Development of U-model enhanced nonlinear dynamic control systems — framework, algorithms and validation

RUOBING LI

A thesis submitted to the University of the West of England, Bristol for the degree of Doctor of Philosophy

School of Engineering
UNIVERSITY OF THE WEST OF ENGLAND

SEPTEMBER 2023

Expanded Abstract

This study aims to develop the classical model-based U-control design framework to enhance its robustness and reduce its dependence on model accuracy. By absorbing the design concepts of other advanced control algorithms, firstly, based on the discrete-time U-control algorithm, a continuous-time (CT) U-model based dynamic inversion algorithm is proposed. Then the CT U-control system design procedures are presented and explained step by step with numerical and simulation demonstrations of the linear and nonlinear U-control system design examples. Secondly, the U-control algorithm develops two mainstream nonlinear robust control algorithms, disturbances suppression and disturbances compensation, while maintaining its system dynamic cancellation characteristics, including two-degree-of-freedom U-model-based internal model control (UTDF-IMC), Disturbance observer-based U-control (DOBUC), sliding mode enhanced U-control (U-SMC) and U-model based double sliding mode control (UDSMC) algorithms. At the same time this study first developed and applied the U-control method to a practical industry application: robust quadrotor trajectory tracking control. The proposed UDSMC method and multiple-input and multiple-output extended-state-observer (MIMO-ESO) established the quadrotor flight control system. The difficulties associated with quadrotor velocity measurement disturbances and uncertain aerodynamics are successfully addressed in this control design. A rigorous theoretical analysis has been carried out to determine whether the proposed control system can achieve stable trajectory tracking performance, and a comparative real-time experimental study has also been carried out to verify the better effectiveness of the proposed control system than the classical SMC and built-in PID control system. This study is clearly novel as the methods and experiments it proposed have not been researched before.

ACKNOWLEDGEMENTS

I would like to express my gratitude to my parents for their financial support, constant care and love. I would like to take this opportunity to express my sincere gratitude to my supervisors, Prof Quanmin Zhu, Dr Alex Yue, and Dr Pritesh Narayan, for their continued encouragement, guidance, and supervision of this research work in the past three years.

I also would like to thank Prof Chenguang Yang, Dr Lingzhong Guo, who have critical reviewed my research and provided useful suggestions. I also want to give my thanks to Dr Hamidreza Nemati, Dr Jianhua Zhang, Dr Weicun Zhang, Dr Baiyang Shi and Dr Peter Kay for wonderful collaboration on work and research.

I am acknowledging the partial PhD studentship for the research project from Engineering Modelling and Simulation Group (EMSG), UWE. Meanwhile, thanks to the Repository Team, IT services department and Graduate school office for their great help and support.

LIST OF PUBLICATIONS

1. Li, R., Zhu, Q., Kiely, J., & Zhang, W. (2020). Algorithms for U-model-based dynamic inversion (UM-dynamic inversion) for continuous time control systems. *Complexity*, 2020, 1-14.

2. Wei, Z., Li, R., & Zhu, Q. (2021). Sliding mode plus U-control method for continuous time SISO dynamic systems. *International Journal of Cybernetics and Cyber-Physical Systems*, 1(1), 68-92.

3. Li, R., Zhu, Q., Narayan, P., Yue, A., Yao, Y., & Deng, M. (2021). U-model-based two-degree-of-freedom internal model control of nonlinear dynamic systems. *Entropy*, 23(2), 169.

4. Zhu, Q., Li, R., & Yan, X. (2022). U-model-based double sliding mode control (UDSM-control) of nonlinear dynamic systems. *International Journal of Systems Science*, 53(6), 1153-1169.

5. Li, R., Zhu, Q., Yang, J., Narayan, P., & Yue, X. (2021). Disturbance-Observer-Based U-Control (DOBUC) for nonlinear dynamic systems. *Entropy*, 23(12), 1625.

6. Li, R., Zhu, Q., Zhang, W., Yue, X., & Narayan, P. (2022). An improved U-control design for nonlinear systems represented by input/output differential models with a disturbance observer. *International Journal of Control*, 1-12.

7. Li, R., Zhu, Q., Nemati, H., Yue, X., & Narayan, P. (2023). Trajectory tracking of a quadrotor using extend state observer based U-model enhanced double sliding mode control. *Journal of the Franklin Institute*, 360(4), 3520-3544.

8. Zhu, QM, Li, RB, Zhang, JH, and Shi, BY. Model-free robust decentralised control of MIMO nonlinear interconnected dynamic systems. *Journal of Vibration and Control*, 2023.

9. Zhu, QM, Li, RB and Zhang, JH. Model-free robust decoupling control of nonlinear nonaffine dynamic systems. *International Journal of Systems Science*, 2023, 1-18.

10. Li, RB, Zhu, QM, Nemati H, and Yue, XC. Adaptive sliding mode attitude control of 2-DOF helicopter system with actuator saturation and disturbances, 2023 (under review).

11. Lei CY, Li, RB, Zhu, QM. Design and Stability Analysis of Semi-Implicit Cascaded Proportional-Derivative Controller for Underactuated Cart-Pole Inverted Pendulum System, *Robotica*, 2023.

12. Book, Li RB and Zhu QM, U-model enhanced robust control and applications, 2023 (under preparation).

Author's declaration

I declare that the work in this dissertation was carried out in accordance with the requirements of the University's Regulations and Code of Practice for Research Degree Programmes and that it has not been submitted for any other academic award. Except where indicated by specific references in the text, the work is the candidate's own work. Work done in collaboration with, or with the assistance of, others, is indicated as such. Any views expressed in the dissertation are those of the author.

SIGNED: .....Ruobing Li..... DATE: .....26/09/2023.....

TABLE OF CONTENTS

LIST OF TABLES

TABLE **Page**

List of Figures

Figure **Page**

CHAPTER 1

INTRODUCTION

Dynamic system modelling and control is a must in many high-tech engineering applications and is an interdisciplinary subject that crosses various technical boundaries. Dynamic systems modelling is used to describe and predict the interactions over time between multiple components of a phenomenon that is viewed as a system [31]. It focuses on the mechanism of how the components and the system evolve over time. Controlling is the managerial function of planning, organizing, implementing and directing. It helps to check errors and take corrective actions during project/machine operations. The control solution quality is increasingly critical in system operations that ensure the optimal performance of controlled products and processes. For example, the quality of the aircraft controller determines the stability, anti-interference ability and accuracy of the aircraft in flight [9]; one more, the vehicle controller also determines the energy saving, cruise manipulability and obstacle avoidance capability of autonomous driving [37]. In regarding the dynamic model structures, even linear models have been widely used as approximations to real plants/processes (almost all are subject to nonlinear), nonlinearity is the most challenging issue in control system analysis/design. It is believed that academic research has been at the front of improving nonlinear control system design. This PhD research takes nonlinear dynamic models as the research background.

1.1 Research motivation

In the process control community, especially in petroleum, chemical, and metallurgical industries, production processes are generally influenced by external disturbances such as variations of raw material quality, fluctuations in production load, and variations of the complicated production environment. In addition, the interactions between different production processes are always sophisticated and difficult to analyze precisely. These factors and their composite actions

usually result in significant degradation of the production quality of these processes [18]. In the mechanical control community, including industrial robotic manipulators [36], motion servo systems [49], maglev suspension systems [110], etc., the control precision is generally affected by different external disturbances, such as uncertain torque disturbances, variations of load torque, vibrations of the horizontal position of rail track, and pivot frictions. Moreover, the control performances of these mechanical systems are also subject to the effects of internal model parameter perturbations caused by the changes in operating conditions and external working environments [18, 36, 49, 110].

As analyzed above, unknown disturbances and uncertainties widely exist in various engineering control systems. The existence of these uncertain factors has great side effects on practical engineering systems. The problem of disturbance rejection is an everlasting research topic since the appearance of control theory and its applications. Since no direct disturbance rejection design is considered, the traditional control methods, such as proportional-integral-derivative (PID) and linear quadratic regulator (LQR) controllers, may be unable to meet the high-precision control specifications in the presence of severe disturbances and uncertainties [42]. The essential reason for this is that these traditional methods do not explicitly take into account disturbance or uncertainty attenuation performance when the controllers are designed.

Therefore, the development of advanced control algorithms with strong disturbance rejection properties has great importance to improve the control precision and of course the production efficiency of practical engineering systems. Due to the significance of disturbance attenuation, many elegant advanced control approaches have been proposed to handle the undesirable effects caused by unknown disturbances and uncertainties since the 1950s, for example, adaptive control (AC) [89, 90], sliding mode control (SMC) [98, 101], disturbance-observer-based control (DOBC) [14, 117], extended state observer (ESO)-based control [54], active disturbance rejection control (ADRC) [42], internal model control (IMC) [26, 84], uncertainty and disturbance estimator (UDE)-based robust control [77]. However, many practical systems, e.g., chemical reactions and PH neutralization, are inherently nonlinear, and their input variables may not be expressed in an affine form. Indeed, the control of these nonaffine nonlinear systems is not only of practical interest but also academically challenging, because of the lack of mathematical tools. To control nonaffine nonlinear systems, the performance of the above control methods [26, 84, 89, 90, 98, 101] is limited or the features of the controlled plants are lost due to the non-affine part being treated as unmeasured disturbance [14, 42, 54, 77, 117].

U-model is a derived control-oriented model set to map almost all classical models into their U-model realization and converts classical models into controller output u based on model with time-varying parameters [115] expressions. U-model establishes a platform for the solution of dynamic inversion by solving roots of polynomial equations, which is more generally attractive compared to the other ad hoc approaches/algorithms [125]. U-model based control [123] (denoted as 'U-control' in short), takes advantage of U-model in dynamic inversion with the following characteristics:

U-model based framework applies dynamic inversion to facilitate holistic control system design and specifies transient and steady-state performance without the need for redundant work when the plant model changes. The difference in U-control between linear models and nonlinear models is the solution with the 1st order or higher order polynomial root solving. The difference in U-control between polynomial models and state space models is the one-layer or multi-layer polynomial root solving. U-control seamlessly integrates with many classical model-based design approaches while enhancing their functionality.

The superiority of U-model has attracted a large number of scholars to conduct research. For example, U-Pole Placement Control (UPPC) [121], U-General Predictive Control (UGPC) [35], U-Neuro-Control (UNC) [129], U-Internal Model Control (UIMC) [47], U-Two-Degree-of-Freedom IMC [53], etc. However, there are critical issues in dynamic inversion before making any designed U-control system applicable in real situations. Because the inverter of the U-controller is highly sensitive and dependent on controlled plants, most existing U-control approaches have assumed that the plant model can be determined without errors or inaccuracies. Accordingly, U-control must consider such robustness in its designed control systems. It should be noted that almost all U-control still stays at its 1st stage of research — with the assumption of the model known exactly, then put the focus on those fundamental structural issues.

From the aforementioned, due to U-model can seamlessly integrate with other control approaches, the main job of this PhD project is to expand the first stage developed results (perfectly matched model-based control system design) into the second stage research (model with uncertainties in analysis/design), that is, in robust control to deal with uncertain plant models and reject system disturbance by combining with other robust control method structures or techniques.

1.2 Aims and objectives of this research

From the aforementioned, this proposed PhD project is aiming at expanding the perfectly matched model-based U-control system design into a robust U-control design with a mismatched model plus external disturbance. Specifically, the main research questions for the project to answer are listed below:

1. How to apply the IMC technology to reduce U-control system design dependence on the model.

2. How to develop DOB based U-control system and expand it to a proper control system that removes the limits of using linear DOBC to control nonlinear plants.

3. How to integrate U-control with sliding mode control, using sliding mode control to compensate dynamic inversion error.

4. How to further reduce U-control's dependence on the model such as using sliding mode control to design dynamic inversion independently.

5. How to apply U-control methods developed with some real-time industrial bench test examples, such as a simple stand-alone inverted pendulum to complex UAVs and robots. Hopefully, these validations can, in return, stimulate further theoretical studies and improve their applicability.

According to the aforementioned questions, the major objectives to continue the process of this project include:

1. Take a critical review of up-to-date artwork on other advanced robust control methodologies and structures and build up a reference database for developing robust U-control platforms. The critical review will give a clear picture 1) what restricts these methods' better development or real-time applications, 2) what the bottleneck issues are in academia and applications to wait for my PhD project to tackle or update.

2. Develop U-control platforms supported by sliding mode control (SMC), internal model control, extend state observer (ESO), disturbance-observer-based control (DOBC), which could facilitate to expand to accommodate U-robust control. Control mathematics will play key roles in the derivations and prove associated performance/properties. Make comparative studies with one or two leading representatives from classical model structures in terms of efficiency, accuracy, and dynamic/static responses.

3. Develop the corresponding Matlab/Simulink simulation programs to make numerical demonstrations from simple to complex, and linear to nonlinear. Discover and solve the problems linked with the proposed control method from the bench tests. Make comparative demonstrations with one or two leading representatives from classical model structures in terms of efficiency, accuracy, dynamic/static responses (user-friendly manual and programs).

4. Extend the proposed control platform derived in objective 2 to deal with the model uncertainty and external environment disturbances problems, provide performance/property analysis and qualify the robust indices. Lyapunov stability analysis and small gain theorem could be the pertinent reference for expansion. Make comparative studies with one or two leading representatives from classical model structures in terms of efficiency, accuracy, dynamic/static responses (two SCI journal publications).

5. Conduct Matlab/Simulink simulation demonstrations for U-control dynamic systems. Provide an integrated U-control framework to deal with both model uncertainty and external environment disturbances problems. Make comparative demonstrations with one or two leading representatives from classical model structures in terms of efficiency, accuracy, dynamic/static responses (user-friendly manual and programs).

1.3 Contributions

The contributions of this thesis are mainly:

1. Generalise U-model based dynamic inversion (UDI) algorithms for continuous-time linear and nonlinear controlled plants, present U-model-based control design procedure for continuous-time dynamic plants in forms of linear/nonlinear and polynomial/state space model. This application does not require the linearized process to nonlinear systems and is illustrated by numerical and simulation bench tests.

2. Propose a general U-model-based Two-Degree-of-Freedom IMC (UTDF-IMC) structure for controlling a class of open-loop stable polynomial/state-space modelled linear and nonlinear dynamic plants. The new control system structure accommodates both linear and nonlinear plants consistently and separates the tracking control filter design from the robust control filter design. Analyze the designed UTDF-IMC control system properties to provide a valid reference for future study expansions and applications, verify the control system performance through benchmark tests of simulated case studies, and illustrate application procedure from an industrial case demonstration.

3. Based on the UDI method, propose a new nonlinear DOB design method, extend the idea of conventional frequency-domain DOB to be applicable to nonlinear systems, which can integrate all external disturbances and internal modelling errors as system input errors. Combining the strengths exhibited in U-control and this new nonlinear DOB to provide an enhanced, fast-response, delay-free, and convenient design control framework, applicable to all linear/nonlinear invertible controlled plants. The control system performance is verified through benchmark tests of simulated case studies.

4. Inspired by high-gain theory, develop a novel U-model based inverter and U-control design framework that only uses the input/output signal from the control system. Additionally, because of the high sensitivity of the U-inverter to the system modelling accuracy and system external disturbances, the proposed U-control design framework is combined with a nonlinear DOB which also only requires the input/output measurements from the control system to improve its robustness. The control system performance is verified through benchmark tests of simulated case studies.

5. Proposal a new sliding mode (SM) technology enhanced U-control design framework (U-SMC), which uses SM to design an inverter to compensate the modelling errors and system external disturbances, accommodating both control-oriented model structure in the U-control method and strong robustness against imperfect model representation in the SMC method. Compared with classical SMC, U-SMC only uses SMC to realize the stability and robustness design and the control performance design is completed by U-control, which

is convenient for users to choose the system control performance by themselves. Also, the control system performance is analyzed through benchmark tests of simulated case studies.

6. Propose a double sliding mode control (DSMC) scheme to establish a robust dynamic inverter for the controlled plant, to cancel the plant's nonlinearities and complex dynamics, which removes the request of plant nominal model and eliminates chattering in the classical SMC design by introducing sliding band (sliding surface plus sliding boundary). Bench tests with computational experiments validate the analytical results.

7. Based on the proposed UDSMC, first apply the U-control method to a real-time application (quadrotor control). Using UDSMC to propose a quadrotor decoupling algorithm, using an indirect control strategy (position control by controlling the angle) turns the original underactuated system into a fully actuated system. Extending the SISO implementation and application of UDSMC to the MIMO system, based on Lyapunov stability, combining it with MIMO-ESO provides a robust quadrotor flight control framework for flight control. Comparative experimental studies with the built-in PID controller (come from the product) and SMC method (advanced control algorithm) are involved to show the efficiency of the proposed controller.

1.4 Structure of the thesis

This thesis is divided into seven chapters. It starts with an introduction to the research in Chapter 1 and ends with conclusions drawn from this research in Chapter 7. Chapter 2 provides the research background, CT U-model based dynamic inversion algorithm and CT U-control design framework. Chapter 3 presents the design of U-model-based Two-Degree-of-Freedom IMC (UTDF-IMC) framework. Chapter 4 presents disturbance-observer based U-control (DOBUC) design framework. Chapter 5 presents a sliding mode enhanced U-control design framework. Chapter 6 presents a quadrotor trajectory tracking control system using UDSMC and MIMO ESO. Chapter 7 concludes this thesis. The outline of the thesis is as follows:

1. Chapter 1 introduces the research motivation, the project aims and objective, and highlights the contributions of this research study.

2. In Chapter 2, Section 2.1 generalises U-polynomial and U-state space model sets, and its associated step-by-step U-control design procedure. Section 2.2 generalises the dynamic inversion algorithms. Section 2.3 presents a series of computational case studies to test/demonstrate the analytical results numerically and provides an effective procedure for testing designed U-control systems with computational experiments. Section 2.4 presents an industrial background case study from modelling, dynamic inversion, and U-control system design to simulation.

3. In Chapter 3, Section 3.1 presents the basis of using IMC and U-control for the next step of development of the new UTDF-IMC system structure. Section 3.2 elaborates on the principle of TDF-IMC structure and establishes the U-model based TDF-IMC (UTDF-IMC) framework; consequently, it analyses the control system properties. Section 3.3 showcases two computational investigations to benchmark test/demonstrate the proposed UTDF-IMC system performance. Then an industrial backgrounded permanent magnet synchronous motors (PMSM) system is added to demonstrate the application procedure and the comparative studies in Section 3.4.

4. In Chapter 4, Section 4.1 states the excited issues of nonlinear system control using DOB methods. Section 4.2 proposes a DOBUC design framework and performance analysis by simulation experiments. Section 4.3 proposes an improved DOBUC method and takes simulation experiments to illustrate and demonstrate the findings of the studies.

5. In Chapter 5, Section 5.1 introduces the basic principles and concepts of the SMC method. Section 5.2 presents the U-SMC system design framework and design procedures, and its control performance is demonstrated by simulation experiments. Based on section 5.2, section 5.3 proposes a U-model based double sliding mode control (UDSMC) method and takes simulation experiments to illustrate and demonstrate the findings of the studies.

6. In Chapter 6, Section 6.2 introduces the dynamical model of the quadrotor and control problems for follow-up development. In section 6.3, the MIMO-ESO is derived to estimate the unmeasured quadrotor's velocities. Section 6.4 presents the UDSMC method first, then comes with its quadrotor flight controller design procedures, coefficients designed principle, and stability analysis. Also, it proposes a new decoupling algorithm for the quadrotor flight operation. Section 6.5 presents the experimental bench tests, which show the experimental setup procedure, design parameters of the involved control methods, and experiment results to compare to demonstrate the efficiency of the proposed control system.

7. In Chapter 7, conclusions are drawn to summarise the study and provided the proposed future research to follow up this research study.

CHAPTER 2

U-MODEL BASED DYNAMIC INVERSION

The model of linear control system can be described by state space model-based and polynomial model-based approaches, which have been well studied and are widely used [41, 85]. However, in an actual production process, nonlinear control is ubiquitous and more difficult as the superposition principle no longer holds, in contrast to linear systems, therefore, how to design a standard-compliant nonlinear control system to match desired performance properly is a hot issue. For nonlinear systems, a variety of analysis and design approaches already exist, and the most commonly used method to design a nonlinear control system is still linearization. However, the linearization method has certain limitations, and most linear control methods cannot be applied to the design of nonlinear systems directly. For example, compared with the linear polynomial model, nonlinear polynomial models, such as the Nonlinear Autoregressive Moving Average with eXogenous inputs (NARMAX) model [6], have appeared widely in applications and academic research publications [125], however, there is no systematic routine to convert it into the equivalent state-space model.

Generally, there are three methodologies for nonlinear plant-model based control system design, two widely used and one less attended. The first approach is using linear expressions to describe the nonlinear state-space models by feedback linearization approach [48, 85], and then designing this linear-expression corresponding control systems by linear state-space approaches, which has been well studied in [41, 85]. However, this case-by-case method requires certain skills in selecting the appropriate coordinate system and solving the equations requires extra effort. Furthermore, this state-space linearization approach cannot be directly applied to nonlinear polynomial models. The second method is to use a time-varying linear model to fit the polynomial model, for example, the state-dependent parameter (SDP) transformation [20] method can use specified (desired) poles to transform a nonlinear closed-loop control system model to a linear

transfer function expression. In summary, it is clear that these approaches for designing a nonlinear control system are trying to convert the original nonlinear system into a quasi-linear domain system first, and then choose a proper linear control approach for the system. In the model structure, the other variables in the system can also determine this quasi-linear SDP transformation's parameters [112]. The nonlinear polynomial model can be converted into a time-varying linear state-space model by the second method, however, there are obstacles to using this method because this design and transform procedure is not unique, that is, personal and subjective for the selection of SDP models.

The third approach is the U-model based design, which is relatively new and less attended. U-model is defined as a polynomial or state space function, with time-varying parameters, representing a class of smooth and analytic systems. In 1991, Zhu Quanmin et al [126] proposed the use of a Newton-Raphson iterative algorithm for the root solving of the controller output function, which provided a basic procedure for the design of controllers in the U-model. Research[121] formally proposed the concept of U-model and established the U-model based control, U-control in short, system design framework, which provides a general routine to convert smooth nonlinear plant models into U-model. The U-model based design method can be recognised as converting nonlinear models to time-varying parameter models associated with controller output u, that is, linear control-oriented model structure.

Regarding the research status of U-model based control, the discrete-time systems have been studied with more attention, especially the representative approaches including, the pole placement control design method [121, 131], U-Smith predictor with input time delay [35], adaptive U-control of total nonlinear dynamic systems [124], U-neural network enhanced control [129], and underactuated coupled nonlinear adaptive control synthesis, using U-model for multivariable unmanned marine robotics [47]. However, most U-control approaches have assumed that the plant model can be detected without errors or inaccuracies. Therefore, designing an adaptive U-model controller when the plant model is inaccurate, especially the robustness control, will be a hotspot and difficult study area for intensive research. At the same time, there is very little research on U-model based control system design for continuous-time systems so far [128]. Consequently, the main purpose of this study is to provide a pack of dynamic inversion routines for U-model based continuous-time control systems.

Compared with methods 1 (linear model approximation) and 2 (time-varying linear model approximation) aforementioned, the main contributions of this U-design method are

1. In dealing with nonlinearity, U-model-based design method does not require linearization of the nonlinear models in advance. Instead, this nonlinear plant model-based system is designed directly using linear design methods.

2. In methodology, using those well-studied linear methods to design nonlinear control systems greatly reduces the complexity of the design procedure.

3. In design, once the closed loop system output is specified, the only remaining work is to calculate the output of the U model controller.

4. U-model-based control system design procedure is more general and effective for designing a linearly behaved control system, which provides new insight and solutions to design the controller.

5. U-control can be applied together with the other well-developed control system design methods, such as pole placement control, sliding mode control, general predictive control, adaptive, Smith predictive control and so on [100].

6. It should be noted that unless the plant model is accurately known, U-model dynamic inversion is very sensitive to internal uncertainties, so the whole control system performs.

Accordingly, the main contributions of this study are:

1. generalize dynamic inversion algorithms for continuous-time U-model.

2. generalize U-model based control system design procedure for continuous-time dynamic plants in forms of linear/nonlinear, polynomial/state space.

3. An industrial backgrounded study – U-control of a wind energy conversion system.

For the rest of the section, Chapter 2.1 generalises U-polynomial and U-state space model sets, and their associated step-by-step U-control design procedure. Chapter 2.2 generalises the dynamic inversion algorithms. Chapter 2.3 presents a series of computational case studies to test/demonstrate the analytical results numerically and provides an effective procedure for testing designed U-control systems with computational experiments. Chapter 2.4 presents an industrial background case study from modelling, dynamic inversion, and U-control system design to simulation. Chapter 2.5 concludes this study.

2.1 U-model and U-control system design

2.1.1 Polynomial U-model: single layer realisation

Consider a general continuous-time U-model [129] for Single-Input and Single-Output (SISO) polynomial dynamic systems with a triplet of (y,u,λ) and $y,u \in R$ for the output, input, and parameter respectively at time $t \in R^+$,

$$y^{(M)} = \sum_{j=0}^{J} \lambda_j(Y_{M-1}, U_{N-1}, \Theta)\left(u^{(N)}\right)^j, \;\; M \geq N \tag{2.1}$$

where $y^{(M)}$ and $u^{(N)}$ are the Mth and Nth order derivatives of the plant output y and the plant input u, respectively. The time-varying parameter $\lambda_j(*) \in R^+$, absorbs all the other terms in

$Y_{M-1} = \left[y^{(m)}, y^{(m-1)}, \cdots, y\right] \in R^M$, $U_{N-1} = \left[u^{(n)}, u^{(n-1)}, \cdots, u\right] \in R^N$ with $m \le M$ and $n \le N$ being derivative orders for y and u, and coefficients Θ associated with the input $\left(u^{(N)}\right)^j$. Here is an example for understanding, consider a classical NAMAX polynomial model,

$$\ddot{y} = (y-1)\dot{y} + \left(1+y^2\right)u + \left(1+\dot{y}^2\right)u^2 + y + \left(y+\dot{y}^2\right)u^3 \tag{2.2}$$

Then its (2.2) U-model realisation can be determined with

$$\left\{ \begin{array}{c} \ddot{y} = \lambda_0 + \lambda_1 u + \lambda_2 u^2 + \lambda_3 u^3 \\ \lambda_0 = (y-1)\dot{y} + y \\ \lambda_1 = 1 + y^2 \\ \lambda_2 = 1 + \dot{y}^2 \\ \lambda_3 = y + \dot{y}^2 \end{array} \right) \tag{2.3}$$

Inspection of (2.2) and (2.3), the U-realisation is straightforward generally. It should be remarked that the U-polynomial is the same as its presented classical polynomials in the model properties, but oriented expression for control system design [130]. The rational model is totally nonlinear [125], and its polynomial expression is a ratio of two polynomials, that is:

$$y^{(M)} = \frac{\sum_{j=0}^{n} \lambda_{nj}(Y_{M-1}, U_{N-1}, \Theta) f_{nj}\left(u^{(N)}\right)}{\sum_{j=0}^{d} \lambda_{dj}(Y_{M-1}, U_{N-1}, \Theta) f_{dj}\left(u^{(N)}\right)}, M \ge N \tag{2.4}$$

Where f_{nj} and f_{dj} are vector functions of the control vector $\left(u^{(N)}\right)^j$ in numerator and denominator, respectively, λ_{nj} and λ_{dj} are the associated parameters vectors absorbing all the other terms in the model. Here is a simple example of the rational model

$$\dot{y} = \frac{0.1y^3 + \sin(u) + 0.5u^3}{1 + \cos(y) + u^2} \tag{2.5}$$

Its U-model realisation can be determined with

$$\dot{y} = \frac{\lambda_{n0} + \lambda_{n1}\sin(u) + \lambda_{n2}u^2 + \lambda_{n3}u^3}{\lambda_{d0} + \lambda_{d1}u + \lambda_{d2}u^2} \tag{2.6}$$

where

$$\left\{ \begin{array}{c} \lambda_{n0} = 0.1y^3 \\ \lambda_{n1} = 1 \\ \lambda_{n2} = 0 \\ \lambda_{n3} = 0.5 \end{array} \right) and \left\{ \begin{array}{c} \lambda_{d0} = 1 + \cos(y) \\ \lambda_{d1} = 0 \\ \lambda_{d2} = 1 \end{array} \right) \tag{2.7}$$

2.1.2 State space U-model: multi-layer realization

Consider a general SISO CT state space model,

$$\left\{ \begin{array}{c} \dot{X} = F(X,u) \\ y = H(X) \end{array} \right) \tag{2.8}$$

where $u, y \in R$. $F \in R^+$ is a smooth mapping to represent the input to the state $X \in R^+$, and $H \in R$ is a smooth mapping to drive the states to the outputs. In this section, assume that there are no unstable zero dynamics and that the state X can be obtained through measurement or observation. Expand state-space model (2.8) into a multi-layer polynormal expression as follows:

$$\left\{\begin{array}{c} \dot{x}_1 = F_1(x_1, x_2, \ldots, x_n) \\ \dot{x}_2 = F_2(x_1, x_2, \ldots, x_n) \\ \vdots \\ \dot{x}_n = F_n(x_1, x_2, \ldots, x_n, u) \\ y = H(x_1, x_2, \ldots, x_n) \end{array}\right\} \tag{2.9}$$

Convert state-space model (2.9) into a multi-layer U-model expression as follows

$$\left\{\begin{array}{c} \dot{x}_1 = \sum_{i=0}^{n} \lambda_{1i} f_{1i}(x_2) \\ \dot{x}_2 = \sum_{i=0}^{n} \lambda_{2i} f_{2i}(x_3) \\ \vdots \\ \dot{x}_n = \sum_{i=0}^{n} \lambda_{ni} f_{ni}(u) \\ y = \sum_{i=0}^{n} h_i(x_1, x_2, \ldots, x_n) \end{array}\right\} \tag{2.10}$$

For each line of (2.10), λ_{ni} and f_{ni} are time-varying parameters absorbing all the other variables and the U-basis function respectively. For illustration, consider a nonlinear SISO system state-space model of

$$\left\{\begin{array}{c} \dot{x}_1 = x_1 + 0.5\sin(x_2) \\ \dot{x}_2 = -x_1 + u \\ y = x_1 \end{array}\right\} \tag{2.11}$$

Using the absorbing rule to convert (2.11) into a multi-layer U-model as

$$\left\{\begin{array}{c} \dot{x}_1 = \lambda_{10} + \lambda_{11} f_{11}(x_2) \\ \dot{x}_2 = \lambda_{20} + \lambda_{21} f_{21}(u) \\ y = x_1 \end{array}\right\} \tag{2.12}$$

where

$$\left\{\begin{array}{c} \lambda_{10} = x_1,\ \lambda_{11} = 0.5,\ f_{11}(x_2) = \sin(x_2) \\ \lambda_{20} = -x_1,\ \lambda_{21} = 1,\ f_{21}(u) = u \end{array}\right\} \tag{2.13}$$

2.1.3 U-control system design

Figure 2.1 shows the classical control system framework, where G_P is the plant model, which could be linear or nonlinear dynamics and can be described by polynomial and state space models [130]. Let G (not shown in the figure) be the closed-loop performance function, specified with ad hoc applications in advance by designers and/or customers, r is the reference, which is the desired output of the control system, e is the difference (error) between the output y and the reference r.

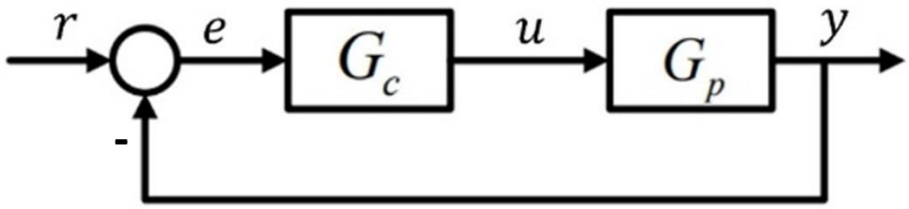

Figure 2.1: Classical control system framework

G_c is the designed controller. The main principles of this kind of control system design framework are to generate a suitable control input signal u to drive the system output trajectory y following a set of specified closed-loop performances (both transient and steady state).

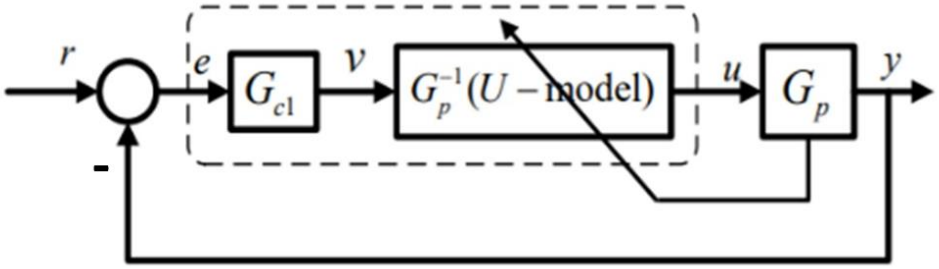

Figure 2.2: U-control system framework

Figure 2.2 shows the U-control system framework, in which G_{c1} is a linear invariant controller, can be designed by $G_{c1} = \frac{G}{1-G}$ while $G_P^{-1}G_P = 1$, where G_P^{-1} is the controlled plant's dynamic inversion. It is clear that this invariant controller is only designed according to the gain of the whole control system G, not the controlled plant G_P. U-control framework is applicable to both linear and nonlinear structures as long as dynamic inversion G_P^{-1} exist. To explain the control system design procedure, consider a CT SISO linear closed-loop feedback control system framework with a set of (F, G_{c1}, G_{ip}),

$$\sum = (F, G_{c1}, G_{ip}) \tag{2.14}$$

where $G_ip = G_P^{-1}G_P$ represents the product of the dynamic inversion and the controlled plant, and F represents such control system framework.

In general, the U-control system design procedure has two separate steps:

1. Assume the plant model G_P is stable and bounded, and its inversion G_P^{-1} exists (the controlled plant should be minimum phase and its dynamic response is not equal to 0).

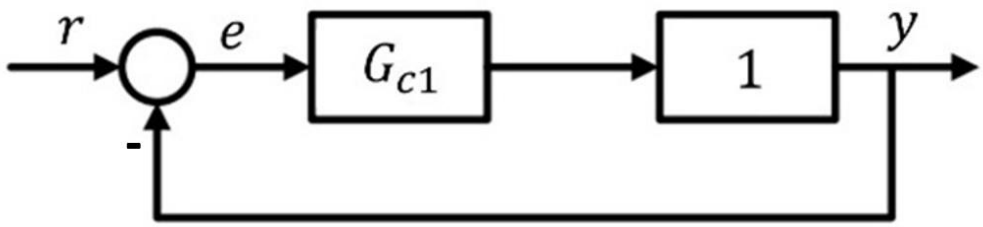

Figure 2.3: U-model based simplified control system

From Figure 2.2, the controller which is shown in the dashed line block has two parts: the invariant controller G_{c1} and the plant's dynamic inversion G_P^{-1}. To facilitate the design of G_P^{-1}, convert plant model G_P into its U-model. Alternatively (2.14) can be expressed as

$$\sum = \left(F, U\left(G_{c1}, G_P^{-1}\right), G_p\right) \tag{2.15}$$

where $\left(G_{c1}, G_P^{-1}\right)$ is defined as U-controller. Determine G_{ip} to work out the controller output u, which is the control input to the plant G_P. The eventual goal is to make plant output equal to the invariant controller output: $v = y$, that is, to reach $G_P^{-1}G_P = 1$ under the proper dynamic inversion.

2. Design the invariant controller G_{c1}. Figure 2.3 shows the U-control structure while $G_P^{-1}G_P = 1$ achieved. That is

$$\sum = (F, G_{c1}) \tag{2.16}$$

This is a type of linear control system. Therefore, the desired closed-loop transfer function G can be expressed as $G = \frac{G_{c1}}{1+G_{c1}}$. where G can be effectively designed with two significant factors shaping linear system response, damping ratio ζ and undamped natural frequency ω_n. Therefore, the invariant controller G_{c1} can be obtained by $G_{c1} = \frac{G}{1-G}$ while $G_P^{-1}G_P = 1$. As the invariant controller G_{c1} design is independent of plant G_P, the U-control system allows once-off design for all stable-nonminimum phase controlled plants, except designing the inverter G_P^{-1} of the considered plant.

2.2 UM-dynamic inversion

Nonlinear dynamic inversion (NDI) is a generic control technique in nature, that is, improving control performance through control system design. Currently, NDI has been a challenging research issue and has practical significance in mechanical motion control systems, such as turbines, robots, and flying vehicles [83]. The basic NDI calculation procedure is differentiating the plant output equation results in N times to find the direct relationship between the input u and Nth order derivative of the output y under the Lie derivative formulation [83]. However, NDI

is very sensitive and unstable in case of model inaccuracies and mismatches. In order to combat the uncertainty of the plant and improve the system robustness, Incremental Nonlinear Dynamic Inversion (INDI) [83] and adaptive INDI [86] have been introduced in another complicated formulation.

Different from the computational complexity of basic NDI under the Lie derivative expression, this study converts the plant model into U-model realization in a systematic concise formulation, which is generically applicable to both polynomial and state space equations. This also establishes a foundation for the future development of robust UM-dynamic inversion. The U-model based dynamic inversion (UM-dynamic inversion) algorithm is to obtain the input u by solving the root from (2.1), that is,

$$G_p^{-1} \Longleftrightarrow u^{(N)} \in y^{(M)} - \sum_{j=0}^{J} \lambda_j(Y_{M-1}, U_{N-1}, \Theta)\Big(u^{(N)}\Big)^j = 0 \tag{2.17}$$

For the solution to exist, the systems must be Bounded Input and Bounded Output (BIBO) stable and have no unstable zero dynamics (nonminimum phase).

2.2.1 Algorithms for polynomial models

Using Laplace transform (S operator, $y^{(j)} = \frac{d^j y}{dt^j} \Leftrightarrow s^j Y$ and $\int \cdots \int y dt \Leftrightarrow \frac{1}{s^j} Y$) to express a set of general linear dynamic plants as

$$Y = \frac{\sum_{j=0}^{j=N} \beta_j s^{N-j}}{\sum_{j=0}^{j=M} \alpha_j s^{M-j}} u = \frac{\beta_0 s^N + \beta_1 s^{N-1} + \ldots + \beta_{N-1} s + \beta_N}{\alpha_0 s^M + \alpha_1 s^{M-1} + \ldots + \alpha_{M-1} s + \alpha_M} U, \;\; M \geq N \tag{2.18}$$

where Y and U are the Laplace transform of the output and input respectively, and M and N are the orders (highest power) of the denominator and numerator functions respectively. Accordingly, its (2.18) U-realisation is given as

$$y^{(M)} = \sum_{j=0}^{1} \lambda_j(Y_{M-1}, U_{N-1}, \Theta)\Big(u^{(N)}\Big)^j \tag{2.19}$$

where

$$\begin{aligned} \lambda_o(Y_{M-1}, U_{N-1}, \Theta) &= \left(- \sum_{j=1}^{j=M-1} \alpha_j s^{(M-j)} Y + \sum_{j=1}^{j=N-1} \beta_j s^{(N-j)} U \right) / \alpha_0 \\ \lambda_1(Y_{M-1}, U_{N-1}, \Theta) &= \frac{\beta_0}{\alpha_0} \end{aligned} \tag{2.20}$$

Convert the operations into integral implementations by multiplying $\frac{1}{s^N}$ on both sides of (2.19), this gives

$$y^{(M-N)} = \frac{\sum_{j=0}^{1} \lambda_j(Y_{M-1}, U_{N-1}, \Theta) u}{s^N} \tag{2.21}$$

where

$$\begin{aligned}\lambda_o(Y_{M-1},U_{N-1},\Theta) &= \left(-\sum_{j=1}^{j=M-1}\alpha_j\frac{s^{M-j}}{s^N}Y+\sum_{j=1}^{j=N-1}\beta_j\frac{s^{N-j}}{s^N}U\right)/\alpha_0\\ \lambda_1(Y_{M-1},U_{N-1},\Theta) &= \frac{\beta_0}{\alpha_0}\end{aligned} \tag{2.22}$$

Therefore, the alternative U-model is

$$y^{(M-N)} = \sum_{j=0}^{1}\lambda_j(Y_{M-1},U_{N-1},\Theta)u^j \tag{2.23}$$

For nonlinear plants, consider the UM-dynamic inversion described in (2.17), and replace all the derivatives with integrals through division by the output derivative order, which is formulated as

$$y^{(j)} = y^{(M)}\left(\frac{1}{s}\right)^{M-j} \tag{2.24}$$

where $y^{(j)} = \frac{d^j y}{dt^j}$. Here is the practical implementation of (2.17),

$$G_p^{-1} \Longleftrightarrow u \in y - \frac{\sum_{j=0}^{J}\lambda_j(Y_{M-1},U_{N-1},)\left(u^{(N)}\right)^j}{s^M} = 0 \tag{2.25}$$

To illustrate the conversion to U-model from a nonlinear polynomial. Consider an example of

$$\ddot{y} = \left(1-y^2\right)\dot{y} - u + (1+y)\dot{u} + \left(1+\dot{y}^2\right)\dot{u}^2 + \dot{u}^3 \tag{2.26}$$

In U-realisation, its derivative-based operation becomes

$$\ddot{y} = \lambda_0 + \lambda_1\dot{u} + \lambda_2\dot{u}^2 + \lambda_3\dot{u}^3 \tag{2.27}$$

where

$$\left\{\begin{array}{c}\lambda_0 = \left(1-y^2\right)\dot{y} - u\\ \lambda_1 = \left(1+y^2+\dot{y}^2\right)\\ \lambda_2 = 1+\dot{y}^2\\ \lambda_3 = 1\end{array}\right\} \tag{2.28}$$

Because $u^{(i)} = u^{(N)}\left(\frac{1}{s}\right)^{N-i}$ and $u^{(i)} = \frac{d^i u}{dt^i}$, convert (2.27) into integration operation, the corresponding U-realisation has form of

$$y = \frac{\lambda_0}{s^2} + \frac{\lambda_1}{s}u + \frac{\lambda_2}{s}u^2 + \frac{\lambda_3}{s}u^3 \tag{2.29}$$

2.2.2 Algorithms for state space models

For a general SISO linear CT state-space system model, it has

$$\left\{\begin{array}{c}\dot{x} = Ax + Bu\\ y = Cx + Du\end{array}\right\} \tag{2.30}$$

Where $u, y \in R$, $x \in R^n$, let $A = \begin{bmatrix} 0 & 1 & 0 & \cdots \\ \cdots & \ddots & \ddots & \cdots \\ -\alpha_1 & \cdots & & -\alpha_n \end{bmatrix}$, $B = [0\ 0 \cdots 1]^T$, $C = \begin{bmatrix} \beta_1 \cdots \beta_n \end{bmatrix}$, and $D = 0$.

Expanding (2.30) gives rise to

$$\left\{ \begin{array}{l} \dot{x}_1 = x_2 \\ \dot{x}_2 = x_3 \\ \vdots \\ \dot{x}_n = \sum_{j=1}^{n} \alpha_j x_j + u \\ y = \sum_{j=1}^{n} \beta_j x_j \end{array} \right\} \tag{2.31}$$

where x is the state vector, u and y are the input and output of the controlled plant, respectively. For taking up such UM-dynamic inversion, firstly use a systematic approach [72] to convert the linear state space model into an input/output transfer function by

$$\frac{Y(s)}{U(s)} = C[sI_n - A]^{-1}B \tag{2.32}$$

where $Y(s)$ and $U(s)$ are the Laplace transforms of the output and input respectively, I_n is an identity matrix with dimension n. Then the linear polynomial dynamic inversion procedure presented in the Chapter 2.2.1 can be applied.

For the nonlinear controlled plant, consider the model in (2.10), the step-by-step UM-dynamic inversion design procedure can be organized as

1. Generate direct mapping between the output y and the input u, by differentiating the state variables in the output equation till directly related to u in the state equation.

2. Use the procedure for nonlinear polynomial dynamic inversion presented in the previous subchapter to determine the solutions. It should be noted that the above computations require the full state variable necessarily available/measurable. To illustrate the realization, consider a nonlinear state space model of

$$\left\{ \begin{array}{c} \dot{x}_1 = x_1 - x_2 - {x_3}^2 \\ \dot{x}_2 = -x_1 + {x_2}^2 - x_3 \\ \dot{x}_3 = -{x_1}^2 - x_2 + x_3 + u \\ y = x_1 \end{array} \right\} \tag{2.33}$$

   Differentiating y twice against x_1 with the output equation gives

$$\left\{ \begin{array}{c} \dot{y} = \dot{x}_1 = x_1 - x_2 - {x_3}^2 \\ \ddot{y} = \dot{x}_1 - \dot{x}_2 - 2x_3\left({x_1}^2 - x_2 + x_3 + u\right) \end{array} \right\} \tag{2.34}$$

   As the second line of (2.34) directly relates the output and the input, it can be used for the dynamic inversion. The corresponding polynomial U-model is given by

$$\left\{ \begin{array}{l} \ddot{y} = \ \lambda_0 + \ \lambda_1 u \\ \lambda_0 = \dot{x}_1 - \dot{x}_2 - 2x_3\left({x_1}^2 - x_2 + x_3\right) \\ \lambda_1 = -2x_3 \end{array} \right\} \tag{2.35}$$

Convert to integral expression as

$$y = \frac{\lambda_0}{s^2} + \frac{\lambda_1}{s^2}u \tag{2.36}$$

2.3 Simulation demonstrations

This simulation demonstration selected four plant models to test the UM-dynamic inversion and their associated U-control systems with the following bullet points

1. To demonstrate the generality and effectiveness of UM dynamic inversion.
2. To demonstrate the principle of model-independent design in U-control, supported by the dynamic inversions.
3. To demonstrate a once-off design with the linear invariant controller in accordance with a closed-loop performance specification irrespective of the plant model structures.
4. To validate the applicability, conciseness, and efficiency of the U-control and UM-dynamic inversion, particularly in designing nonlinear control systems.

2.3.1 U-control system design

With reference to the previous U-model based algorithm introduction in Chapter 2.2, For these simulations, design a unique U-control system with a desired system output response in terms of damping ratio $\zeta = 0.7$, undamped natural frequency $\omega_n = 1$, and zero steady-state error to a step reference input [35]. Accordingly, this closed-loop transfer function was specified as

$$\frac{Y(S)}{R(S)} = G(S) = \frac{1}{s^2 + 1.4s + 1} \tag{2.37}$$

The invariant controller G_{c1} was determined by taking the inverse of (2.37) as

$$G_{c1} = \frac{G}{1-G} = \frac{1}{s^2 + 1.4s} \tag{2.38}$$

2.3.2 Case 1: Linear polynomial and state space models

Consider a linear polynomial controlled plant as plant 1

$$G_P(s) = \frac{3s^2 + 6s + 4}{s^2 + 2s + 1} \tag{2.39}$$

The corresponding U-model will be

$$\left\{ \begin{array}{c} y = \frac{\lambda_0}{s^2} + \lambda_1 u \\ \lambda_0 = -2\dot{y} - y + 6\dot{u} + 4u \\ \lambda_1 = 3 \end{array} \right) \tag{2.40}$$

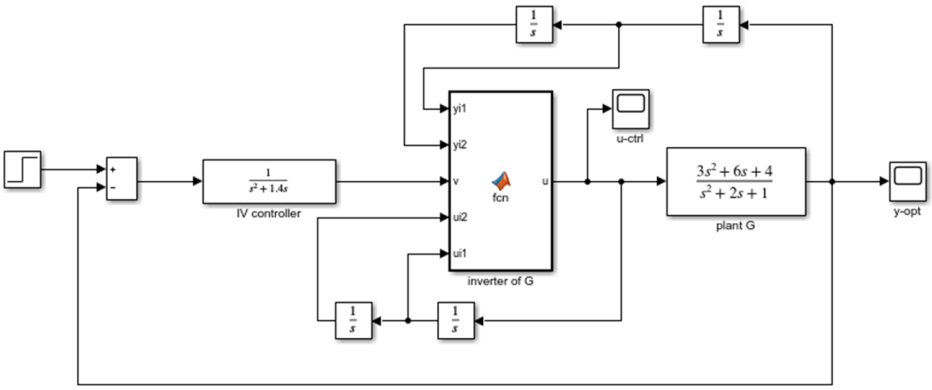

Figure 2.4: U-control system for plant 1

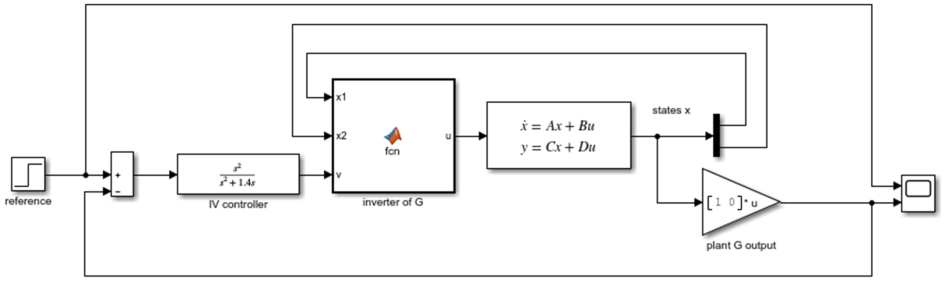

Figure 2.5: U-control system for plant 2

Then consider a state-space based controlled plant as plant 2

$$\left\{ \begin{array}{c} \begin{bmatrix} \dot{x_1} \\ \dot{x_2} \end{bmatrix} = \begin{bmatrix} 0 & 1.5 \\ -0.5 & -2 \end{bmatrix} \begin{bmatrix} x_1 \\ x_2 \end{bmatrix} + \begin{bmatrix} 0 \\ 1 \end{bmatrix} \\ y = \begin{bmatrix} 1 & 0 \end{bmatrix} \begin{bmatrix} x_1 \\ x_2 \end{bmatrix} + [0] \end{array} \right\} \tag{2.41}$$

The corresponding U-model is

$$\left\{ \begin{array}{c} \ddot{y} = \lambda_0 + \lambda_1 u \\ \lambda_0 = 1.5(-0.5x_1 - 2x_2) \\ \lambda_1 = 1.5 \end{array} \right\} \tag{2.42}$$

The U-control systems frameworks designed for plant 1 and plant 2 are shown in Figure 2.4 and Figure 2.5, their control performance can be observed in Figure 2.6 and Figure 2.7. Both control systems' outputs can converge to the desired followed by the designed control performance specification.

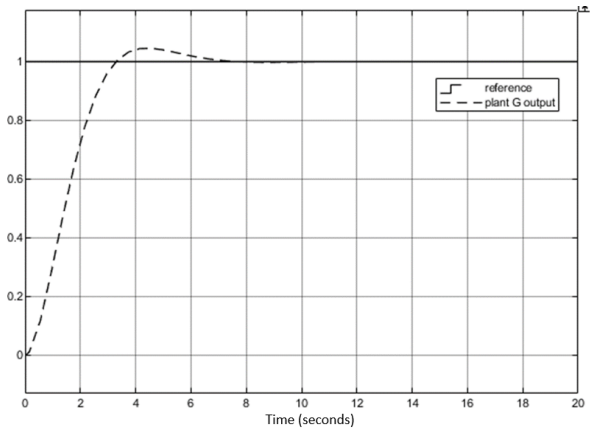

Figure 2.6: Plant output and reference

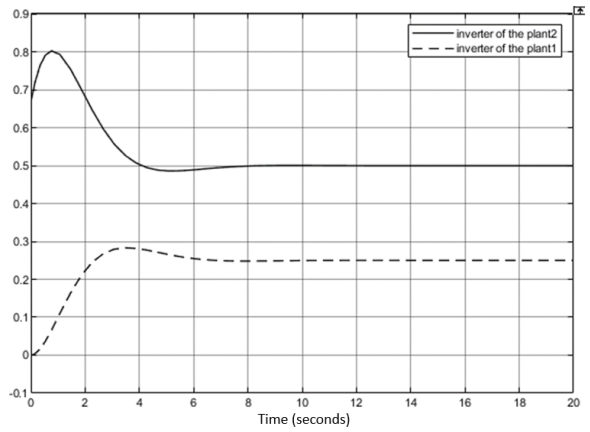

Figure 2.7: Controller outputs for plant1 and plant2

2.3.3 Case 2: Nonlinear polynomial and state space models

Consider a nonlinear polynomial controlled plant as plant 3

$$\dot{y} = \dot{u}^3 + \dot{u}^2 - \dot{u} - 0.5y + \sin(u) \tag{2.43}$$

The corresponding U-model will be

$$\left\{ \begin{array}{c} \dot{y} = \lambda_0 + \lambda_1 \dot{u} + \lambda_2 \dot{u}^2 + \lambda_3 \dot{u}^3 \\ \lambda_0 = -0.5y + \sin(u) \\ \lambda_1 = -1 \\ \lambda_2 = \lambda_3 = 1 \end{array} \right\} \tag{2.44}$$

Then consider a nonlinear state-space based controlled plant as plant 4

$$\left\{ \begin{array}{c} \dot{x}_1 = x_2 \\ \dot{x}_2 = \sin(x_1) + u \\ y = x_1 \end{array} \right\} \tag{2.45}$$

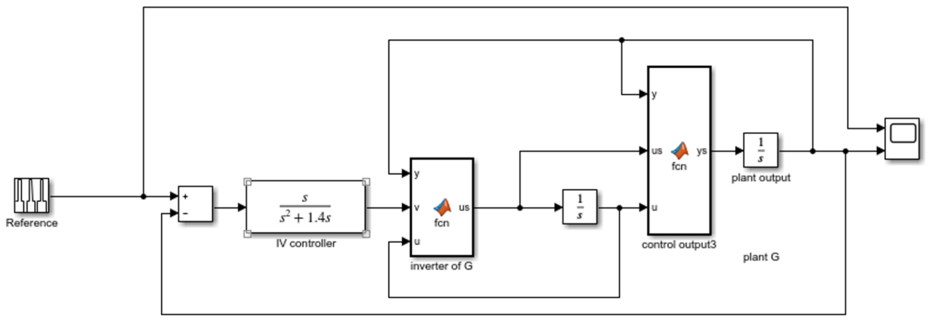

Figure 2.8: U-control system for plant 3

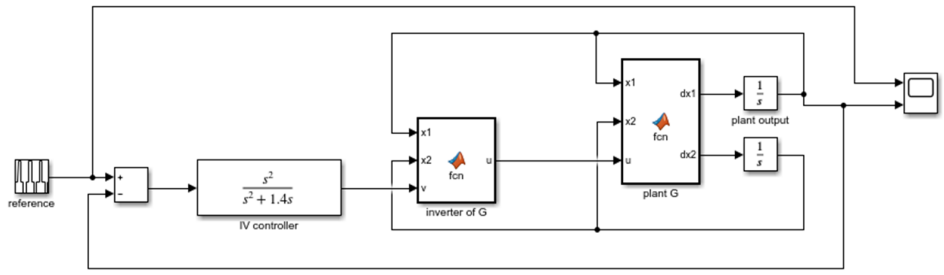

Figure 2.9: U-control system for plant 4

Its corresponding U-model model is

$$\left\{\begin{array}{c} \ddot{y} = \lambda_0 + \lambda_1 u \\ \lambda_0 = \sin(x_1) \\ \lambda_1 = 1 \end{array}\right. \tag{2.46}$$

The U-control systems framework designed for plant 3 and plant 4 are shown in Figure 2.8 and Figure 2.9, their control performance can be observed in Figure 2.10 and Figure 2.11. Both control systems' outputs can converge to the desired followed by the designed control performance specification. All of these simulation tests have demonstrated that the purposes outlined at the beginning of the Chapter have been achieved.

2.4 Test of U-control of a wind energy conversion system

2.4.1 Brief review of wind energy conversion control systems

Wind power is a clean natural resource to supplement the other power resources from fossil fuels, coal, solar, and so on. This rich power source is widely distributed, renewable has no greenhouse gas emissions, and uses little land [32]. In the conversion of wind power, in which air flows drive wind turbines to generate electrical power, the need for effective control strategies for cost

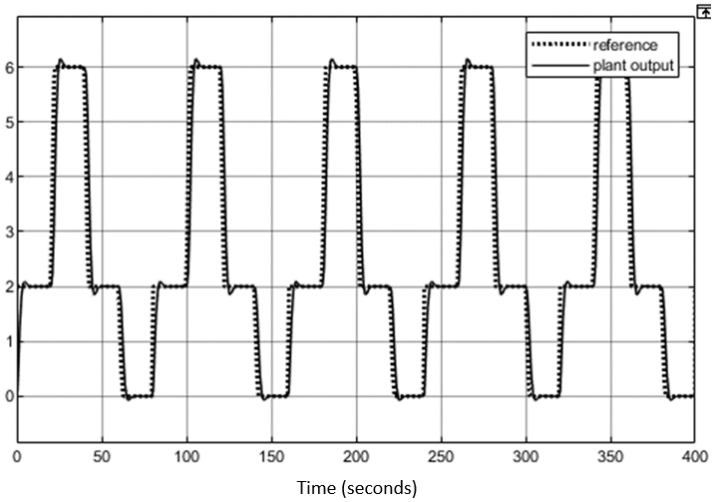

Figure 2.10: Plant output and reference

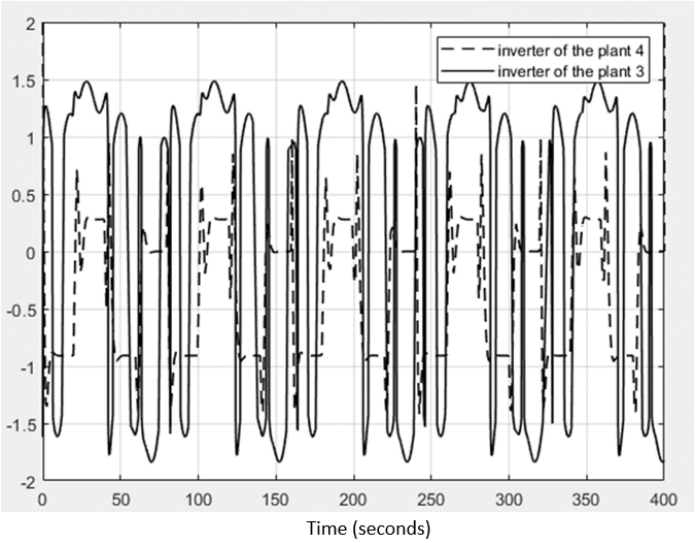

Figure 2.11: Controller outputs for plant3 and plant4

reduction and power acquisition performance is commonly recognized. Particularly, such control system design is very critical for Variable Speed Wind Turbines (VSWT). The other unavoidable issue in wind energy conversion is that the turbine performs according to linear dynamics, but the power conversion is nonlinear from the multiplication of two dynamic variables (the wind power is obtained as a product of torque/input and rotor angular speed). Designing such control systems is challenging in formulation and implementation. [73] gives a collection of up-to-date research on advanced control and optimization paradigms for wind energy systems. Regarding U-control of the wind energy conversion systems, [120] presents the 1st U-model based control system formulation and design for wind energy conversion systems. In contrast, this study removes the demand for solving the Diophantine equation for pole placement assignment and directly uses closed-loop inversion to design the invariant controller. Further, this study is a continuous time control and gives emphasis on the illustration of the general platform for industrial applications using Simulink block diagram connections, rather than Matlab-coded programs.

2.4.2 Plant model

Modelling of wind turbines has played a significant role in the understanding of the behaviour of the wind turbine over its region of operation because it allows for the development of comprehensive control systems that aid in the optimal operation of a wind turbine [64]. Such mathematical models are the foundation to quantify the control performance of energy systems. Further, these models are essential references for the design of the turbines and minimize generation costs leading to cost reduction in wind energy, consequently making it an economically viable alternative source of energy. This Chapter characterizes these wind turbine model into an integrated nonlinear dynamic plant operational model to describe input/output relationships.

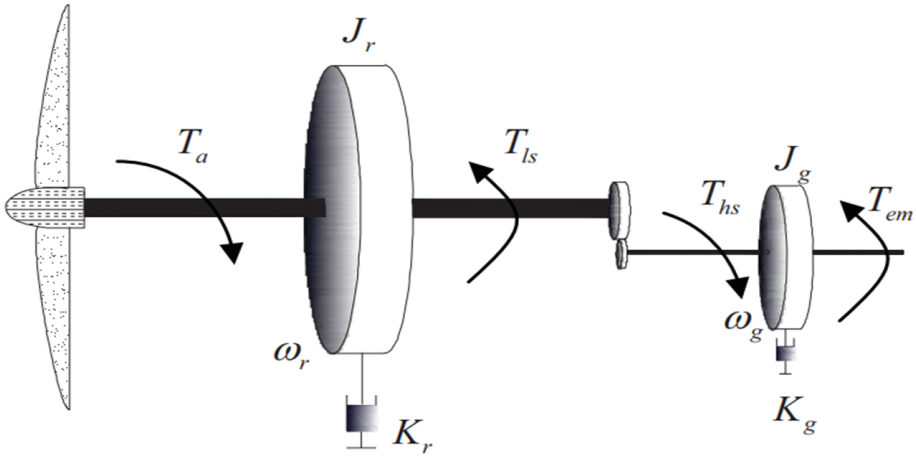

Figure 2.12: Schematic diagram of drive train [120]

The structure of this drive train model is presented in Figure 2.12, and here is the nomencla-

ture list.

- ω_r: rotor angular speed aerodynamic torque
- J_r and J_g: rotor and generator inertias respectively
- K_r and K_g are rotors and generator external damping respectively
- J_t: integrated inertia
- K_t: integrated damping
- T_{em}: converted electromagnetic torque
- T_a: rotor torque, from external wind power in practical systems
- T_g: generator torque, regulates the system operation to generate power

The rotor speed ω_r is driven by the rotor torque T_a and the low-speed torque T_{ls}. The generator speed ω_g is driven by the high-speed torque T_{hs} and the electromagnetic torque T_{em}. It should be noted that using a gearbox can change the generator speed. The dynamics of the rotor and the generator can be described by Newton's law in the form of

$$\left\{ \begin{array}{c} J_r\dot{\omega_r} = T_a - K_r\omega_r - T_{ls} \\ J_g\dot{\omega_g} = T_{hs} - K_g\omega_g - T_{em} \end{array} \right) \tag{2.47}$$

Then define gearbox ratio n_g as

$$n_g = \frac{\omega_g}{\omega_r} = \frac{T_{ls}}{T_{hs}} \tag{2.48}$$

Invoking (2.48), the generator dynamic in (2.47) can be rewritten as

$$n_g{}^2 J_g\dot{\omega_r} = T_{ls} - n_g{}^2 K_g\omega_r - n_g T_{em} \tag{2.49}$$

Thus, the drive train model can be described by combining (2.47) with (2.49) as

$$J_t\dot{\omega_r} = T_a - K_t\omega_r - T_g \tag{2.50}$$

where

$$\left\{ \begin{array}{c} J_t = J_r + n_g^2 J_g \\ K_t = K_r + n_g^2 K_g \\ T_g = n_g T_{em} \end{array} \right) \tag{2.51}$$

P_g, the power output from the generator, is given by $P_g = T_g\omega_r$. In system (2.47), the external wind is the source of the driven force. The wind speed torque is given by

$$T_a = \frac{1}{2}\rho\pi R^3 C_q\big(\lambda,\beta\big)(\hat{v} - \xi)^2 \tag{2.52}$$

where ρ, v, R are the air density, wind speed, and rotor radius, respectively; β is the blade pitch angle, $\lambda = \frac{R\omega_r}{v}$ is the tip-speed ratio; $\hat{v}$ is the estimation of the effective wind speed v, which can be measured via anemometer and ξ denotes the measurement noise; $C_q(\lambda,\beta)$, the efficiency for the wind turbine power conversion, is given by

$$C_q(\lambda,\beta) = \frac{0.22}{\lambda}\left(\frac{116}{m} - 0.4\beta - 5\right)\exp\left(\frac{-12.5}{m}\right) \tag{2.53}$$

with $\frac{1}{m} = \frac{1}{\lambda+0.08\beta} - \frac{0.035}{\beta^3+1}$. Accordingly, from the above physical principle models, the energy conversion input-output model for control system design can be expressed as

$$\dot{P_g}T_g - \dot{T_g}P_g = \frac{1}{J_t}T_a{T_g}^2 - \frac{K_t}{J_t}P_gT_g - \frac{1}{J_t}{T_g}^3 \tag{2.54}$$

where the control input is the generator torque T_g and the plant output is the power output P_g. Collect the maximum quantity of energy embedded in the low-speed wind region from system (2.47), it requires

$$P_d = n_p P_{amax} \tag{2.55}$$

with $P_{amax} = \frac{1}{2}\rho\pi R^2 C_{pmax} v^3$, where C_{pmax} for the maximum power coefficient, n_p for the ratio between the desired generator power P_d and the maximized available power P_{amax}.

2.4.3 U-control system design

The U-control system was the same as designed in Chapter 2.3.1. The U-realisation of the input-output plant model was derived as

$$\dot{P_g} = \lambda_0 + \lambda_1\dot{T_g} \tag{2.56}$$

with $\lambda_0 = \frac{\frac{1}{J_t}T_a{T_g}^2 - \frac{K_t}{J_t}P_gT_g - \frac{1}{J_t}{T_g}^3}{T_g}$ and $\lambda_1 = \frac{P_g}{T_g}$

2.4.4 Simulation results

The selected generator, equipped with three blades, a horizontal axis, and wind variable speed wind turbine, generate a 1.5 MW electrical output, made by WINDEY Co. This category of generators has been used worldwide [73]. The major parameters are listed in Table 2.1.

Accordingly, for U-model expression in (2.56), its time-varying parameters are assigned with $\lambda_1 = \frac{P_g}{T_g}$ and $\lambda_0 = \frac{1}{5.7998\times10^6}T_aT_g - 7.609\times10^{-4}P_g - \frac{1}{5.7998\times10^6}P_g^2$. The rest of the simulation conditions/parameters include the desired power P_d from (2.56), wind torque T_a from (2.52), the specified wind speed v with a mean of 9m/s and turbulence intensity of 10%, sensor noise represented by a uniformly distributed random sequence of [-0.3, 0.3], n_p=0.8 for the ratio between the desired generator power P_d and the maximum available power P_{amax}, C_{pmax} = 0.4382 for the maximum power ratio and ρ = 1.12 for the air density. Figure 2.13 shows the constructed U-control system in Simulink block diagrams. Figures below show the simulation results which are the

Rated power	1.5MW
Rotor radius R	38.5m
Rotor inertia Jr	4456761 kg.m2
Generator inertia Jg	123 kg.m2
Rotor friction coefficient Kr	45.52N.m/rad/s
Generator friction coefficient Kg	0.4N.m/rad/s
Gearbox ratio n_g	104.494

Table 2.1: Parameters for WECS

same as those obtained from [120]. However, the differences are 1) this study is a continuous time control system against the discrete time control systems [120]; 2) this study uses concise closed loop inversion to determine the invariant controller against solving the complicated Diophantine equation; 3) this study uses Simulink block diagram to build up the control system against using Matlab functions to develop coded programs, which block diagram based simulation is much more engineering meaningful, transparent, cost-effective than coded programming. Inspection of the generated plots: Figure 2.14 shows the simulated wind speed profile. Figure 2.15 shows the generated output power properly follows the specified power trajectory and is similar to the wind speed profile even though with wind measurement noise. Figure 2.16 shows the variation of the rotor torque following the wind force. Figure 2.17 shows the tracking error amplitude converged to zero mean and small variance, this indicates that the U-control system has converted into the maximum available power from the wind power.

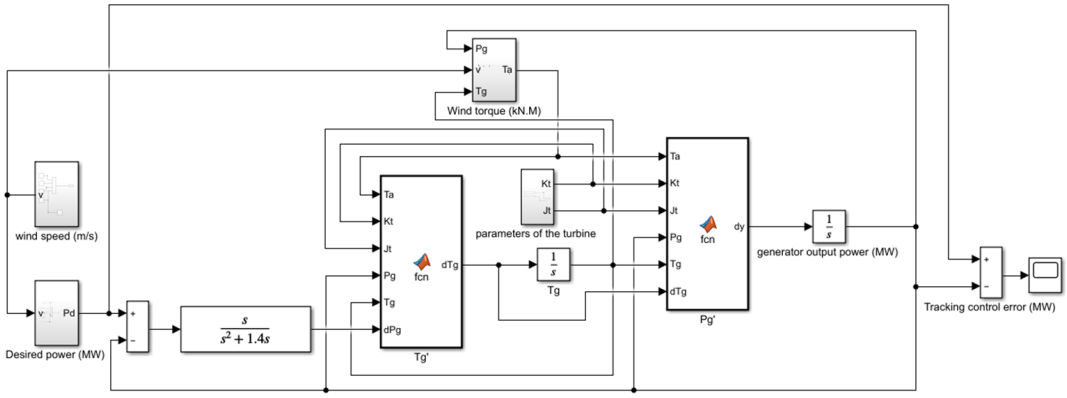

Figure 2.13: U-control of the wind energy conversion system

2.5 Summary

In U-control system design/operation, the condition of $G_p^{-1}G_p = 1$ is the backbone. Therefore, this requires an accurate model of G_p and an effective routine/algorithm for the UM-dynamic inversion G_p^{-1}. This study provides a generalized methodology, with the assumption of an accurate

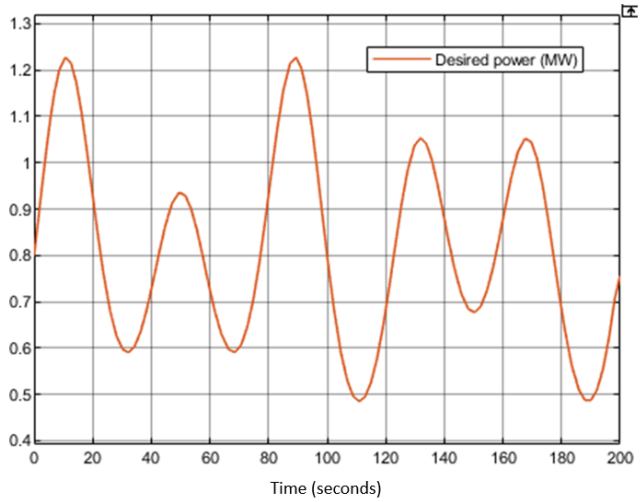

Figure 2.14: Effective wind speed $v(t)$

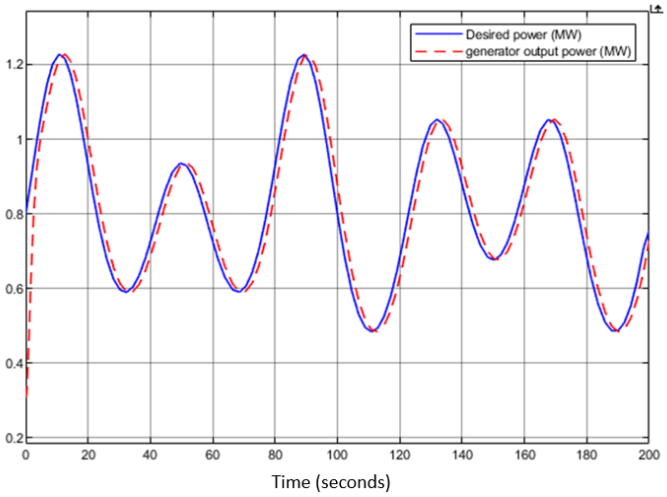

Figure 2.15: Desired power $P_d(t)$ and generator output power $P_g(t)$

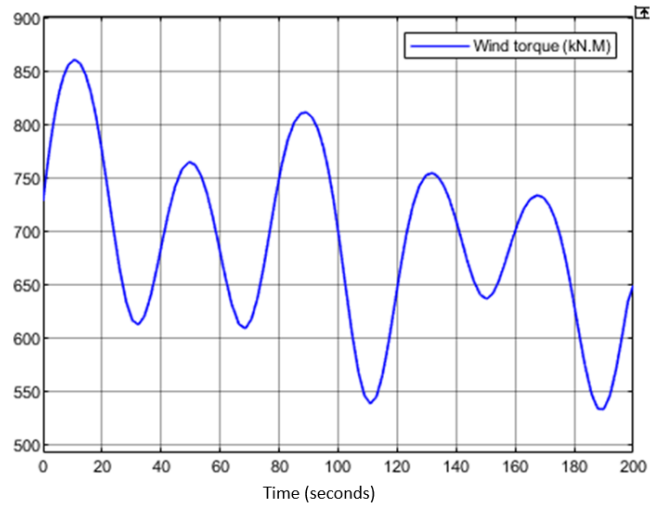

Figure 2.16: Wind torque $T_a(t)$

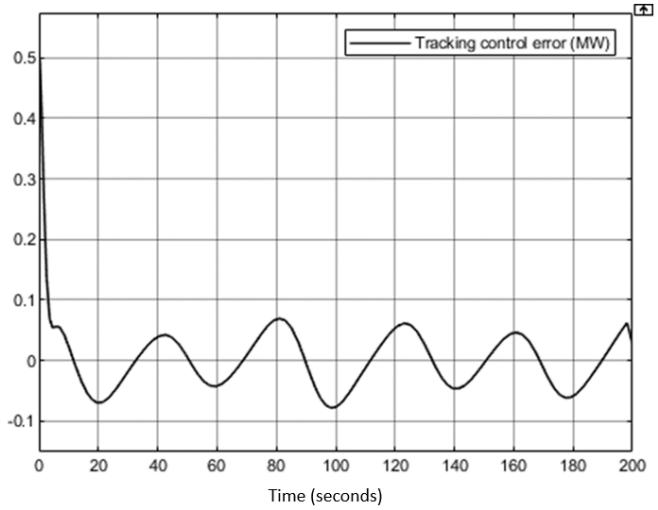

Figure 2.17: Tracking error

model of G_p, a set of algorithms for the UM-dynamic inversion G_p^{-1}. Simulated bench examples have demonstrated the analytical results and provided an effective procedure in testing designed control systems with computational experiments.

The remaining challenging issues with UM-dynamic inversion are robust UM-dynamic inversion dealing with uncertainties in model G_p and data-driven dynamic inversion (DD-dynamic inversion) for an unknown model of G_p. These solutions, no doubt will significantly make U-control realistically feasible and supplementary to the other existing approaches for a wide range of applications.

CHAPTER 3

U-MODEL BASED TWO-DEGREE-OF-FREEDOM INTERNAL MODEL CONTROL

Model validity is a fundamental basis for model-based control systems design. A better model makes control systems design and tuning easier/more efficient. However, for most engineering systems, there can be difficulties in obtaining accurate plant/process models, primarily due to equipment diversity and environment complexity; such as internal uncertainties and external disturbances. Even though a mathematical model can be established from physical principles (such as energy conservation law) and/or data-driven (identification), it is usually taken as a nominal reference (a nominal model is an approximate description of an accurate model). Internal Model Control (IMC) [34] has been widely accepted as an efficient robust control approach. IMC selects the model inverse as the controller and integrates a robust filter to control an explicit plant/process model. The IMC structure is characterised by 1) capable robustness to overcome model uncertainties and system disturbances, 2) effective procedures for designing and tuning, 3) successful application across different industries [58, 76, 87]. However, the control performance of classical IMC is not desirable, because the adjustable parameters only exist in the filter. At the same time, higher robustness demand could degrade tracking performance [79], which must compromise with some of the other performances. Although a Two-Degree-of-Freedom IMC (TDF-IMC) structure can solve the aforementioned problems with the classical IMC structure, its control performance still cannot be separately designed [84, 87, 127].

When a linear model is completely reversible, the design of linear IMC is straightforward to take the controller as the inverse of the model and select a suitable filter. Even when the model is not completely reversible, the model can be decomposed into reversible parts and irreversible parts, in which the inverse of the reversible part is taken as the controller. Appropriate filter selection can then also ensure that the control system has the smallest output variance for both

stabilization and tracking control. However, for controlling nonlinear plants/processes, these approaches are not applicable, and effective algorithms for nonlinear dynamic inversion are very limited [74]. To deal with nonlinear control plants/processes, the approaches used by most of the IMC structures can be divided into 1) linearizing the controlled plants/processes and using the linear method to invert [26]; 2) using PID [21], neural network [8, 91] and fuzzy control-based [1, 116] dynamic inversion; 3) using some numerical tools, such as the Newton–Raphson method [26]. However, the linearized and the other approximating modelling methods could lose an accurate representation of the input-output relationship and degrade the performance of the designed systems. Therefore, deriving the nonlinear model inversion and enabling the two performance indicators (i.e. tracking and robustness) of the IMC structure to be independently designed are the main challenges and focuses of this chapter. Accordingly, this study proposes a framework of U-model based Two-Degree-of-Freedom Internal Model Control (U-TDF IMC) of nonlinear dynamic systems

According to Chapter 2, U-model is a derived control-oriented model set to map almost all classical models into their U-model realisation and converts classical models into controller output u based on time-varying parameters [115] expressions. This chapter is aimed at using U-control, an enhanced tool supplemented with classical approaches, to integrate the strengths exhibited in U-control and IMC to provide an enhanced version of IMC with strength in system configuration and nonlinear dynamic inversion. In order to further improve TDF-IMC, this study expands the previous IMC work [47, 80] by effectively introducing U-model based dynamic inversion within a revised system structure configuration. By doing so, the new framework presents a new U-model based two-degree-of-freedom IMC (UTDF-IMC) structure to achieve a completely independent design in rejecting disturbance and tracking operational set-point. Compared with the classical IMC and TDF-IMC, this proposed structure has better control performance and more convenient tuning methods without introducing additional design work and maintaining the same hardware configuration. Accordingly, the major impacts of this research are outlined below:

1. Propose a general U-model based Two-Degree-of-Freedom IMC (UTDF-IMC) structure for controlling a class of open-loop stable polynomial/state-space modelled linear and nonlinear dynamic plants. The new control system structure accommodates both linear and nonlinear plants consistently and separates the tracking control filter design from the robust control filter design.

2. Tailor the UM-dynamic inversion platform [31] in conjunction with IMC, which removes the necessity of either linearizing the nonlinear model or converting it to a quasi-linear parameter-varying (quasi-LPV) model in advance. This UM-dynamic inversion platform directly provides algorithms dealing with all types of inversions in IMC structured systems.

3. Analyse the designed UTDF-IMC control system properties to provide a valid reference for future study expansions and applications.

4. Verify the control system performance through benchmark tests of simulated case studies and illustrate application procedure from an industrial case demonstration.

For the remainder of this chapter, Chapter 3.1 presents the basis of using IMC and U-control for the next step of development of the new UTDF-IMC system structure. Chapter 3.2 elaborates on the principle of TDF-IMC structure and establishes the U-model based TDF-IMC (UTDF-IMC) framework; consequently, it analyses the control system properties. Chapter 3.3 showcases two computational investigations to benchmark test/demonstrate the proposed UTDF-IMC system performance. Then an industrial backgrounded permanent magnet synchronous motors (PMSM) system is added to demonstrate the application procedure and the comparative studies in Chapter 3.4. Chapter 3.5 concludes this study with key findings and observations.

3.1 Internal model control (IMC)

A classical IMC control scheme [34] is shown in Figure 3.1, in which the plants/process P is approximated by model P_0 (specifically named as the internal model) and the controller Q. Figure 3.2 shows the equivalently rearranged IMC structure, in which the controller is expressed in the inner loop

$$C = \frac{Q}{1 - QP_0} \tag{3.1}$$

For a given set-point reference r, the control system is designed to keep the output y following a pre-specified output response y_m (Figure 3.1) with the desired transient and steady-state performance. With reference to Figure 3.1, it has

1. Plant output:
$$y = \frac{QP}{1 + Q(P - P_0)} r + \frac{1 - QP_0}{1 + Q(P - P_0)} d \tag{3.2}$$

2. Error output:
$$e = \frac{1}{1 + Q(P - P_0)} (r - d) \tag{3.3}$$

3. Controller output:
$$u = \frac{Q}{1 + Q(P - P_0)} (r - d) \tag{3.4}$$

Remark 1: (3.2) can also be rewritten as:

$$y = \alpha r + \beta d \tag{3.5}$$

where $\alpha = \frac{QP}{1+Q(P-P_0)}$ specifies tracking performance and $\beta = \frac{1-QP_0}{1+Q(P-P_0)}$ denotes the contribution to robustness. These two weights meet the condition of $\alpha + \beta = 1$

The main features of IMC [34] include:

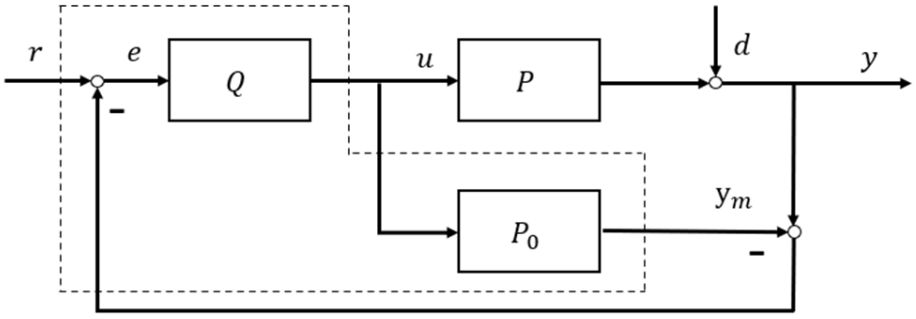

Figure 3.1: Internal model control structure

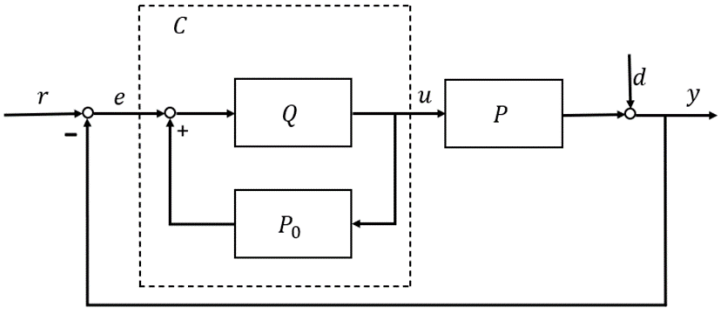

Figure 3.2: Equivalent IMC structure

1. Dual stability: For $P = P_0$ and $d = 0$, and $y = y_m$, the feedback error signal e is obviously zero. IMC system becomes an open loop structure and both controller Q and plant P are stable.

2. Perfect control: This requests plant $P = P_0$ minimum-phase and invertible and controller as the model inverse $Q = {P_0}^{-1}$. Accordingly (3.2) becomes

$$y = \frac{{P_0}^{-1}P}{1+{P_0}^{-1}P-{P_0}^{-1}P_0}r + \frac{1-{P_0}^{-1}P_0}{1+{P_0}^{-1}(P-P_0)}d = r \tag{3.6}$$

   where $\alpha = 1$ and $\beta = 0$

3. Augmented robust IMC is shown in Figure 3.3. It decomposes model and dynamic inversion by factorizing P_0 into P_{0+} and P_{0-}, namely: $P_0 = P_{0+}P_{0-}$, where P_{0+} is the part containing pure delay and uncertain zero, and P_{0-} is the minimum-phase part. There are certain factorization techniques, like simple factorization, and all-pass factorization [79]. Hence, the controller is kept as the inverse of the plant/process model with an invertible portion, that is,

$$Q_1 = \frac{1}{P_{0-}} \tag{3.7}$$

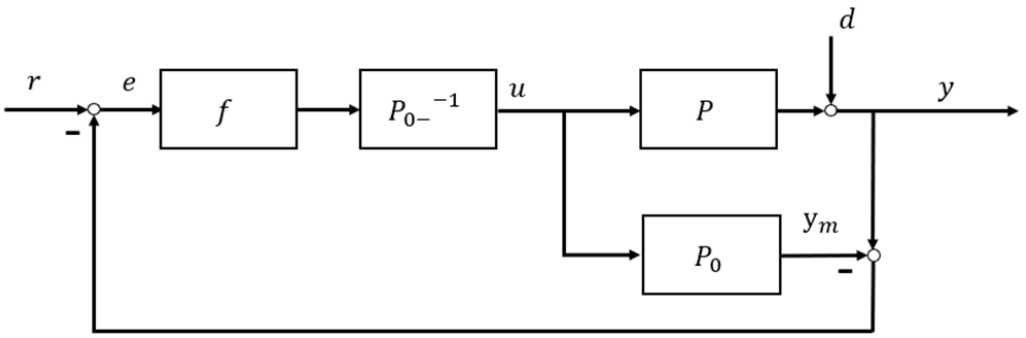

Figure 3.3: Robust IMC structure

4. Filter: When designing the IMC controller, it should add a low-pass filter for the inverse of the factorized minimum phase model to ensure the controller is proper and robust against model mismatching and disturbance. Define the IMC controller and the filter as

$$Q = fQ_1 \tag{3.8}$$

$$f = \frac{1}{(1+\lambda s)^{\rho}} \tag{3.9}$$

where β is the order of the filter, normally assigned with a large value to ensure Q_1 is proper or semi-proper; λ is the time constant, the sole design parameter of the controller and is inversely proportional to the closed loop response speed. Therefore, λ is a trade-off between the performances.

Remark 2: Substituting (3.7) and (3.8) into (3.2) obtains the plant output

$$\begin{aligned} y &= \frac{\frac{f}{P_{0-}}P}{1+\frac{f}{P_{0-}}P-\frac{f}{P_{0-}}P_0}r+\frac{1-\frac{f}{P_{0-}}P_0}{1+\frac{f}{P_{0-}}P-\frac{f}{P_{0-}}P_0}d \\ &= \frac{\frac{f}{P_{0-}}P}{(1-fP_{0+})+\frac{f}{P_{0-}}P}r+\frac{1-fP_{0+}}{(1-fP_{0+})+\frac{f}{P_{0-}}P}d \end{aligned} \tag{3.10}$$

To track the reference signal with a faster speed and effectively reject the modelling errors and system disturbance, it requires output (3.10) satisfying $fP_{0+} = 1$ necessarily, which is achieved by selecting λ in the filter.

3.2 U-model based Two-Degree-of-Freedom IMC (UTDF-IMC)

3.2.1 Classical Two-Degree-of-Freedom IMC (TDF-IMC) structure

Figure 3.4 shows a TDF-IMC structure to be incorporated with U-control, which comprises feedback controller F added in the external loop within the classical IMC structure. Clearly, if the feedback filter F is a unit constant, this structure is the same as that in Figure 3.1. From

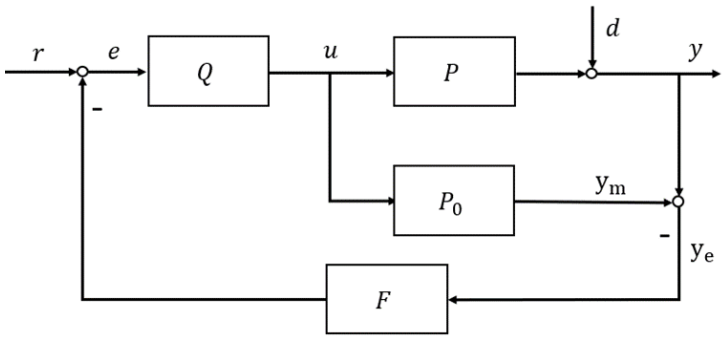

Figure 3.4: IMC structure with the feedback filter

Figure 3.4, the system output $y = y_m + y_e$. Therefore,

$$\begin{aligned} y &= (r - y_e F)QP_0 + y_e \\ &= rQP_0 + y_e(1 - FQP_0) \end{aligned} \tag{3.11}$$

In the TDF-IMC system, if the controlled plant is a minimum-phase system, then the controller $Q(s) = \frac{f(s)}{P_0(s)}$. The output of (3.11) can be re-organized as

$$y = rf + y_e(1 - Ff) \tag{3.12}$$

The explicit input/output relationships from Figure 3.4 can be written as follows:

$$u = \frac{Q}{1 + (P - P_0)FQ}(r - dF) \tag{3.13}$$

$$y = \frac{QP}{1 + (P - P_0)FQ}r + \frac{1 - QFP_0}{1 + (P - P_0)FQ}d \tag{3.14}$$

If the controlled system does not contain uncertain parameters or control disturbance, then $y_e = 0$, otherwise, $|y_e| > 0$. From (3.2), rf determines the system tracking performance, while $y_e(1-F)f$ determines the system robustness. To achieve desired control performance, a condition must hold true below:

$$\lim_{t \to \infty} f(t) = 1, \quad \lim_{t \to \infty} L^{-1}(F(s)f(s)) = 1 \tag{3.15}$$

Where $L^{-1}(*)$ is the inverse Laplace transform operator, $F(s)$ and $f(s)$ are the Laplace functions of filters F and f respectively. Thus, output y equals the reference r eventually, and the system disturbance and modelling errors will be eliminated. The performance of the IMC control system will depend on these two filters F and f. The setting time and rise time of these two filters should be as short as possible. However, response speeds that are too fast will cause the amplitude of the controller output signal to increase sharply. From Figure 3.4, the controller $Q(s)$ output u is:

$$u = (r - y_e F) \tag{3.16}$$

From (3.13), when controller Q is determined, the faster the response of the filter F, the larger value of the initial controller output u. In general, it can be observed from (3.12) that the tracking

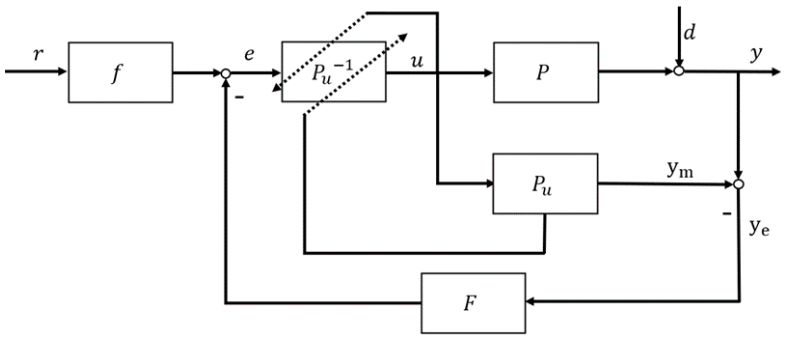

Figure 3.5: U-model based Two-Degree-of-Freedom IMC structure

ability and robustness of the IMC system cannot be separately designed, as well as its design flexibility is relatively limited. Therefore, this is one of the project's research aims, to separate IMC's design of tracking ability control and robustness and improve its design effectiveness without affecting its desired control performance.

3.2.2 U-model based Two-Degree-of-Freedom IMC (UTDF-IMC) structure

On the basis of the IMC, the problem stated in the introduction and TDF-IMC analysis in Chapter 3.2.1, this chapter changes the classical TDF-IMC structure in Figure 3.4 to a UTDF-IMC structure as shown in Figure 3.5. In Figure 3.5, the original controller Q in classical TDF-IMC shown in Figure 3.4 has been split into two parts: the feedforward filter f and the inversion ${P_u}^{-1}$ of the U-realization controlled plant model P_u, where the original IMC's controller $Q = f{P_0}^{-1}$. Different from the classical IMC structure, feedforward filter f appears outside the system feedback loop. Generally, the plant model inversion ${P_0}^{-1}$ cannot exist alone because of its irrationality and unrealizable property. For polynomial-based modelling of the controlled plant expressed by the Laplace transfer function, its inversion will make the order of the numerator higher than the order of the denominator, which cannot be achieved in the actual control system. Therefore, this chapter introduces the UM-dynamic inversion algorithm to design the plant's inversion part ${P_u}^{-1}$ in the UTDF-IMC structure.

3.2.3 UTDF-IMC Design procedures

Figure 3.5 presents the U-model based Two-Degree-of-Freedom IMC system framework, where f and F are the designed feedforward and feedback filters respectively. P is the controlled plant or process, which is allowed to be linear or nonlinear. P_u is U-model based approximation to the controlled plant P. ${P_u}^{-1}$ is the inverter designed by the U-model based root solving algorithm. From (2.17), the parameters absorbed by λ_i can be obtained from the output signal y_m of the plant model $P_u(s)$ and controller output u. In general, similar to the classical IMC design, UTDF-IMC system design has the following two steps:

1. Assume the controlled plant or process P is stable and bounded, and its inverse P^{-1} exists. Use the U-model to describe P or convert the plant model P_0 into its U-realization P_u. The specific U modelling process can refer to Chapter 2. Different from the classical IMC or classical TDF-IMC, U-realization of the original model P_0 can comfortably cover nonlinear dynamics, therefore, remove linearization restrictions.

2. Design filters f and F according to system control performance requirements, then re-optimize the parameters of the filters according to the controller output limit. The feedforward filter determines the system's set-point tracking ability (response time) while the feedback filter determines the system's robustness. Because the control system performance is completely designed according to the two filters independently, designers can select the appropriate filters according to performance requirements, hardware limitations, controller output limitations, etc.

3.2.4 Property analysis

1. Dual stability: Assume the plant model is perfectly matched ($P_u = P$) and system disturbance is absent $d = 0$, then from Tables 3.1, the closed-loop stability is characterized by the stability of the plant $P(P^-1)$ and the feedforward filter f. In this case, the system output signal will be: $y = fr$.

2. Perfect control: Assume that the dynamic inverter P_u^{-1} is satisfied with $P_u = P$ and P is stable, then the closed-loop control system is stable and perfectly controlled. In this case, the system output is $y = fr + (1-F)d$. The faster the response speed of feedback filter F, the better the system robustness.

3. Zero offset: Assume that the steady-state gain of the controller equals to the steady-state gain of the inverse model, and this closed-loop system is input-output stable with this controller, then offset-free control is obtained asymptotically to step or ramp type inputs and disturbances.

4. Separability of designing the tracking filter and the robust filter: This is shown in the tables, in which UTDF-IMC has no product of the two filters Ff.

In comparison with IMC and TDF-IMC, Tables 3.1 and 3.2 list the three IMC types of control system configurations against disturbance and model mismatching respectively. For UTDF-IMC the typical properties are analyzed below. From Table 3.1, the factor associated with d is called the disturbance rejection design. It is clear that this rejection part only depends on the feedforward filter f in IMC, depends on two filters F and f in TDF-IMC but only depends on the feedback filter F in UTDF-IMC structure. In case of model mismatch, it can also use the output error signal y_e to analyse the system performance in Table 2: From Table 3.2, regarding UTDF-IMC,

	Controller output u	System output y
IMC	$u = \frac{1}{P_0+(P-P_0)f}(rf-df)$	$y = \frac{fP}{P_0+(P-P_0)f}r + \frac{P_0(1-f)}{P_0+f(P-P_0)}d$
TDF-IMC	$u = \frac{1}{P_0+(P-P_0)Ff}(rf-dFf)$	$y = \frac{fP}{P_0+(P-P_0)Ff}r + \frac{P_0(1-fF)}{P_0+(P-P_0)Ff}d$
UTDF-IMC	$u = \frac{1}{P_u+(P-P_u)F}(rf-dF)$	$y = \frac{fP}{P_u+(P-P_u)F}r + \frac{P_u(1-F)}{P_u+(P-P_u)F}d$

Table 3.1: Input/output comparison of IMC, TDF-IMC and UTDF-IMC against disturbance

	System output y
IMC	$y = rf-(1-f)y_e$
TDF-IMC	$y = rf-(1-Ff)y_e$
UTDF-IMC	$y = rf+(1-F)y_e$

Table 3.2: Output comparison of IMC, TDF-IMC and UTDF-IMC against model mismatching

the function associated with y_e is robustness designed, where y_e absorbs all whole modelling error and system disturbance; the function associated with signal r is for tracking designed. Obviously, all the tracking design only depends on the feedforward filter f and the robustness designed is the same as previously discussed. In summary, compared with the classical IMC and TDF-IMC structure, the main differences in UTDF-IMC structure are as follows:

1. Classical TDF-IMC structure can make tracking ability and robustness be designed separately but not wholly independent due to the product term of Ff in robustness specification. The UTDF-IMC overcomes this shortcoming without resorting to a more complex structure. Therefore, when the robustness performance of the system is determined, the UTDF-IMC control system will have a faster response speed than the classical TDF-IMC control system.

2. U-model is used to facilitate control system design, which can easily form an inversion of the plants to cancel both dynamic and nonlinearities. Accordingly, it converts the nonlinear control system into a linear model based control with a nonlinear dynamic inverter.

3. UM-dynamic inversion algorithm is used to design the inversion part in UTDF-IMC structure, which provides a faster convergence speed and allows the inversion part exists alone properly without the feedforward filter.

4. This structure where the feedforward filter f from outside the control loop allows the tracking ability and robustness performance to be completely independently designed.

5. The improved control performance is not complicating the system structure and/or increase the additional computation burden throughout the design process.

3.3 Simulation demonstrations

This simulation demonstration selects two plants to test the proposed U-model based TDF-IMC structure. Both plants will be controlled by IMC, TDF-IMC and UTDF-IMC structures.

3.3.1 Linear controlled plant

Consider a linear controlled plant as plant 1

$$P_0(s) = \frac{{\omega_n}^2}{s^2 + 2\zeta\omega_n s + {\omega_n}^2} = \frac{1}{s^2 + 3s + 1} \tag{3.17}$$

(3.17) is characterised with the damping ratio $\zeta = 1.5$ and the undamped natural frequency $\omega_n = 1$. For designing the UTDF-IMC system:

1. Convert plant model (3.17) into its corresponding U-model

$$\left\{ \begin{array}{c} P_u(s): \ \ddot{y} = u - 3\dot{y} - y = \lambda_0 + \lambda_1 u \\ \lambda_0 = -3\ddot{y}\frac{1}{s} - \dot{y}\frac{1}{s^2} \\ \lambda_{11} = 1 \end{array} \right) \tag{3.18}$$

2. Design the inverter of the plant model $P_u(s)$:

$$u = \ddot{y} + 3\ddot{y}\frac{1}{s} + \dot{y}\frac{1}{s^2} \tag{3.19}$$

3. Design the feedforward filter $f(s)$ and the feedback filter $F(s)$. In this chapter, based on the UTDF-IMC system design procedure in Chapter 3.2, to make the system achieve a fast response speed and no overshoot, $f(s) = \frac{1}{(0.2s+1)^2}$ and $F(s) = \frac{1}{(0.1s+1)^2}$. To compare control performance fairly, the TDF-IMC system uses the same filters as UTDF-IMC. To ensure the same robustness, the classical IMC system uses $f'(s) = \frac{1}{(0.1s+1)^2}$.

To test the performance of the designed control system, assume the plant a 2nd order dynamic with $\zeta = 1$ and $\omega_n = 0.5$, and an external disturbance added at the system output, that is,

$$P(s) = \frac{1}{4s^2 + s + 1} + D(s) \tag{3.20}$$

The system disturbance is a band-limit white noise with changing rate of 1hz, and a system signal-noise ratio (SNR) of 26.9db. The noise sequence is shown in Figure 3.6. From Figure 3.7 and Figure 3.8, UTDF-IMC and IMC have better robustness performance in the rejection of system disturbance and modelling errors. IMC system has the fastest tracking speed because of its fast respond-speed filter, however, due to modelling error, stronger tracking ability brings more overshoot. The simulation results also demonstrate the analysis in Chapter 3.2.4. From Figure 3.9, the UTDF-IMC structure does not increase the maximum peak output of the controller compared with the TDF-IMC structure. However, fast-tracking speed brings a large controller output peak in the IMC system, which may cause the controller to overload applications. Considering the control performance and controller load, in the case of selecting the same filters (control parameters), the UTDF-IMC system also shows better control performance.

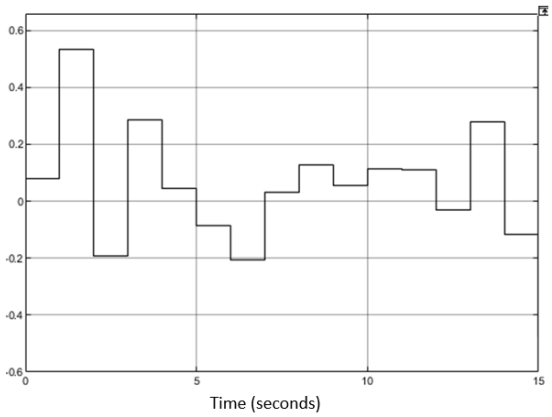

Figure 3.6: System disturbance noise

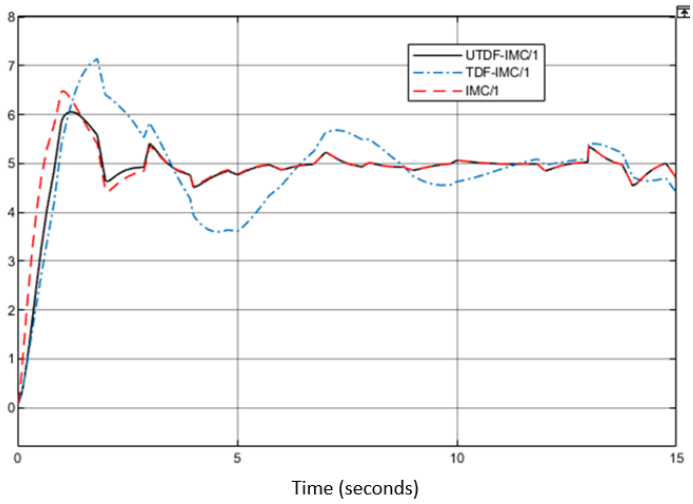

Figure 3.7: System outputs for plant 1

3.3.2 Nonlinear controlled plant

Consider a nonlinear controlled plant as plant 2

$$P_0: \quad \dot{y} = a\dot{u}^3 + b\dot{u}^2 - c\dot{u} - ky + e^u \tag{3.21}$$

where the coefficients $a = b = c = 1, k = 0.5$. Then design the UTDF-IMC system:

1. Convert the plant (3.21) into its corresponding U-model:

$$\left\{ \begin{array}{c} P_u(s): \dot{y} = \lambda_0\dot{u} - \lambda_1\dot{u} + \lambda_2\dot{u}^2 + \lambda_3\dot{u}^3 \\ \lambda_0 = -0.5\dot{y}\frac{1}{s} + e^u \\ \lambda_1 = \lambda_2 = \lambda_3 = 1 \end{array} \right) \tag{3.22}$$

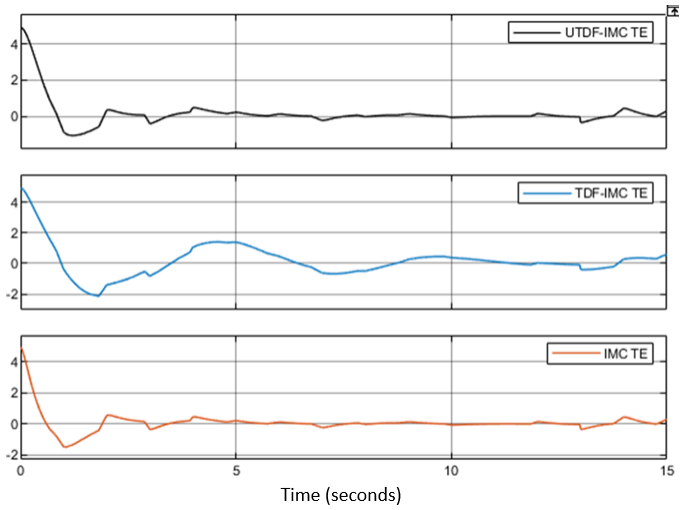

Figure 3.8: Tracking errors for plant 1

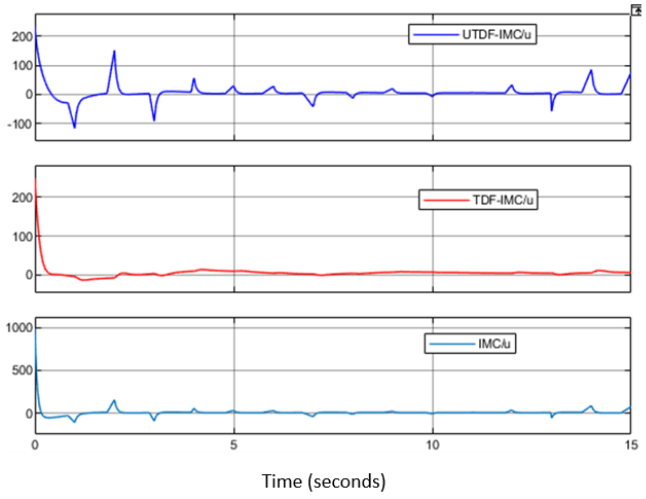

Figure 3.9: Controller outputs for plant 1

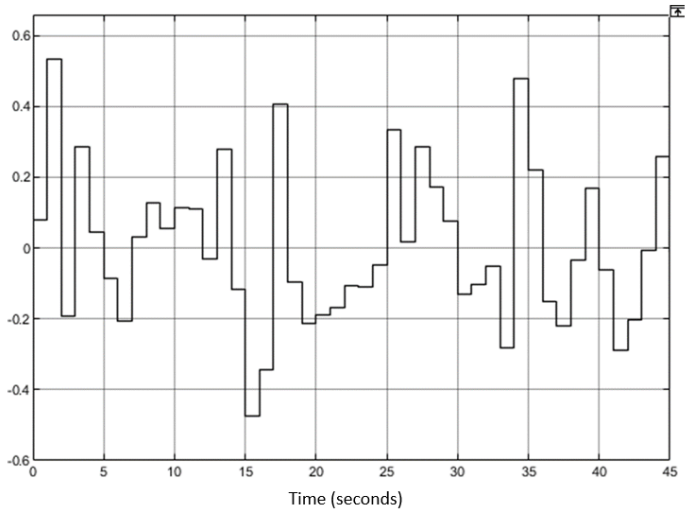

Figure 3.10: System disturbance d for plant 2

2. Design the inverter of the plant model $P_u s$

$$u = root\left(\lambda_0 \dot{u} - \lambda_1 \dot{u} + \lambda_2 \dot{u}^2 + \lambda_3 \dot{u}^3 - \dot{y} = 0\right) \tag{3.23}$$

It should be noted that because equation (3.23) is a cubic equation of one variable about u. In order to ensure that the controller output is rational, the real root of equation (3.23) is selected as the output of the controller.

3. Design the feedforward filter $f(s)$ and the feedback filter $F(s)$ Same as previous work, to make the system achieve a fast response speed and no overshoot, this chapter chooses $f(s) = \frac{1}{(0.1s+1)^2}$ and $F(s) = \frac{1}{(0.2s+1)^2}$ for the plant 2. To compare control performance fairly, the TDF-IMC system uses the same filters as UTDF-IMC. To ensure the same tracking speed, the classical IMC system uses $f'(s) = \frac{1}{(0.2s+1)^2}$.

To demonstrate the performance of the designed control system, assume the real plant with the same structure as the IM, but $c = 1.4$ and $k = 0.8$ for modelling errors, and an external noise added to the system output, that is

$$P(s): \quad \dot{y} = \dot{u}^3 + 1.4\dot{u}^2 - \dot{u} - 0.8y + e^u + d \tag{3.24}$$

The system noise is a band-limit white noise with changing rate of 1Hz and SNR of 20.9db. The noise sequence is shown in Figure fig310. From Figure 3.11 and Figure 3.12, UTDF-IMC both has a better robustness performance in rejection of system disturbance and modelling error and the fastest tracking speed. When the reference signal suddenly jumps sharply, the response of the TDF-IMC system also shakes sharply although it has the same filters as UTDF-IMC. These simulation results demonstrate the analysis in Chapter 3.2.4. From Figure 3.13, the UTDF-IMC structure does not increase the burden on the controller, although it has a better

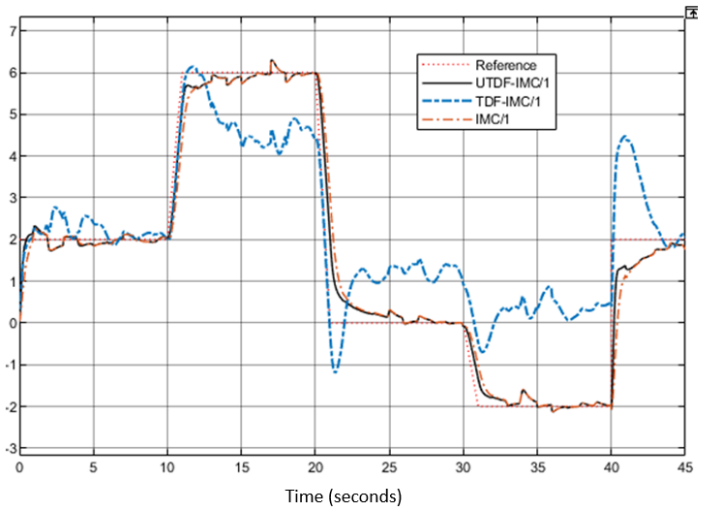

Figure 3.11: System outputs for plant2

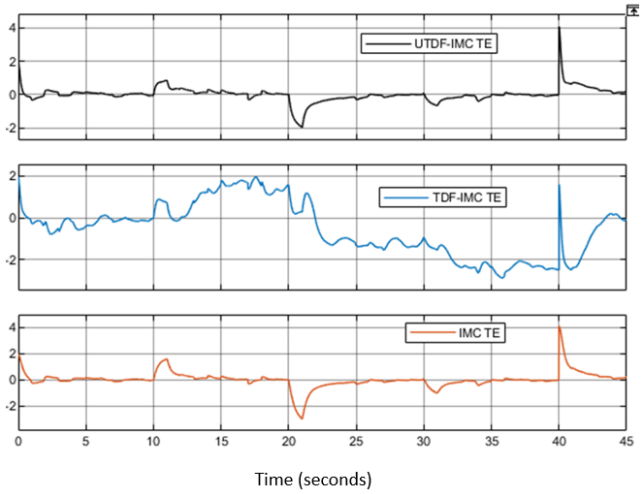

Figure 3.12: Tracking errors for plant2

control performance. The output of the controller shows that the UTDF-IMC is not overloaded. Once again, considering the control performance and controller load, in the case of selecting the same filters (control parameters), the UTDF-IMC system shows a better control performance.

3.4 Test of U-control of a wind energy conversion system

In the past few decades, Permanent Magnet Synchronous Motors (PMSM) have been widely used in industry because of their high-power density, high efficiency, and large torque inertia ratio. PMSM is essentially a non-linear Multiple-Input-Multiple-Output (MIMO) system, so parameter uncertainty and interference acting on torque will make it difficult for PMSM control systems to

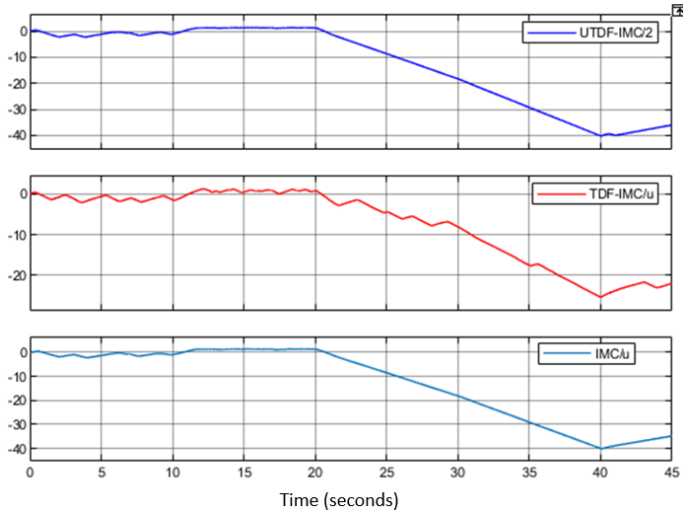

Figure 3.13: Controller outputs for Plant2

obtain higher control performance [99]. Most advanced control strategies [30, 92, 113] for PMSM servo system angular position control ignore the nonlinear term in the speed equation, assuming that A=B and load torque disturbance does not change. Therefore, it is still a challenge to provide an efficient set-point value tracking control strategy for a general PMSM system affected by time-varying system disturbance and uncertain parameters. Therefore, this Chapter applies the proposed UTDF-IMC structure combined with the U-modelling of the PMSM system to achieve high-precision set-point robust tracking control of the PMSM operation.

3.4.1 Modelling of PMSM system

It should be noted that the permanent magnets used in the PMSM are a type of modern rare-earth varieties with high resistivity, so the induced current in the rotor can be negligible. The model of the PMSM is based on s number of equations in the d-q reference frame [102], where the “d” and “q” axes are the single-phase representations of the flux contributed by the three separate sinusoidal phase quantities at the same angular velocity. The “d” axis, also known as the direct axis, is the axis by which flux is produced by the field winding. The “q” axis, or the quadrature axis is the axis on which torque is produced. Converting the mathematical model of the motor to this coordinate system can realize the decoupling of the “d” axis and “q” axis, thereby obtaining good control characteristics [65]. The electric torque of the PMSM is

$$T_e = \frac{3}{2} p \left[\Phi_v i_q + \left(L_d - L_q \right) i_d i_q \right] \tag{3.25}$$

And its motor dynamics can be modeled as

$$T_e = T_L + B\omega_r + J\Delta\omega_r \tag{3.26}$$

The relationship between voltages and currents in a motor are:

$$\begin{bmatrix} V_d \\ V_q \end{bmatrix} = \begin{bmatrix} R_s + L_d\Delta & -p\omega_r L_q \\ p\omega_r L_d & R_s + L_q\Delta \end{bmatrix} \begin{bmatrix} i_d \\ i_q \end{bmatrix} + \begin{bmatrix} 0 \\ p\omega_r \Phi_v \end{bmatrix} \tag{3.27}$$

The rotor flux rotates at rotor speed ω_r and is positioned by the rotor angular position:

$$\theta_r = \int \omega_r dt \tag{3.28}$$

Therefore, the PMSM in the rotating d-q reference frame can be modelled in the following state-space equation [102]

$$\left\{ \begin{array}{l} \frac{d\theta_r}{dt} = \omega_r \\ \frac{d\omega_r}{dt} = \frac{3p\Phi_v}{2J} i_q + \frac{3p}{2J}\left(L_d - L_q\right) i_d i_q - \frac{B}{J}\omega_r - \frac{1}{J}T_L \\ \frac{di_d}{dt} = -\frac{R_s}{L_d} i_d + \frac{pL_q}{L_d} i_q \omega_r + \frac{1}{L_d} V_d \\ \frac{di_q}{dt} = -\frac{R_s}{L_d} i_q - \frac{pL_d}{L_q} i_d \omega_r - \frac{p\Phi_v}{L_q}\omega_r + \frac{1}{L_q} V_q \end{array} \right) \tag{3.29}$$

with Δ: differential operator $((d*)/dt)$, θ_r and ω_r: the rotor angular position and rotor speed, i_d, i_q and V_d, V_q: stator currents and voltages in d-q reference frame, L_d and L_q: axes inductances in d-q reference frame, T_L: load torque, Φ_v:rotor flux, J: inertia, R_s: stator resistance, B: viscous friction coefficient and p: number of pole pairs. The design aim is controlling voltages V_d and V_q in (3.28) to make rotor angular position θ_r track a desired constant reference angular position θ_d and the current i_d is regulated to zero asymptotically, concretely, this PMSM control system is two-input two-output with $u = [u_1\ u_2] = \begin{bmatrix} V_d\ V_q \end{bmatrix}$ and $y = [y_1\ y_2] = [\theta_r\ i_d]$. The same as used [102], the commonly used nonlinear load torque disturbance to test the system performance is generated by the following disturbance dynamic model:

$$\left\{ \begin{array}{l} \dot{v}_1 = v_2 \\ \dot{v}_2 = -a v_1 + b\left(1 - {v_1}^2\right) v_2 \end{array} \right) \tag{3.30}$$

where $v_1 = T_L$ is the solution of this Van der Pol oscillator. Let

$$\left\{ \begin{array}{l} x_1 = \theta_r, x_2 = \omega_r, x_3 = i_d, x_4 = i_q \\ a_1 = \frac{3p\Phi_v}{2J}, a_2 = \frac{3p}{2J}\left(L_d - L_q\right), a_3 = \frac{B}{J}, a_4 = \frac{1}{J} \\ b_1 = \frac{R_s}{L_d} i_d, b_2 = \frac{pL_q}{L_d}, b_3 = \frac{1}{L_d} \\ c_1 = \frac{R_s}{L_d}, c_2 = \frac{pL_d}{L_q}, c_3 = \frac{p\Phi_v}{L_q}, c_4 = \frac{1}{L_q} \end{array} \right) \tag{3.31}$$

Then the system (3.28) can be rewritten into a standard state space equation of:

$$\left\{ \begin{array}{l} \dot{x}_1 = x_2 \\ \dot{x}_2 = a_1 x_4 + a_2 x_3 x_4 - a_3 x_2 - a_4 v_1 \\ \dot{x}_3 = -b_1 x_3 + b_2 x_3 x_2 + b_3 u_1 \\ \dot{x}_4 = -c_1 x_4 - c_2 x_3 x_2 - c_3 x_2 + c_4 u_2 \end{array} \right) and \left\{ \begin{array}{c} y_1 = x_1 + d \\ y_2 = x_3 \end{array} \right) \tag{3.32}$$

where d is the system disturbance. Linearize system (3.32) gives

$$\dot{X} = AX + BU, \quad Y = CX + d \tag{3.33}$$

where $A = \begin{bmatrix} 0 & 1 & 0 & 0 \\ 0 & -a_3 & a_1 & 0 \\ 0 & -b_3 & -b_1 & 0 \\ 0 & 0 & 0 & -c_1 \end{bmatrix}, B = \begin{bmatrix} 0 & 0 \\ 0 & 0 \\ b_4 & 0 \\ 0 & c_3 \end{bmatrix}, C = \begin{bmatrix} 1 & 0 & 0 & 0 \\ 0 & 0 & 1 & 0 \end{bmatrix}$

3.4.2 Experiment set up

In this Chapter, the following three controllers are compared with simulation tests.

1. IMC: The filter time parameter shown in equation (3.9) is chosen as $\lambda = 0.01$, use linearization to approximate the inverse of PMSM.

2. TDF-IMC: Based on the structure in Figure 3.4, the feedforward filter and feedback filter are chosen as $f = \frac{1}{(1+0.1s)^\gamma}$ and $F = \frac{1}{(1+0.01s)^\gamma}$, use UM-dynamic inversion to design the inverse of PMSM.

3. UTPF-IMC: To test the performance of UTDF-IMC fairly, based on the structure in Figure 3.5, the feedforward filter and feedback filter are chosen as $f = \frac{1}{(1+0.1s)^\gamma}$ and $F = \frac{1}{(1+0.01s)^\gamma}$, use UM-dynamic inversion to design the inverse of PMSM.

The comparison test of controller 1 and controller 3 is to demonstrate the superiority of the UM-dynamic inversion algorithm for modelling nonlinear controlled plants/processed and inversion calculation, and the comparison test of controller 2 and controller 3 is to show the efficiency of the proposed UTPF-IMC structure under the same modelling and calculation accuracy. The nominal values of PMSM parameters [102] for the simulations are $p = 3$, $R_s = 1.2\Omega$, $\Phi_v = 0.18Vs/rad$, $\overline{L_d} = 0.011H$, $\overline{L_q} = 0.015H$, $\overline{B} = 0.0001Nms/rad$, $\overline{J} = 0.006kgm^2$. Choose $a = 9$,$b = 1$. The initial state values are chosen as follows: $\theta_r(0) = 0\ rad$, $\omega_r(0) = 0\ rad/s$, $i_d(0) = 0A$, $i_q(0) = 0A$.

3.4.3 Experiment 1: Matched model with system disturbance

To test property 2 in Chapter 3.2.4 while the process model is perfectly matched, that is, $P_0 = P$, assign the step reference signal with tracking angles $\theta_d = \pi$ rad and current $i_d = 0$, plus a squared disturbance shown in Figure 3.14 is added. Clearly, based on the observed experimental results from Figure 3.15 to Figure 3.19, all the controllers can track the desired set-point and reject the system disturbance but the robustness of the TDF-IMC system is worse than others. IMC system has the fastest response speed, however, it has overshoot due to restricting accuracy caused by linearization. From Figure 3.16, when ω_r reaches the designated angular position, rotor speed ω_r is stabilized at zero. From Figure 3.17, all control systems' current i_d can maintain at 0, but its peak value in the IMC control system is much larger than the others obviously. These

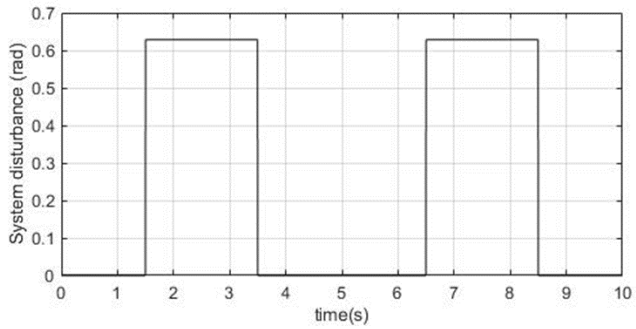

Figure 3.14: System disturbance for PMSM control experiments

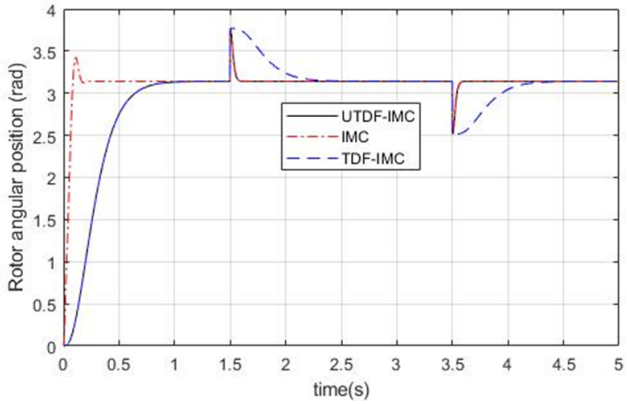

Figure 3.15: Output angular position ω_r in experiment 1

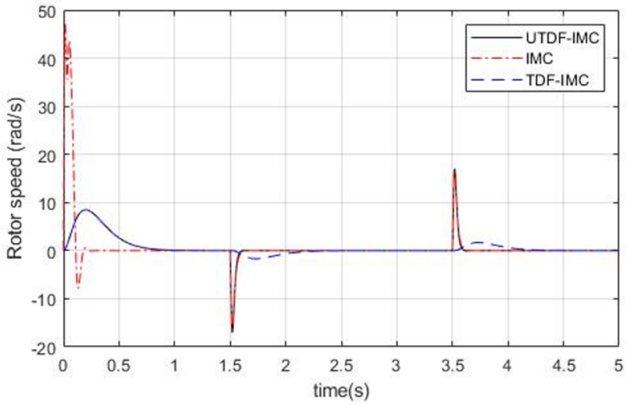

Figure 3.16: Output rotor speed ω_r in experiment 1

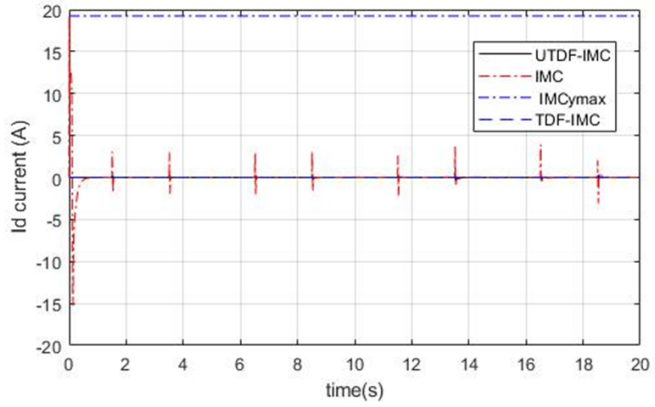

Figure 3.17: Output current i_d in experiment 1

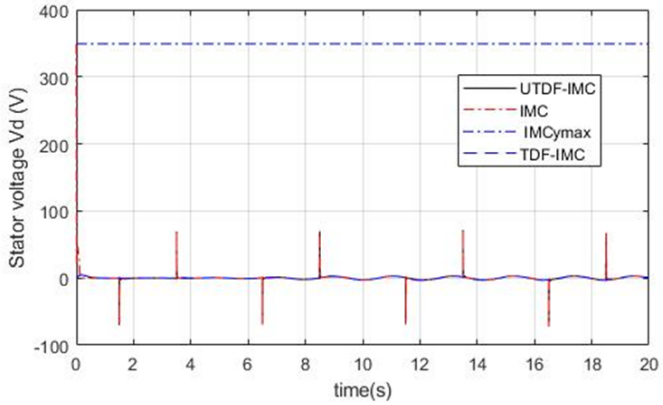

Figure 3.18: Input voltage V_d in experiment 1

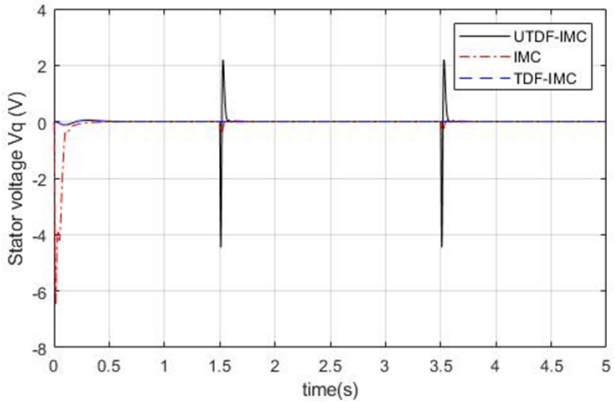

Figure 3.19: Input voltage V_q in experiment 1

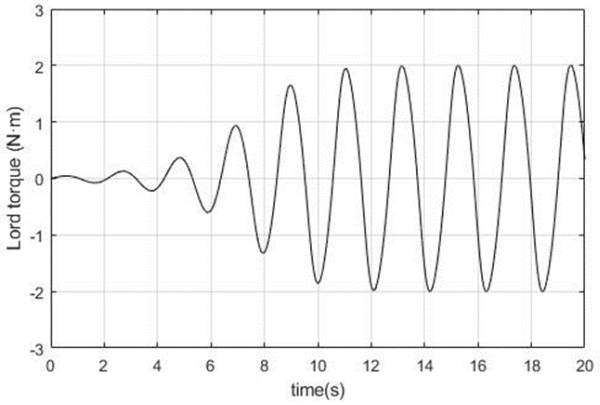

Figure 3.20: Load torque disturbance

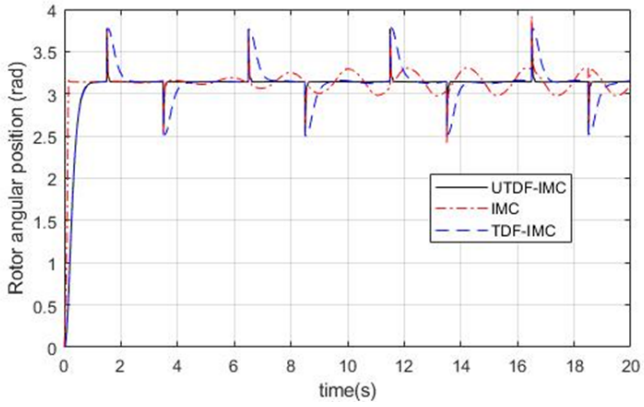

Figure 3.21: Output angular position ω_r in experiment 2

simulation results demonstrate properties justified in Chapter 3.2.4. From Figures 3.18 and 3.19, the controller outputs have large peak values at the initial phase in the IMC system.

3.4.4 Experiment 2: Mismatched model with system disturbance

In this part, three controllers under the actual situation (with modelling error) will be tested to investigate property 3 in Chapter 3.2.4. The parameters of PMSM become: $L_d = 0.5\overline{L_d}$, $L_q = 1.3\overline{L_q}$, $B = 1.45\overline{B}$ and $J = 0.75\overline{J}$. The load torque disturbance generated by (3.30) with initial values of $v_1(0) = 0$ and $v_2(0) = 0.1$ is also added in the PMSM system, which is shown in Figure 3.20. System disturbance is the same as shown in Figure 3.14, and the comparative simulation results are showed from Figure 3.21 to Figure 3.25

From Figure 3.21, the IMC system has a tracking error due to the accuracy limitation of linearization, which makes IMC unable to reject load torque disturbance. Both TDF-IMC and UTDF-IMC control systems can reach the prescribed set-point tracking performance because

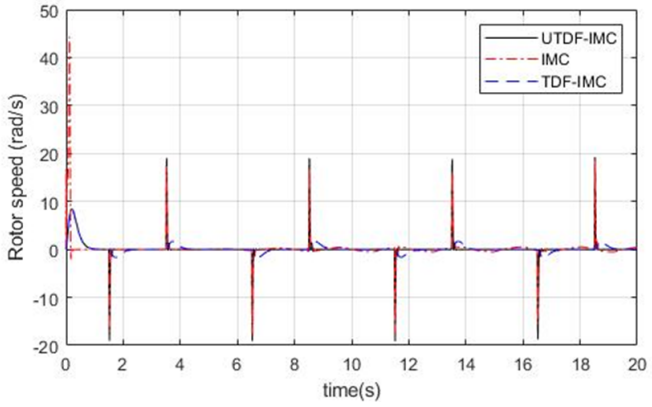

Figure 3.22: Output rotor speed ω_r in experiment 2

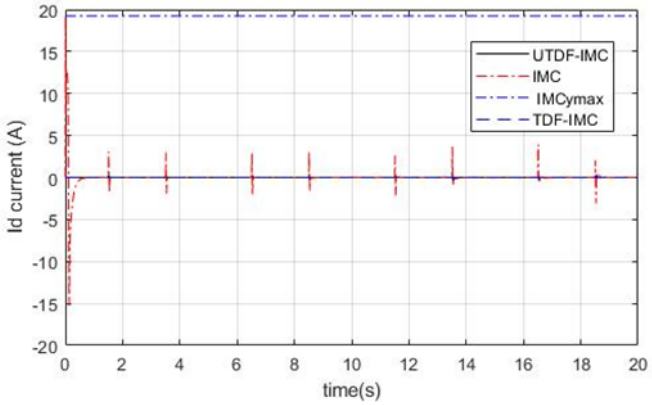

Figure 3.23: Output current i_d in experiment 2

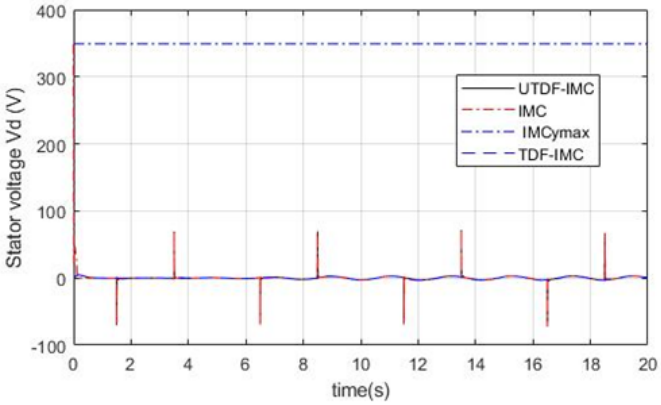

Figure 3.24: Input voltage V_d in experiment 2

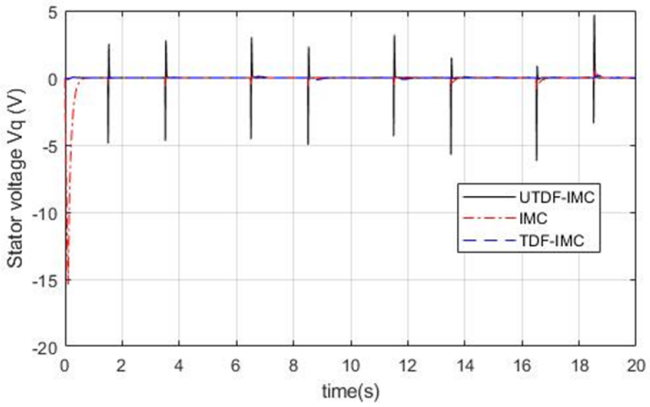

Figure 3.25: Input voltage V_q in experiment 2

UM-dynamic inversion does not lose nonlinear features. UTDF-IMC system has better robustness than the TDF-IMC system due to its superior structure. From Figure 3.22, when θ_r reaches the designated angular position, rotor speed ω_r in UTDF-IMC and TDF-IMC systems is stabilized at zero, however, the rotor revolves slightly in the IMC system. From Figure 3.23, all the current i_d staying at zero but its peak value in the IMC control system is much larger than the others, this is because of the cost of faster response speed in the IMC system. From Figures 3.24 and 3.25, the large peak values from controller outputs at the initial phase in the IMC system can be observed.

In summary, from all simulation results, the control system using the linearization method does degrade the control performance while there is a strong nonlinear disturbance. Additionally, by using UM-dynamic inversion, both UTDF-IMC and TDF-IMC systems can achieve reasonably good set-point tracking performance, and the UTDF-IMC system has better robustness than the classical TDF-IMC system with the same parameters chosen in the filters.

3.5 Summary

This chapter introduces an effective U-model based Two-Degree-of-Freedom IMC framework. Consistently with the simulation test results of linear and nonlinear controlled plants, the proposed UTDF-IMC framework shows its strong robustness and effectiveness in control system design compared with the classical IMC and TDF-IMC approaches. It is believed that UTDF-IMC, enhanced with the nonlinear dynamic inverter, could be applied more effectively to a wide range of industrial control system designs. Therefore, this study has established a platform for possible further expansion, for example controlling Multi-Input and Multi-Output (MIMO) systems, which involves solution challenges with the nonlinear set equations in case of under, full, and over-actuated control system design. Another research direction is to expand the UTDF-IMC to deal with nonminimum phase/unstable zero dynamic systems.

CHAPTER 4

DISTURBANCE-OBSERVER-BASED U-CONTROL

It is believed that unknown system uncertainties and disturbances universally exist in various engineering control systems [17]. These uncertainties have critical side effects on practical engineering system operations and academic research. The issue of disturbance rejection is an ongoing topic since the appearance of control theory and applications, among which Disturbance-Observer-Based Control (DOBC) has shown its efficiency because of its potential feature of the "separation principle" for the ease of control design [14, 17, 96]. In DOBC systems, there are two separate design control loops: a baseline feedback controller to satisfy the desired tracking performance and a Disturbance Observer (DOB) to estimate the system disturbances and uncertainties. When the control system is matched perfectly, the DOB is not activated, and consequently, the DOBC reduces to a feedback control system [17]. Different from the worstcase robust control methods which need to sacrifice control performance, the DOBC can preserve the nominal performance to achieve better robustness.

The method to estimate system uncertainties and disturbances accurately is the core element in DOBC design. The fundamental idea of the DOB is to integrate all the external disturbances and internal uncertainties into single lumped errors. The basic DOB structure was first proposed in frequency-domain in the 1980s by Ohnishi [71], which estimates the disturbance by using the difference between the system control input and the calculation input obtained through the inversion of the controlled plant model. It should be noted that frequency-domain DOB requires the linear control systems or ignoring the nonlinear parts in nonlinear systems and regarding them as disturbances. However, for most control systems, nonlinear dynamic modelling is achievable, and its parameters are measurable [17], the estimation performance by the linear DOB approach is much limited, so that, instead of broadly assuming as unknown elements, reasonably using this knowledge could facilitate more effective controller designs. Accordingly,

the estimation and attenuation of disturbances and uncertainties can be remarkably improved by utilizing the recognized non-linear dynamics in the design.

Chen [16] firstly proposed a universal nonlinear DOB (NDOB) for disturbance torques estimation caused by unknown friction in nonlinear robotic manipulators, then Chen [14] used Lyapunov stability theory to illustrate the estimation error of disturbances will converge exponentially to 0 eventually. The NDOB described in [16] was investigated further in [15], where the control performance of a missile autopilot system had been improved. In addition, NDOB approaches have been widely implanted to many real-time applications, such as the roll, attack and sideslip angle control design for UAV [11], the position control of seven degrees of freedom manipulator [68], and roll tracking control design of Quadrotor [2]. It may be seen that the previously discussed NDOB approaches are proposed in time domain, with the disturbance estimation in each system state variables' channel. Compared with time-domain DOB, frequency-domain DOB has its unique advantage: can integrate all the external system disturbances and internal modelling uncertainties into control input error, which is more intuitive, less computation and its adjustment object is only the design of the low-pass filter [88]. However, because frequency-domain DOB rechoirs the inversion of the plant model, which is difficult to obtain for a nonlinear system, it cannot be directly applicable to nonlinear systems. Therefore, if one can construct the inverse dynamic of nonlinear systems, the lumped disturbance can then be estimated directly using the difference between system input and calculated input.

Another aspect of DOBC is the baseline controller designed to satisfy the required system performance specifications. U-model based control (U-control) proposed and developed by [115, 125], takes the efficiency of UM dynamic inversion and can be applied as a proper control strategy. By getting an inversion, the controlled plant can be compensated into "1" (a unit constant), which brings a designer's requested system response and phase delay-free between system inputs and outputs. However, there are critical issues in dynamic inversion before making any designed U-control system applicable in real situations. Because the inverter of the U-controller is highly sensitive and dependent on the credibility/accuracy of the controlled plants, most existing U-control approaches require accurate modelling without uncertainties. Accordingly, U-control must consider such robustness in its designed control systems. It should be noted that almost all U-control is still focused on its early research—model matched control, that is, with the assumption of the model known exactly, then put the focus on those fundamental structural issues.

Motivated by the advantages of the U-control and the frequency-domain DOB, this chapter aims to develop a nonlinear DOB design framework, which is analogous to the conventional frequency-domain DOB. Promisingly, as described in U-Model (UM) based dynamic inversion algorithm [52], the inverse of the nonlinear system has been used to design a part of the U-controller. Based the simulation experiments, also verifies the efficiency of UM based dynamic inversion algorithm can be applied to not only affine nonlinear systems but also nonaffine

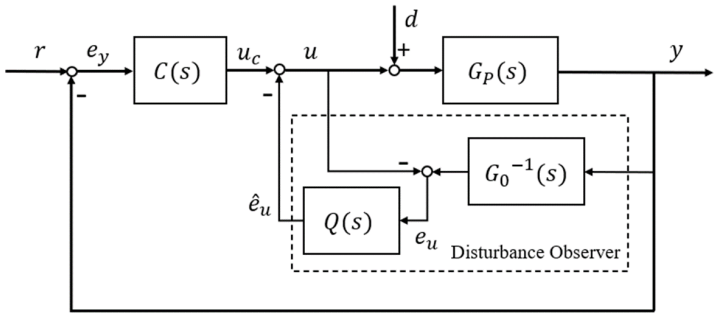

Figure 4.1: Conceptual diagram of frequency-domain disturbance observer based control DOBC

nonlinear systems. This offers the possibility of extending the idea of frequency-domain DOB into a new disturbance estimation approach using the difference between system input and calculated input. In summary, there are two main contributions to the chapter. The first one is to propose a new nonlinear DOB design method, extend the idea of conventional frequency-domain DOB being applicable to a nonlinear system, which can integrate all external disturbances and internal modelling uncertainties as system input error, whereas the conventional time-domain nonlinear DOB estimates the disturbance in system state variables' channel. The second one is combining the strengths exhibited in U-control and this new nonlinear DOB to provide an enhanced, fast-response, delay-free, and convenient design control framework, applicable to all linear/nonlinear invertible controlled plants.

The remainder of this chapter is organized as follows: Chapter 4.1 states the excited issues of nonlinear system control using DOB methods. Chapter 4.2 proposes a DOBUC design framework and performance analysis by simulation experiments. Chapter 4.3 proposes an improved DOBUC method and takes simulation experiments to illustrate and demonstrate the findings of the studies. Finally. conclusions are presented in Chapter 4.4.

4.1 Issues of Nonlinear System Control Using DOB

4.1.1 Frequency Domain DOBC

Ohnishi [71] firstly proposed the basic diagram (shown in 4.1) of frequency-domain DOB by ignoring the outer feedback loop, which is implementable for minimum-phase systems. As described in [88], it is extended to nonminimum-phase systems. However, both frequency-domain DOB requires linear systems, or their nonlinear properties must be estimated as disturbance variables. Figure 4.1 shows the basic structure of the frequency-domain DOB control system.

Where $G_P(s)$ is the actual physical plant, $G_0(s)$ is its nominal model, r is the reference signal, d is the external system disturbance, e_u is the lumped disturbance, and e_u is the estimate of the lumped disturbance. From Figure 4.1, the baseline controller $C(s)$ in the outer loop is designed

according to the desired tracking performance and the observer in the inner loop is designed to reject disturbance and suppress uncertainty. The tracking and robustness requirements can be implemented by separately designing the normal feedback loop and disturbance compensation loop. It should be noted that when system modelling is without disturbance and uncertainty, the disturbance estimation and compensation module in the inner loop will not be activated. Consider a SISO linear minimum phase system by:

$$y = G_P(s)[u + d] \tag{4.1}$$

where u is the ideal control system input, u_c and y are the controller and the control system output, respectively. It should be clarified that both external system disturbances caused by noise and internal disturbances caused by modelling uncertainties can be estimated by frequency-domain DOB. The lumped disturbance e_u in Figure 4.1 contains two items as

$$\begin{aligned} e_u &= yG_0(s)^{-1} - u \\ &= G_P(s)[u+d]G_0(s)^{-1} - u \\ &= G_P(s)G_0(s)^{-1}[u+d] - G_P(s)G_P(s)^{-1}[u+d] + d \\ &= \left[G_P(s)^{-1} - G_0(s)^{-1}\right]G_P(s)[u+d] + d \\ &= \left[G_P(s)^{-1} - G_0(s)^{-1}\right]y + d \end{aligned} \tag{4.2}$$

The first item in (4.2) relates to the modelling errors between the controlled plant $G_P(s)$ and its nominal model $G_0(s)$, and the second relates to the external disturbance d. Therefore, e_u contains all of the disturbances and uncertainties. After letting it pass a filter $Q(s)$, the lumped disturbance estimation e_u is:

$$\hat{e}_u = Q(s)G_0(s)^{-1}y - Q(s)u = Q(s)e_u \tag{4.3}$$

The lumped disturbance estimation error, that is, $\hat{e}_u - e_u$ will need to be zero when time goes to infinity. Clearly, filter $Q(s)$ should be selected as a low-pass filter, that is, in the frequency range of $Q(j\omega) = 1$. It is derived that the control system output is:

$$\begin{aligned} y &= G_P(s)\left[\frac{G_0(s)}{G_0(s) + Q(s)[G_P(s) - G_0(s)]}u_c - \frac{G_P(s)Q(s)}{G_0(s) + Q(s)[G_P(s) - G_0(s)]}d + d\right] \\ &= \frac{G_0(s)G_P(s)}{G_0(s) + Q(s)[G_P(s) - G_0(s)]}u_c + \frac{G_P(s)G_0(s)[1 - Q(s)]}{G_0(s) + Q(s)[G_P(s) - G_0(s)]}d \end{aligned} \tag{4.4}$$

Clearly, the filter $Q(s)$ should be selected as a low-pass filter, that is, in the frequency range of $Q(j\omega) = 1$, it follows from (4.4) that:

$$\lim_{\omega \to 0} y = G_0(j\omega)u_c + 0d \tag{4.5}$$

Equation (4.5) implies that the disturbances and uncertainties in the system have been eliminated by the frequency-domain DOB.

Remark 1. The difference order degree of LPF $Q(s)$ between the denominator and the numerator should be larger than that of the nominal model $G_0(s)$ to ensure that $Q(s)G_0(s)^{-1}$ be proper.
Remark 2. Based on (4.3) Design the LPF $Q(s)$ is close to 1 in all frequency range to guarantee accurate estimation of the lumped disturbance that is, $e_u = \hat{e}_u$.

4.1.2 Nonlinear DOBC

DOBC for the linear system has been developed and employed in engineering for over three decades. Ohnishi [71] pioneered the development of DOBC for motion control systems. After that, DOBC has been employed in many mechatronic systems including disk drivers, machining centres, dc/ac motors, and manipulators. However, this observer may make the DOB not implementable due to the requirement of the inverse of the nominal plant G_P^{-1}, especially for nonlinear plant [17]. To deal with nonlinear plants and uncertainty, one of the famous solutions is developing DOB into nonlinear DOB (NDOB). Consider a classical nonlinear system:

$$\left\{ \begin{array}{c} \dot{x} = f(x) + g_1(x)u + g_2(x)d \\ y = h(x) \end{array} \right\} \tag{4.6}$$

where $x \in R^n$, $d \in R^n$, $u \in R$, and $y \in R$ are the state vector, the lumped disturbance vector, and the system input and output. It is assumed that $f(x)$, $g_1(x)$, $g_2(x)$, and $h(x)$ are smooth functions in terms of x. [17] proposed a NDOB to estimate the disturbance for system (4.6) as:

$$\left\{ \begin{array}{c} \dot{z} = -l(x)g_2(x)z - l(x)[g_2(x)p(x) + f(x) + g_1(x)u] \\ \hat{d} = z + p(x) \end{array} \right\} \tag{4.7}$$

where $\hat{d} \in R^n$ is an estimate of all the disturbances and uncertainties, and $z \in R^n$ is the estimate of the internal states of the nonlinear observer. Although NDOBC has been successfully applied in a wide range of fields such as industrial control [117] and aircraft control [78], it cannot be denied that its design is complicated [55]. Where $l(x)$, $p(x)$ are functions that need to be designed according to the system and need to be stable and satisfied by [14]:

$$l(x) = \frac{\partial p(x)}{\partial x} \; and \; \dot{e}_d = -l(x)g_2(x)e_d \tag{4.8}$$

where $e_d = d - \hat{d}$ is the disturbance estimation error. Concretely, NDOBC realizes the efficient control to nonlinear plants by extending the linear disturbance observer to a nonlinear disturbance observer. However, time-domain NDOB proposed by [14] is still defective in the following aspects:

1. The design in time-domain NDOB [14] is more complex than frequency-domain DOB, and therefore the design process of mentioned NDOB is more complicated and requires more expensive computation [55].

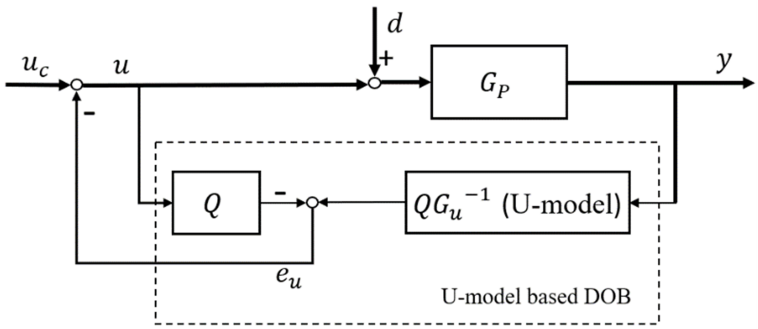

Figure 4.2: Conceptual structure of UDOB

2. The hypothesis of NDOB: the lumped disturbance d changes slowly with time [55], because of the limitation of the convergence speed of NDOB; from [55], the state variables of the plant's model are known or can be directly measured.

3. The lumped disturbances estimated require the dynamics of the disturbance observer to be faster than that of the closed-loop dynamics, which may put pressure on industrial design.

4. The estimation results from NDOB cannot be used for compensation directly because the disturbances and control inputs are not in the same channels, where $d \in R^n$ but $u \in R$.

4.2 Conventional disturbance observer based U-Control

4.2.1 U-model enhanced DOB (UDOB)

From Chapter 4.1, both DOB-based control methods have their shortages. Therefore, another interesting and potential solution is considered to only change the inversion method to re-meet the requirements of the frequency-domain DOB of nominal plant G_P and expand it to adapt to the inversion of the nonlinear system. Inspired by U-model based (UM) dynamic inversion algorithm [52], which can convert nonlinear inversion into linear expression without losing or ignoring plants' features or nonlinear functions. Based on the linear frequency-domain DOBC structure in Figure 4.2, combining the advantages of UM dynamic inversion algorithm, a novel UDOB is generated in this chapter.

From Figure 4.2, G_u is the U-relation of nominal plant G_P, $G_u{}^{-1}$ is the U-model based inversion of G_u, d is the disturbance, u_c is the controller output, u and y are control system input and output, respectively. UDOB is similar to frequency-domain DOB in structure, and the core of both is the inversion of controlled plant G_P and the design of the proper low-pass filter Q. The use of UM inversion algorithm expands the inversion of the traditional linear transfer function into an inversion method that can adapt to linear/nonlinear, transfer function/state space/polynomial

based plants, and therefore expands its application range on the basis of frequency-domain DOB. Compared with NDOB, this UDOB has the following advantages:

1. The computation of UDOB is cheaper (only the inversion of controlled plant ${G_u}^{-1}$ is required), and there are fewer parameters to be designed and adjusted (only parameters in the filter Q).

2. The estimates of UDOB can be used to compensate for the disturbances directly since the estimation disturbances are in the same channels with the control inputs, where $d \in R$ and $u \in R$.

3. UDOB does not require the assumption that "the lumped disturbance d changes slowly with time" in [55] because the inversion process happens almost instantaneously if the response of G_{c1} is fast enough and the computation tool is very powerful.

4.2.2 DOB based U-Control (DOBUC)

Although U-control shows high efficiency in the case of model matching, its high sensitivity to inversion [52] limits its real-time control application. UDOB stated its advantages in observing a lumped disturbance in Chapter 4.2.1, by combining the lumped disturbance and system input into the same channel, the control system design and disturbance compensation will be much more easily realized. Accordingly, U-control can cooperate with UDOB's rapid response, and UDOB can reduce U-control's sensitivity to accurate modelling of the controlled plants (improving system robustness). Therefore, combining the advantages of both, this chapter proposes a novel UDOB-enhanced U-control method (DOBUC). The structure of DOBUC is shown in Figure 4.3.

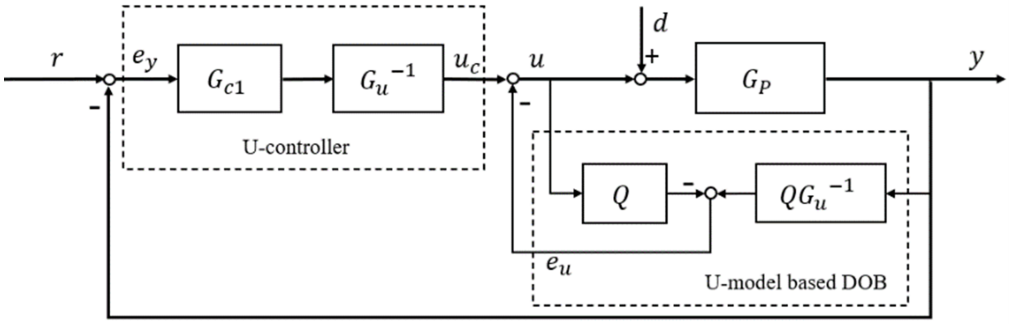

Figure 4.3: Conceptual structure of disturbance observer based U-control DOBUC

From Figure 4.3, this DOBUC has two loops inside and outside. UDOB of the inner loop can estimate the lumped disturbances including the system input disturbances and modelling errors due to uncertainties, U-controller of the outer loop will provide the system tracking performance specifications required by the user. Manifestly, if the control system is perfectly matched and without disturbances, the inner UDOB has no contribution to the system. In this case, the system

tracking preference can be designed directly through the U-control method. When the system has modelling errors or disturbances, the inner loop is activated and will reject the disturbance and suppress uncertainty. Substantiated in Chapter 4.2.1, the estimate of the lumped disturbance in UDOB can be used directly for compensation in the input channel of the U-control system. As demonstrated in Chapter 2.1.3, when the inversion of the controlled plant is realized, a proper low-pass filter will force the lumped disturbances to be suppressed eventually. Based on the structure of DOBUC in Figure 4.3, the U-controller output is:

$$u_c = (r-y)G_{c1}G_u^{-1} \tag{4.9}$$

The control system input can be calculated by:

$$y = u_c G_P - \left(yG_u^{-1} - u\right)QG_P + dG_P \tag{4.10}$$

where $y = (u+d)G_P$ from Figure 4.3. Then it derived from (4.10) that:

$$\begin{aligned} u_c G_P - \left(((u+d)G_P)G_u^{-1} - u\right)QG_P + dG_P &= (u+d)G_P \\ u_c G_P + dG_P - dG_P\left(1+G_u^{-1}QG_P\right) &= uG_P\left(1+G_u^{-1}QG_P - Q\right) \\ u &= \frac{G_u}{G_u + Q\left(G_P - G_u\right)}u_c - \frac{G_P Q}{G_u + Q\left(G_P - G_u\right)}d \end{aligned} \tag{4.11}$$

Therefore, the DOBUC system output can be calculated by:

$$\begin{aligned} y &= G_P(u+d) \\ &= G_P\left[\frac{G_u}{G_u + Q\left(G_P - G_u\right)}u_c - \frac{G_P Q}{G_u + Q\left(G_P - G_u\right)}d + d\right] \\ &= G_P\left[\frac{G_u}{G_u + Q(G_P - G_u)}(r-y)G_{c1}G_u^{-1} - \frac{(1-Q)G_u}{G_0 + Q(G_P - G_u)}d\right] \\ &= \frac{G_P G_{c1}}{G_u + Q(G_P - G_u)}r - \frac{G_P G_{c1}}{G_u + Q\left(G_P - G_u\right)}y - \frac{(1-Q)G_u G_P}{G_0 + Q\left(G_P - G_u\right)}d \end{aligned} \tag{4.12}$$

Accordingly, the control system output from (4.12) becomes:

$$y\left(\frac{G_P G_{c1}}{G_u + Q(G_P - G_u)} + 1\right) = \frac{G_P G_{c1}}{G_u + Q(G_P - G_u)}r - \frac{(1-Q)G_u G_P}{G_0 + Q\left(G_P - G_u\right)}d \tag{4.13}$$

It is derived from (4.13) that the system output y equals:

$$\begin{aligned} y &= \frac{G_P G_{c1}}{(1-Q)G_u + G_P(Q+G_{c1})}r - \frac{G_P G_u(1-Q)}{(1-Q)G_u + G_P(Q+G_{c1})}d \\ &= \frac{G_P G_{c1}}{G_u + Q\left(G_P - G_u\right) + G_P G_{c1}}r - \frac{G_P G_u[1-Q]}{G_u + Q\left(G_P - G_u\right) + G_P G_{c1}}d \end{aligned} \tag{4.14}$$

Clearly, if the filter $Q(s)$ is selected as a low-pass form, that is, $\lim_{\omega\to 0} Q(j\omega) = 1$, it follows from (4.14) that:

$$\lim_{\omega\to 0} y = \frac{G_{c1}}{1+G_{c1}}r + 0d \tag{4.15}$$

From (4.15), modelling errors between G_P and G_u will not affect system performance and the external disturbances will be eliminated by the UDOB, then the structure of DOBUC is equivalent to the structure presented in Figure 4.4. In summary, the design procedures of this DOBUC are:

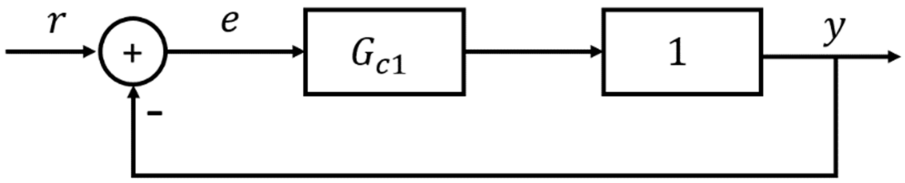

Figure 4.4: Equivalent structure after UDOB compensation

1. Convert the controlled plant G_P into its U-model based expression G_u, then design its dynamic inverter G_u^{-1} through UM dynamic inversion algorithm. Accordingly, the model inversion G_u^{-1} should exist and satisfy the Lipschitz continuity globally uniformly:

$$\begin{aligned} \|G(x_1) - G(x_2)\| &\leq \gamma_1 G \|x_1 - x_2\|, \ \forall x_1, x_2 \in \mathbb{R}^n \\ \left\|G^{-1}(x_1) - G^{-1}(x_2)\right\| &\leq \gamma_2 G^{-1} \|x_1 - x_2\|, \ \forall x_1, x_2 \in \mathbb{R}^n \end{aligned} \tag{4.16}$$

2. Based on the dynamic inverse in (4.14) to design a disturbance observer with a suitable low-pass filter $Q = \frac{1}{(1+\lambda s)^\rho}$. Parameter ρ should be selected large enough to ensure ${G_u}^{-1}$ be proper; λ is the filter time constant, which has an inverse relationship with the speed of closed-loop response. It is noted that the smaller the value of λ, the higher accuracy in disturbance estimation.

3. Design invariant controller G_{c1} with user-desired damping ratio ζ and undamped natural frequency ω_n. Where $G_{c1} = \frac{G}{1-G}$ and $G = \frac{{\omega_n}^2}{s^2+2\omega_n s+{\omega_n}^2}$.

Remark 3. UDOB can be combined with any other baseline control methods because it can integrate the lumped disturbances and system input in the same channel. The use of the U-control method here is not only because of its superior control tracking performance but also because it is very convenient and elementary to design a U-controller based on the realization of controlled plants' inversion.

Remark 4. Because of the restriction of model based dynamic inversion algorithm, UDOB is not effective enough for non-minimum phase systems, while time-domain DOB does not have this restriction [55]. Therefore, although UDOB shows its superiority, it is still necessary to select a suitable disturbance observer according to the controlled plants in practice.

4.2.3 Control of wind energy conversion system (WECS)

The WECS model can be referred to (2.54) in Chapter 2.4.2, and its parameters can be referred to Table 2.1.

Experiment 1: Tracking performance under uncertain wind speed and generator parameters

The wind speed v is chosen to be the same in [64] with a mean of 9m/s and turbulence intensity

of 10%. Because the speed measurement is inevitably inaccurate, this simulation experiment should consider the speed sensor noise.

Case 1: The speed measurement disturbance is chosen as a random value from -0.5 to 0.5 with a sample time of 0.1s. Figure 4.5 shows the ideal wind speed for modelling and its real-time measurement trajectory.

The simulation results for **Case 1** are shown below. The generator output response and desired

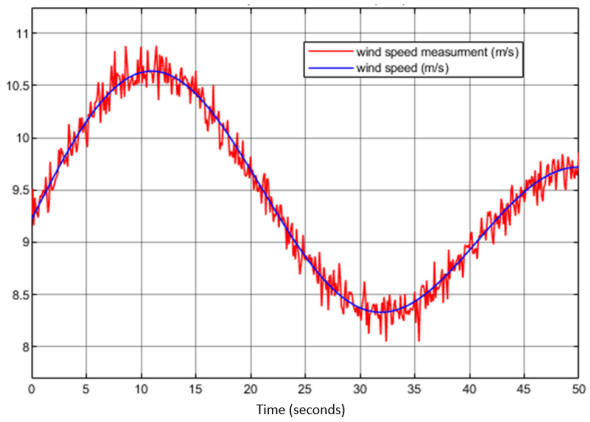

Figure 4.5: Ideal wind speed with its measurement

power output curves are shown in Figure 4.6, both control methods obtain fine tracking performance in the presence of unknown measurable disturbance, whereas the DOBUC method has a smaller tracking error in Figure 4.7. Figure 4.8 shows the disturbance observed result for system input compensation and Figure 4.9 shows the system input with little difference between the two control methods. When WECS only has unmeasurable wind speed disturbance, both control methods show robustness for rejection.

Case 2: The speed measurement disturbance is chosen as a random value from -0.5 to 0.5, mean-

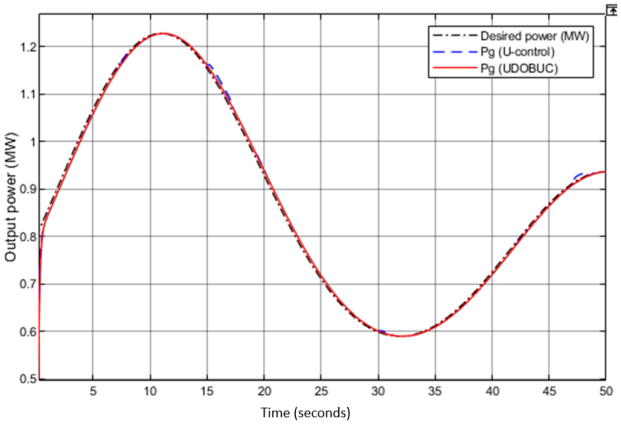

Figure 4.6: Generator output power trajectory in case 1

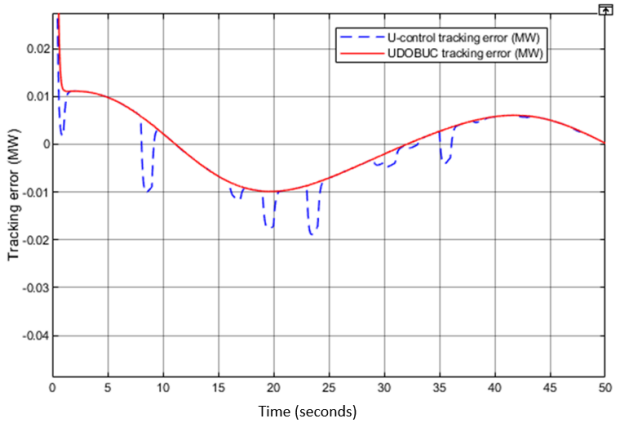

Figure 4.7: Tracking error in case 1

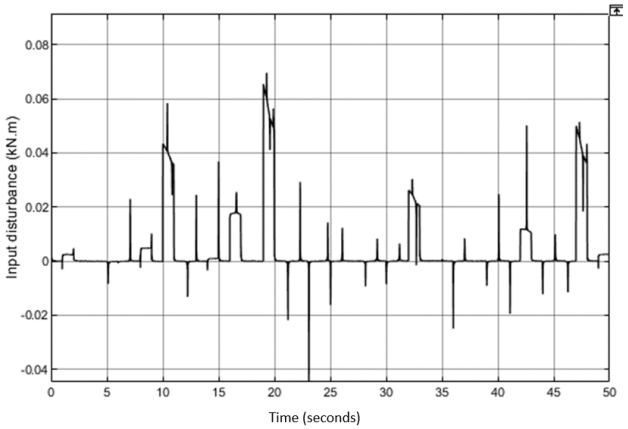

Figure 4.8: Disturbance observer result in case 1

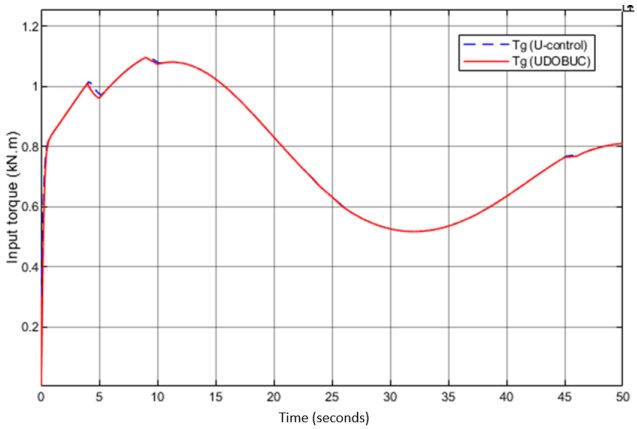

Figure 4.9: System input total torque in case 1

while, modelling errors appear in the experiment with $\Delta J_t = -0.2J_t$, $\Delta K_t = -0.2K_t$. Therefore, WECS system from (2.54) changed to:

$$\dot{P_g}T_g - P_g\dot{T_g} = \frac{1.25}{J_t}T_a{T_g}^2 - \frac{1.625K_t}{J_t}P_gT_g - \frac{1.25}{J_t}{T_g}^3 \tag{4.17}$$

To demonstrate the superiority of the proposed control method further, the generator's parameters are supposed to have variations from their nominal operation values. The simulation results for **Case 2** can be observed below that the proposed control method attains better tracking performance (4.10). UDOB's contribution is already very obvious from Figure 4.12, and the tracking error under the DOBUC method is therefore much smaller than the U-control method from Figure 4.11. When WECS only has both unmeasurable wind speed disturbance and modelling errors, the proposed UDOB demonstrates its efficiency in improving control system robustness.

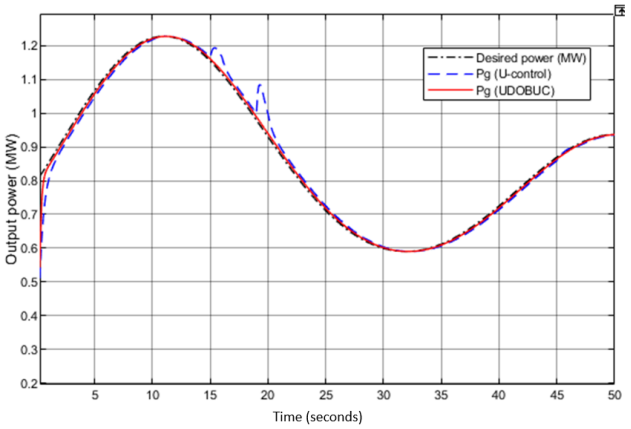

Figure 4.10: Generator output power trajectory in case 2

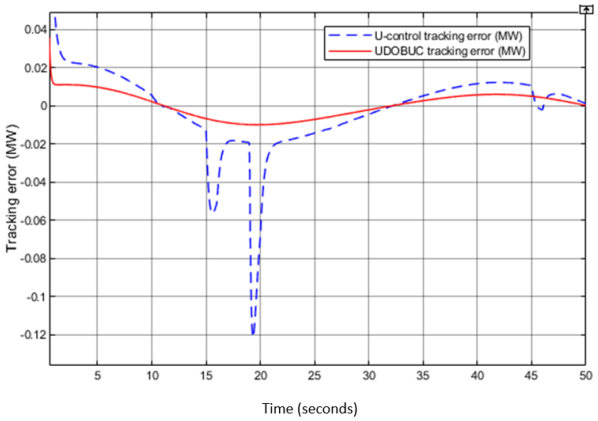

Figure 4.11: Tracking error in case 2

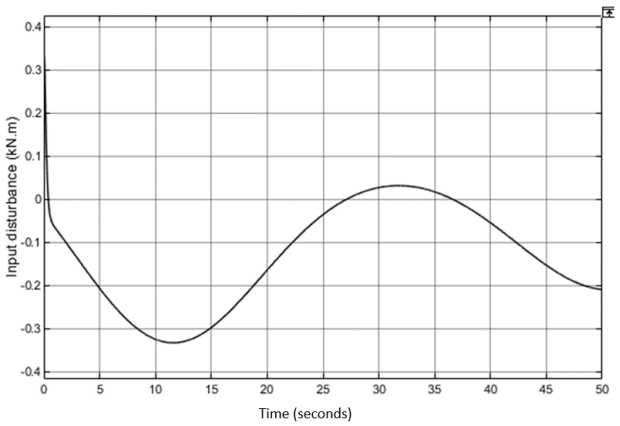

Figure 4.12: Disturbance observer result in case 2

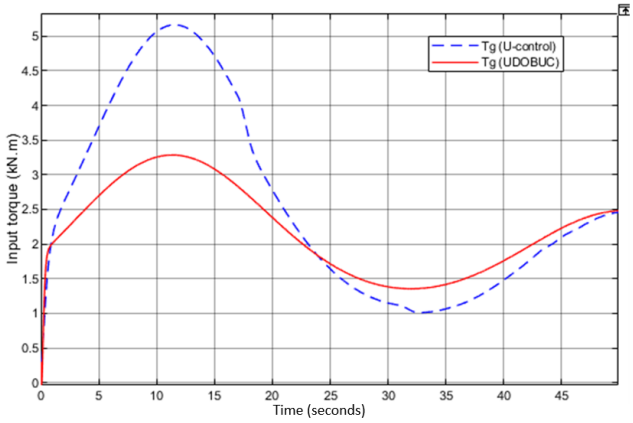

Figure 4.13: System input total torque in case 2

Experiment 2: Tracking performance under uncertain wind speed, generator parameters and system input noise

In real-time control applications, the interference caused by noise or other signals in the environment to the system input of this WECS is unpreventable. Therefore, **Experiment 2** introduces a disturbance to the input control signal channel, a sinusoidal signal with amplitude 0.3(kN.m) and frequency of 1 Hz to further test the robustness of the proposed control method. The generator response results are shown below. When the disturbance appears in the input channel of the control system, the tracking curve of the U-control method has a large fluctuation, and DOBUC can perfectly track the desired power from both Figures 4.14 and 4.15. The proposed UDOB can accurately observe the input disturbance, and integrate all other errors including unmeasurable wind speed and system uncertainties into the input disturbance and then compensate from both Figures 4.16 and 4.17. Impartially, the proposed UDOB shows strong strength in disturbance observation and integration, and this input compensation control method for suppressing lumped disturbance is very convenient for the control system design and use.

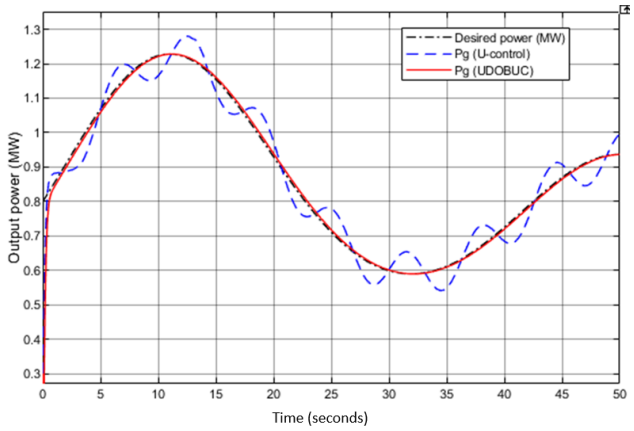

Figure 4.14: Generator output power trajectory in Experiment 2

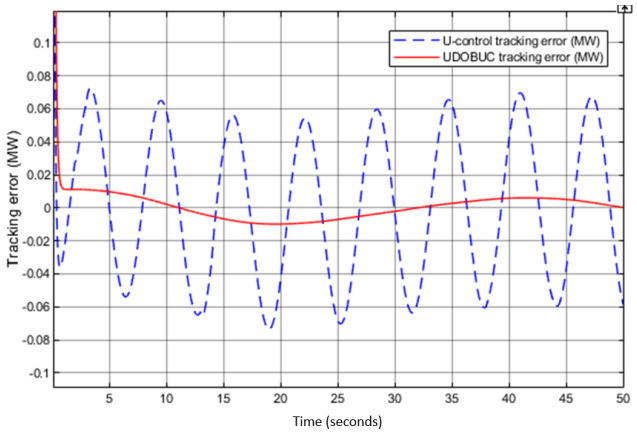

Figure 4.15: Tracking error in Experiment 2

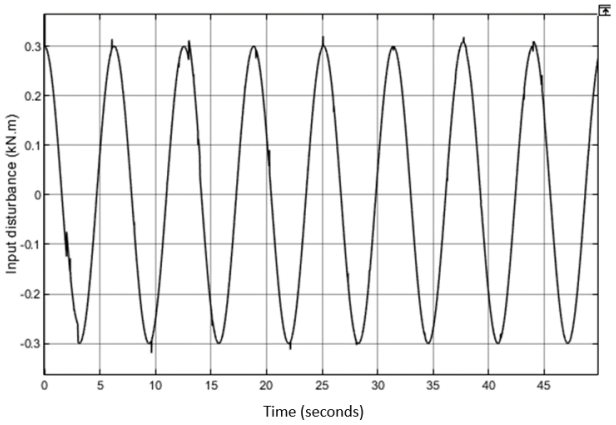

Figure 4.16: Disturbance observer result in Experiment 2

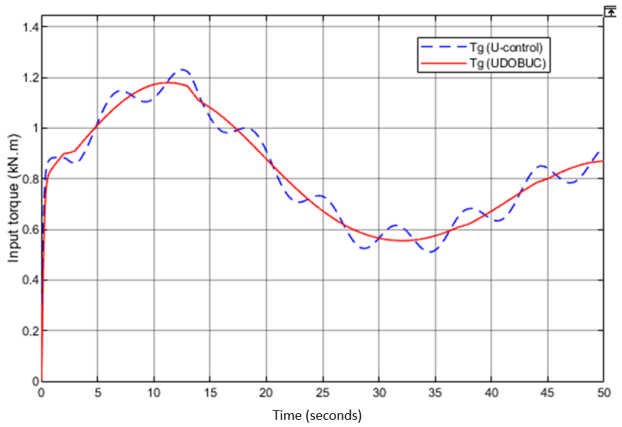

Figure 4.17: System input total torque in Experiment 2

4.3 Imporved disturbance observer based U-Control

4.3.1 Problem Statement

This study considers the following SISO input/output differential equation to describe a general nonlinear dynamic system

$$y_1^{(n)} = f(Y_1) + g_0(Y_1)u + \cdots + g_m(Y_1)u^{(m)},\ m \le n \tag{4.18}$$

where y_1 is the system output, u is the system input, Y_1 absorbs all the system output y_1 and its derivatives except the highest order one $y_1^{(n)}$, that is

$$Y_1 = \left(y_1, \dot{y}_1, \ddot{y}_1, \cdots, y_1^{(n-1)}\right) \tag{4.19}$$

Remark 5: Model (4.18) is widely used to describe a kind of flat nonlinear systems [22]. Generally, $g_i(Y_1) = 0,\ i \in N^+$ can be applied in many practical applications, which means the high order derivatives of system input $u^{(i)},\ i \in N^+$ do not exist. When the system considers the actuator, $g_i(Y_1) = 0,\ i \ge 2$, which means the control system only needs system input u and its derivative $\dot{u}$.
Assumption 1: The system output y_1 and its related higher-order derivatives $\dot{y}_1, \ddot{y}_1, \cdots, y_1^{(n-1)}$ can be bounded with a proper control input u.
Assumption 2: The following dynamic system meets global asymptotic stability

$$g_0(Y_1)u + g_0(Y_1)\dot{u} + \cdots + g_m(Y_1)u^{(m)} = 0 \tag{4.20}$$

Remark 6: **Assumption 1** is applicable to a lot of nonlinear control systems that satisfy the smoothing prerequisite described in (4.18). Technically, this assumption would limit the field of application of the proposed control system; practically, it would not have much impact. From the author's point of view, the core point of the control system is to make the controlled object operate to meet and complete the designer's requirements, which means that the controlled object

is stable in normal conditions. In this case, "the output y and its derivatives are bounded" is reasonable in practical applications.
Meanwhile, the zero dynamics of system (4.18) is

$$g_0(0)u + g_0(0)\dot{u} + \cdots + g_m(0)u^{(m)} = 0 \tag{4.21}$$

The dynamic system (4.21) is globally asymptotically stable when it satisfies **Assumption 2**, which means the control system described in (4.18) is minimum-phase. When using (4.18) to describe the linear system, it turns to:

$$y_1^{(n)} + a_{n-1}y_1^{(n-1)} + \cdots + a_1\dot{y}_1 + a_0 y_1 = b_m u^{(m)} + b_{m-1}u^{(m-1)} + \cdots + b_0\dot{u} + b_0 u,\ m \le n \tag{4.22}$$

Then **Assumption 2** turns to:

$$b_m u^{(m)} + b_{m-1}u^{(m-1)} + \cdots + b_0\dot{u} + b_0 u = 0 \tag{4.23}$$

The above equation (4.23) directly leads to the property of minimum-phase for linear control system from equation (4.22). The next step is to use the U-control method to design the baseline controller to cancel both the nonlinearity and dynamic of (4.18) and design a DOB to improve its robustness. It should be mentioned that all design of this new composite control system only uses the measurement from the control input u and the output y from the model (4.18), rather than requiring other information like high-order derivatives of system output $y^{(n)}$ and system state variables.

4.3.2 Imporved U-inverter design

Chapter 2.2 has explained the basic concept/configuration of the U-control system. Manifestly, the solving process of the controlled plant's inversion (2.25) requires the system input u and output y and their related high-order derivatives u^m) and y^n. In this section, a new U-inverter design based on the input/output model (4.18) is presented. The dashed area in Figure 4.18 shows the basic design framework of this new U-inverter, in which r is the input of the U-inverter (marked in the dashed zone), u and y_1 are the controlled plant input/output respectively. Based on the U-control framework, U-inverter is designed to convert the controlled plant into an identity matrix or unit constant. When there are no modelling errors and external disturbances from the system, $G_0^{-1}G_P = 1$. In this case, the input of the U-inverter equals the output of the controlled plant, that is, $r = y_1$. Let the controlled plant input u be

$$U = k_1(r - y_1) \tag{4.24}$$

where $k_1 > 0$ is a sufficiently large constant. It follows from (4.24) that

$$\left\{\begin{array}{l} u = k_1(r - y_1) \\ \dot{u} = k_1(\dot{r} - \dot{y}_1) \\ \vdots \\ u^{(n)} = k_1\left(r^{(n)} - y_1^{(n)}\right) \end{array}\right\} \tag{4.25}$$

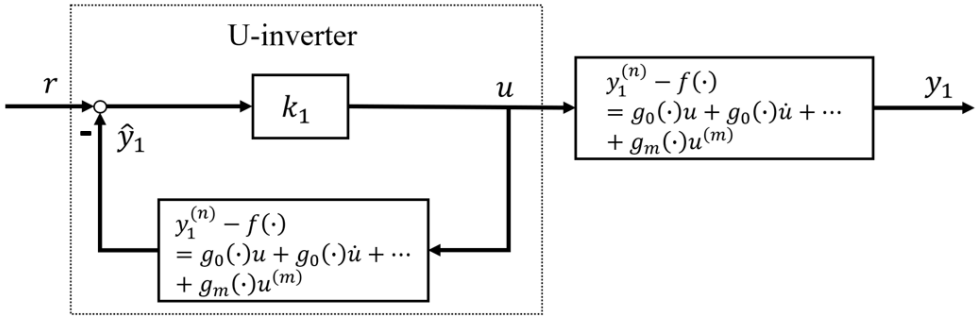

Figure 4.18: The design framework of new U-inverter

Clearly, from equations (4.24) and (4.25) and Figure 4.18, the proposed U-inverter only requires the signal information of system output y_1 and reference r. Different from the general U-inverter, high-order derivatives of y_1 are not required in the whole design procedure. From (4.25), it follows that

$$\left\{\begin{array}{l} y_1 = r - \frac{u}{k_1} \\ \dot{y}_1 = \dot{r} - \frac{\dot{u}}{k_1} \\ \vdots \\ y_1^{(n-1)} = r^{(n-1)} - \frac{u^{(n-1)}}{k_1} \\ y_1^{(n)} = r^{(n)} - \frac{u^{(n)}}{k_1} \end{array}\right. \tag{4.26}$$

Therefore, system (4.18) turns to

$$\begin{aligned} y_1^{(n)} =& f\left(y_1, \dot{y}_1, \ddot{y}_1, \cdots, y_1^{(n-1)}\right) \\ &+ g_0\left(y_1, \dot{y}_1, \ddot{y}_1, \cdots, y_1^{(n-1)}\right) u \\ &+ \cdots + g_m\left(y_1, \dot{y}_1, \ddot{y}_1, \cdots, y_1^{(n-1)}\right) u^{(m)} \\ r^{(n)} - \frac{u^{(n)}}{k_1} =& f\left(r - \frac{u}{k_1}, \dot{r} - \frac{\dot{u}}{k_1}, \cdots, r^{(n-1)} - \frac{u^{(n-1)}}{k_1}\right) \\ &+ g_0\left(r - \frac{u}{k_1}, \dot{r} - \frac{\dot{u}}{k_1}, \cdots, r^{(n-1)} - \frac{u^{(n-1)}}{k_1}\right) u \\ &+ \cdots + g_m\left(r - \frac{u}{k_1}, \dot{r} - \frac{\dot{u}}{k_1}, \cdots, r^{(n-1)} - \frac{u^{(n-1)}}{k_1}\right) u^{(m)} \end{aligned} \tag{4.27}$$

Add the same term $f(R) + g_0(R)u + \cdots + g_m(R)u^{(m)}$ to each side of (4.27) with

$$R = \left(r, \dot{r}, \ddot{r}, \cdots, r^{(n-1)}\right) \tag{4.28}$$

Then system (4.27) turns to:

$$\begin{aligned} r^{(n)}-\frac{u^{(n)}}{k_1} =& f(R)+g_0(R)u+\cdots+g_m(R)u^{(m)} \\ &+f\left(r-\frac{u}{k_1},\dot{r}-\frac{\dot{u}}{k_1},\cdots,r^{(n-1)}-\frac{u^{(n-1)}}{k_1}\right)-f\left(r,\dot{r},\cdots,r^{(n-1)}\right) \\ &+g_0\left(r-\frac{u}{k_1},\dot{r}-\frac{\dot{u}}{k_1},\cdots,r^{(n-1)}-\frac{u^{(n-1)}}{k_1}\right)u-g_0\left(r,\dot{r},\cdots,r^{(n-1)}\right)u \\ &+\cdots+g_m\left(r-\frac{u}{k_1},\dot{r}-\frac{\dot{u}}{k_1},\cdots,r^{(n-1)}-\frac{u^{(n-1)}}{k_1}\right)u^{(m)}-g_m\left(r,\dot{r},\cdots,r^{(n-1)}\right)u^{(m)} \end{aligned} \tag{4.29}$$

Because the functions $f\left(r,\dot{r},\cdots,r^{(n-1)}\right)$ and $g_i\left(r,\dot{r},\cdots,r^{(n-1)}\right),\ i\in N$ are both smooth, the following inequalities exist at least locally

$$\begin{aligned} &\left\|f\left(r-\frac{u}{k_1},\dot{r}-\frac{\dot{u}}{k_1},\cdots,r^{(n-1)}-\frac{u^{(n-1)}}{k_1}\right)-f\left(r,\dot{r},\cdots,r^{(n-1)}\right)\right\| \\ &\qquad\le\gamma_1\left\|\left(\frac{u}{k_1},\frac{\dot{u}}{k_1},\cdots,\frac{u^{(n-1)}}{k_1}\right)\right\|=\frac{\gamma_1}{k_1}\left\|\left(u,\dot{u},\cdots,u^{(n-1)}\right)\right\| \end{aligned} \tag{4.30}$$

And

$$\begin{aligned} &\left\|\left(r-\frac{u}{k_1},\dot{r}-\frac{\dot{u}}{k_1},\cdots,r^{(n-1)}-\frac{u^{(n-1)}}{k_1}\right)-g_i\left(r,\dot{r},\cdots,r^{(n-1)}\right)\right\| \\ &\qquad\le\gamma_2\left\|\left(\frac{u}{k_1},\frac{\dot{u}}{k_1},\cdots,\frac{u^{(n-1)}}{k_1}\right)\right\|=\frac{\gamma_2}{k_1}\left\|\left(u,\dot{u},\cdots,u^{(n-1)}\right)\right\| \end{aligned} \tag{4.31}$$

where γ_1 and γ_2 are Lipschitz constants. For a convenient description, let

$$U=\left\|\left(u,\dot{u},\ddot{u},\cdots,u^{(n-1)}\right)\right\| \tag{4.32}$$

Move term $f(R)+g_0(R)u+\cdots+g_m(R)u^{(m)}$ to the left side of the equation (4.29), organize it according to principles described in (4.30) and (4.31), then equation (4.29) turns into

$$\begin{aligned} &\left|r^{(n)}-\frac{u^{(n)}}{k_1}-\left(f(R)+g_0(R)u+\cdots+g_m(R)u^{(m)}\right)\right| \\ &\qquad\le\frac{\gamma_1}{k_1}U+\frac{\gamma_2}{k_1}U|u|+\frac{\gamma_2}{k_1}U|u|+\cdots+\frac{\gamma_2}{k_1}U\left|u^{(m)}\right| \end{aligned} \tag{4.33}$$

From (4.33), it is clearly that when $k_1\to\infty$, the right side of the equation (4.33) has

$$\lim_{k_1\to\infty}\frac{\gamma_1}{k_1}U+\frac{\gamma_2}{k_1}U|u|+\frac{\gamma_2}{k_1}U|\dot{u}|+\cdots+\frac{\gamma_2}{k_1}U\left|u^{(m)}\right|=0 \tag{4.34}$$

Therefore, the left side of the equation (4.33) correspondingly has

$$\begin{aligned} &\lim_{k_1\to\infty}\left|r^{(n)}-\frac{u^{(n)}}{k_1}-\left(f(R)+g_0(R)u+\cdots+g_m(R)u^{(m)}\right)\right|=0 \\ &\lim_{k_1\to\infty}r^{(n)}-\frac{u^{(n)}}{k_1}=\ f(R)+g_0(R)u+\cdots+g_m(R)u^{(m)} \end{aligned} \tag{4.35}$$

Let (4.18) subtract (4.35), it then comes

$$\begin{aligned} y_1^{(n)} - \left(r^{(n)} - \frac{u^{(n)}}{k_1}\right) &= f(Y_1) - f(R) + g_0(Y_1)u - g_0(R)u + \cdots + g_m(Y_1)u^{(m)} - g_m(R)u^{(m)} \\ &= f(Y_1) - f(R) + (g_0(Y_1) - g_0(R))u + \cdots + (g_m(Y_1) - g_m(R))u^{(m)} \end{aligned} \tag{4.36}$$

Since the functions $f\left(r,\dot{r},\cdots,r^{(n-1)}\right)$ and $g_i\left(r,\dot{r},\cdots,r^{(n-1)}\right),\ i \in N$ are smooth, the following inequalities exist at least locally

$$\begin{aligned} &\left\| g_i\left(r,\dot{r},\cdots,r^{(n-1)}\right) - g_i\left(y_1,\dot{y}_1,\cdots,y_1^{(n-1)}\right)\right\| \\ \leq &\gamma_3 \left\|\left(r-y_1,\dot{r}-\dot{y}_1,\cdots,r^{(n-1)}-y_1^{(n-1)}\right)\right\| = \frac{\gamma_3}{k_1}\left\|\left(u,\dot{u},\cdots,u^{(n-1)}\right)\right\| \end{aligned} \tag{4.37}$$

where γ_3 is the Lipschitz constant. Move term $f(Y_1) - f(R)$ to the left side of the equation (4.36), it has

$$\begin{aligned} &\left| y_1^{(n)} - \left(r^{(n)} - \frac{u^{(n)}}{k_1}\right) - (f(Y_1) - f(R))\right| \\ \leq &\frac{\gamma_3}{k_1}U|u| + \frac{\gamma_3}{k_1}U|\dot{u}| + \cdots + \frac{\gamma_3}{k_1}U\left|u^{(m)}\right| = \frac{\gamma_3}{k_1}U\left(|u| + |\dot{u}| + \cdots + u^{(m)}\right) \end{aligned} \tag{4.38}$$

When $k_1 > 0$ tends to infinity, the right term in (4.38) has

$$\lim_{k_1 \to \infty} \frac{\gamma_3}{k_1}U\left(|u| + |\dot{u}| + \cdots + u^{(m)}\right) = 0 \tag{4.39}$$

Substituting (4.39) into (4.38), it comes

$$\left| y_1^{(n)} - \left(r^{(n)} - \frac{u^{(n)}}{k_1}\right) - (f(Y_1) - f(R))\right| = 0 \tag{4.40}$$

Based on (4.26), (4.40) becomes to

$$y_1^{(n)} - \left(r^{(n)} - \frac{u^{(n)}}{k_1}\right) = y_1^{(n)} - y_1^{(n)} = 0 \tag{4.41}$$

Because the term $y_1^{(n)} - \left(r^{(n)} - \frac{u^{(n)}}{k_1}\right)$ equals to 0, it can be concluded from (4.37) that

$$|f(Y_1) - f(R)| = 0 \tag{4.42}$$

Substituting (4.42) into (4.36), it is clear that the left side of the equation (4.36) is equal to 0 as well as the term $f(Y_1) - f(R)$, then it comes from (4.36) that

$$(g_0(Y_1) - g_0(R))u + (g_1(Y_1) - g_1(R))\dot{u} + \cdots + (g_m(Y_1) - g_m(R))u^{(m)} = 0 \tag{4.43}$$

Extend (4.43) by (4.25), then it becomes

$$\begin{aligned} &(g_0(Y_1) - g_0(R))u + (g_1(Y_1) - g_1(R))\dot{u} + \cdots + (g_m(Y_1) - g_m(R))u^{(m)} \\ =&k_1((g_0(Y_1) - g_0(R))(r - y_1) + (g_1(Y_1) - g_1(R))(\dot{r} - \dot{y}_1)) \\ +&k_1\left(\cdots + (g_m(Y_1) - g_m(R))\left(r^{(m)} - y_1^{(m)}\right)\right) = 0 \end{aligned} \tag{4.44}$$

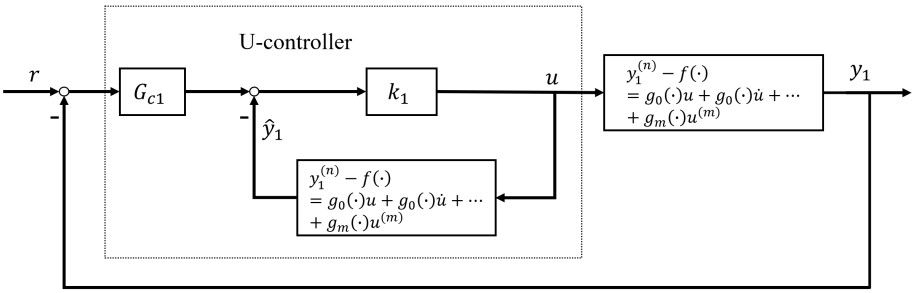

Figure 4.19: New U-control system design framework

Let the error e_1 between the reference r and y_1, that is, $e_1 = r - y_1$. Because constant $k_1 > 0$, it follows (4.44) that

$$(g_0(Y_1) - g_0(R))e_1 + (g_1(Y_1) - g_1(R))\dot{e}_1 + \cdots + (g_m(Y_1) - g_m(R))e_1^{(m)} = 0 \tag{4.45}$$

From **Assumption 2**, the system (4.45) is globally asymptotically stable. Accordingly, the error e_1 between the reference r and y_1 approaches zero asymptotically, which implies that y_1 converges to r with a large enough parameter k_1. When $y_1 = r$, the system dynamic inversion is implemented, which also means the cancellation of system dynamics and nonlinearities is achieved. Therefore, the structure in Figure 4.18 can be used to design U-inverter.

Remark 7: From (4.39) to (4.45), the error between the reference and system output will converge to zero asymptotically when the parameter k_1 adjusted to infinity. It seems this proposed U-inverter is similar to the high-gain feedback controller, but it is not the case. Generally, the high-gain controller requires system states variables [50, 61], and the high-gain controller is designed to achieve desired system control performance, whereas the purposes of the proposed U-inverter is the cancellation of system dynamics and nonlinearity. Additionally, this U-inverter is only a part of the U-control system, which aims to construct an inverse model of the controlled plant. Therefore, the basic idea of the proposed U-inverter is different from the high-gain feedback controller. Any point that should be mentioned is that the proposed U-inverter only requires information on the controlled plant input and output. [51] does not require system state variables, but the frequency response and pole-zero locations are selected to design the system controller.
According to the U-control system design framework in Chapter 2.1.3, the updated U-control system design framework is shown in Figure 4.19, in where the dashed area shows this new U-controller, which contains both invariant controller G_{c1} and the proposed U-inverter. Clearly, only system output and controller output signals are required in the system design process.

4.3.3 Imporved DOB design

From Chapter 2.1.3 and 4.3.2, a new U-controller design is proposed based on this new U-inverter. However, from Figure 4.19, the model in U-controller is required to be the same as the controlled

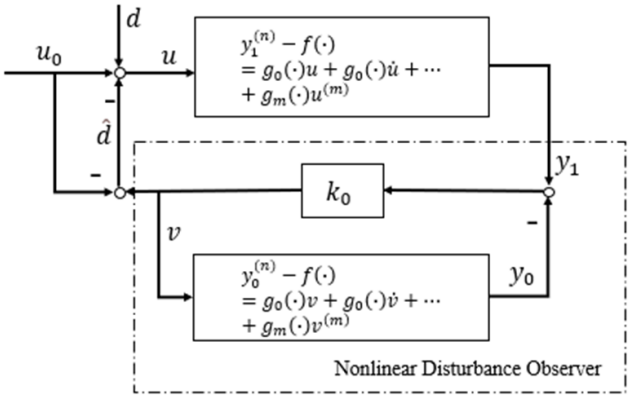

Figure 4.20: The framework of nonlinear DOB

model, that is, the whole U-control system is designed without system internal uncertainties and external disturbances. In practice application, this “perfect modelling” is hardly existed. Therefore, inspired by [23], a nonlinear input/output model-based DOB is introduced in the U-control system design, which also only requires the information of system input and output. The framework of [23] is shown in Figure 4.20. Set the nominal model of system (4.18) as follows for NDOB design:

$$y_0^{(n)} = f(Y_0) + g_0(Y_0)v + \ldots + g_m(Y_0)v^{(m)},\ m \le n \tag{4.46}$$

Where y_0 and v are the observer system output and input, respectively, $f(Y_0)$ and $g_i(Y_0)$ are smooth function associated with

$$Y_0 = \left(y_0, \dot{y}_0, \ddot{y}_0, \ldots, y_0^{(n-1)}\right) \tag{4.47}$$

Let the input of the nominal modeled system (4.46) be

$$v = k_0(y_1 - y_0) \tag{4.48}$$

Where y_1 is the practice system output and k_0 is a large constant. Thus, the disturbance d and other modelling uncertainties can be observed as $\hat{d} = v - u_0$. It follows from (4.48) that

$$\left\{ \begin{array}{l} v = k_0(y_1 - y_1) \\ \dot{v} = k_0(\dot{y}_1 - \dot{y}_0) \\ \vdots \\ v^{(n)} = k_0\left(y_1^{(n)} - y_0^{(n)}\right) \end{array} \right) \tag{4.49}$$

where $k_0 > 0$ is a sufficiently large constant, from (4.48), it follows that,

$$\left\{\begin{array}{l} y_0 = y_1 - \frac{v}{k_0} \\ \dot{y}_0 = \dot{y}_1 - \frac{\dot{v}}{k_0} \\ \vdots \\ {y_0}^{(n-1)} = {y_1}^{(n-1)} - \frac{v^{(n-1)}}{k_0} \\ {y_0}^{(n)} = {y_1}^{(n)} - \frac{v^{(n)}}{k_0} \end{array}\right) \tag{4.50}$$

Then substituting (4.50) into (4.46), it comes

$$\begin{aligned} {y_1}^{(n)} - \frac{v^{(n)}}{k_0} =& f\left(y_1 - \frac{v}{k_0}, \dot{y}_1 - \frac{\dot{v}}{k_0}, \ldots, {y_1}^{(n-1)} - \frac{v^{(n-1)}}{k_0}\right) \\ &+ g_0\left(y_1 - \frac{v}{k_0}, \dot{y}_1 - \frac{\dot{v}}{k_0}, \ldots, {y_1}^{(n-1)} - \frac{v^{(n-1)}}{k_0}\right)v \\ &+ \ldots + g_m\left(y_1 - \frac{v}{k_0}, \dot{y}_1 - \frac{\dot{v}}{k_0}, \ldots, {y_1}^{(n-1)} - \frac{v^{(n-1)}}{k_0}\right)v^{(m)} \end{aligned} \tag{4.51}$$

Add the same term $f(Y_1) + g_0(Y_1)v + \ldots + g_m(Y_1)v^{(m)}$ to each side of the equation (4.51), then it becomes

$$\begin{aligned} {y_1}^{(n)} =& \frac{v^{(n)}}{k_0} + f(Y_1) + g_0(Y_1)v + \ldots + g_m(Y_1)v^{(m)} \\ &+ \left(f\left(y_1 - \frac{v}{k_0}, \dot{y}_1 - \frac{\dot{v}}{k_0}, \ldots, {y_1}^{(n-1)} - \frac{v^{(n-1)}}{k_0}\right) - f\left(y_1, \dot{y}_1, \ldots, y_1^{(n-1)}\right)\right) \\ &+ \left(g_0\left(y_1 - \frac{v}{k_0}, \dot{y}_1 - \frac{\dot{v}}{k_0}, \ldots, {y_1}^{(n-1)} - \frac{v^{(n-1)}}{k_0}\right) - g_0\left(y_1, \dot{y}_1, \ldots, y_1^{(n-1)}\right)\right)v \\ &+ \ldots + \left(g_m\left(y_1 - \frac{v}{k_0}, \dot{y}_1 - \frac{\dot{v}}{k_0}, \ldots, {y_1}^{(n-1)} - \frac{v^{(n-1)}}{k_0}\right) - g_m\left(y_1, \dot{y}_1, \ldots, y_1^{(n-1)}\right)\right)v^{(m)} \end{aligned} \tag{4.52}$$

Because the functions $f\left(r, \dot{r}, \ldots, r^{(n-1)}\right)$ and $g_i\left(r, \dot{r}, \ldots, r^{(n-1)}\right),\ i \in N$ are smooth, the following inequalities exist at least locally

$$\begin{aligned} &\left\| f\left(y_1 - \frac{v}{k_0}, \dot{y}_1 - \frac{\dot{v}}{k_0}, \ldots, {y_1}^{(n-1)} - \frac{v^{(n-1)}}{k_0}\right) - f\left(y_1, \dot{y}_1, \ldots, y_1^{(n-1)}\right)\right\| \\ &\qquad \le \gamma_4 \left\| \left(\frac{v}{k_0}, \frac{\dot{v}}{k_0}, \ldots, \frac{v^{(n-1)}}{k_0}\right)\right\| = \frac{\gamma_4}{k_0}\left\|\left(v, \dot{v}, \ldots, v^{(n-1)}\right)\right\| \end{aligned} \tag{4.53}$$

And

$$\begin{aligned} &\left\| g_i\left(y_1 - \frac{v}{k_0}, \dot{y}_1 - \frac{\dot{v}}{k_0}, \ldots, {y_1}^{(n-1)} - \frac{v^{(n-1)}}{k_0}\right) - g_i\left(y_1, \dot{y}_1, \ldots, y_1^{(n-1)}\right)\right\| \\ &\qquad \le \gamma_5 \left\| \left(\frac{v}{k_0}, \frac{\dot{v}}{k_0}, \ldots, \frac{v^{(n-1)}}{k_0}\right)\right\| = \frac{\gamma_5}{k_0}\left\| v, \dot{v}, \ldots, v^{(n-1)}\right)\right\| \end{aligned} \tag{4.54}$$

Where γ_4 and γ_5 are Lipschitz constants. Then move term $f(Y_1) + g_0(Y_1)v + \ldots + g_m(Y_1)v^{(m)}$ to the left side of the equation (4.52), organize it according to principles described in (4.53) and (4.54),

then equation (4.52) can be turned into

$$\begin{aligned}\left|{y_1}^{(n)}-\left(f(Y_1)+g_0(Y_1)v+\ldots+g_m(Y_1)v^{(m)}\right)\right| \\ \leq \frac{v^{(n)}}{k_0}+\frac{\gamma_4}{k_0}H+\frac{\gamma_5}{k_0}H\left(|v|+|\dot{v}|+\ldots+v^{(m)}\right)\end{aligned} \tag{4.55}$$

When k_0 goes infinite, the right side of the equation (4.55) has

$$\lim_{k_0\to\infty}\frac{v^{(n)}}{k_0}+\frac{\gamma_4}{k_0}H+\frac{\gamma_5}{k_0}H\left(|v|+|\dot{v}|+\ldots+v^{(m)}\right)=0 \tag{4.56}$$

Therefore, the left side of the equation (4.55) turns into

$$\begin{aligned}\left|{y_1}^{(n)}-\left(f(Y_1)+g_0(Y_1)v+\ldots+g_m(Y_1)v^{(m)}\right)\right|=0 \\ {y_1}^{(n)}=\ f(Y_1)+g_0(Y_1)v+\ldots+g_m(Y_1)v^{(m)}\end{aligned} \tag{4.57}$$

Combining (4.57) and (4.18), it gives

$$\begin{aligned}{y_1}^{(n)}-{y_1}^{(n)}=&f(Y_1)+g_0(Y_1)u+\ldots+g_m(Y_1)u^{(m)} \\ &-\left(f(Y_1)+g_0(Y_1)v+\ldots+g_m(Y_1)v^{(m)}\right) \\ =&g_0(Y_1)(v-u)+g_1(Y_1)(\dot{v}-\dot{u})+\ldots+g_m(Y_1)\left(v^{(m)}-u^{(m)}\right)\end{aligned} \tag{4.58}$$

It is clear that the left side of the equation (4.58) equals to 0, let the error e_2 be $e_2=v-u$, it comes from (4.58) that

$$g_0(Y_1)e_2+g_1(Y_1)\dot{e}_2+\ldots+g_m(Y_1)e_2^{(m)}=0 \tag{4.59}$$

From **Assumption 2**, system (4.59) is globally asymptotically stable. Accordingly, the error between u and v approaches zero asymptotically. Therefore, the observed $\hat{d}$ can converge to the lumped disturbance represented by the practical disturbance d and modelling uncertainties asymptotically.

4.3.4 Imporved DOBUC design

The proposed U-control in 4.3.2 shows the efficient control design which only requires the system output, however, this efficiency strictly appears in the case of the model matched. In practice, the modelling errors and system external noise will exist and restrict the proposed U-control performance. The input/output model-based DOB described in 4.3.3 presented its main advantages in observing the system disturbances with only system input/output information. This DOB can amalgamate all uncertainties and system disturbances into the system input channel, which will make disturbance compensation be implemented easily. Accordingly, the combination of this nonlinear DOB and the proposed U-control makes it possible to reduce U-control's sensitivity and improve the robustness of the control system.

Based on the new U-control system design framework in 4.3.2 and DOB described in 4.3.3, this study proposed a new DOBUC design framework shown in Figure 4.21. Concretely, this DOBUC

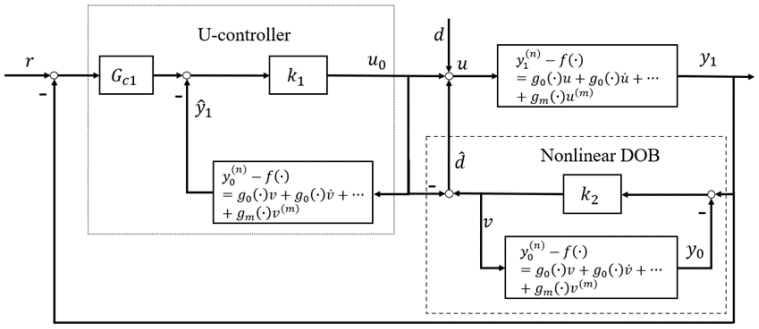

Figure 4.21: New DOB based U-control design framework

has three loops: DOB in the inner loop can estimate the disturbance caused by modelling errors and system noises, and then amalgamate them into the system input channel; U-inverter in the inner loop will cancel both the system dynamics and nonlinearity, convert the controlled plant to an identity matrix or unit constant when combined with its dynamic inversion; G_{c1} in the outer loop is used to design the desired control performance. Manifestly, if the control system is perfectly modelled and free of system external disturbance, the inner DOB will not be activated and the system will be converted into a simple linear closed-loop feedback control system with the dynamic cancellation from U-inverter; when disturbance exists in the system, U-controller will compensate the disturbance estimated by activated DOB into the input channel. Finally, the framework of DOBUC is equivalent to the following framework in Figure 4.22:
Accordingly, the design procedures for the proposed DOBUC are:

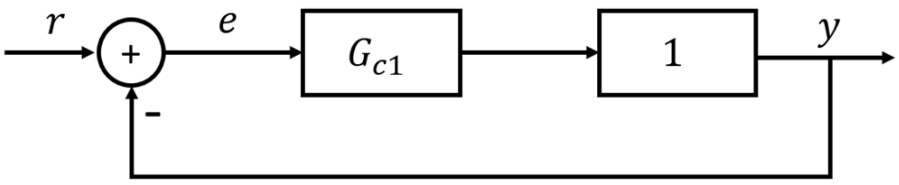

Figure 4.22: Equivalent U-control framework after NDOB compensation

1. Design the U-inverter based on Chapter 4.3.2. The design parameter k_1 should be selected large enough to satisfy (4.34) to implement an efficient U-inverter. It should be mentioned that the model inversion should exist and satisfy the Lipschitz continuity globally uniformly:

$$\begin{aligned} |G(x_1) - G(x_2)| &\le \gamma_1 G\,|x_1 - x_2|,\ \forall x_1, x_2 \in R^n \\ \left\|G^{-1}(x_1) - G^{-1}(x_2)\right\| &\le \gamma_2 G^{-1}\,\|x_1 - x_2\|,\ \forall x_1, x_2 \in R^n \end{aligned} \tag{4.60}$$

2. Design the nonlinear DOB based on Chapter 4.3.3. The design parameter k_0 should be large enough to satisfy (4.56) and guarantee that the disturbance estimation error can converge to a small region.

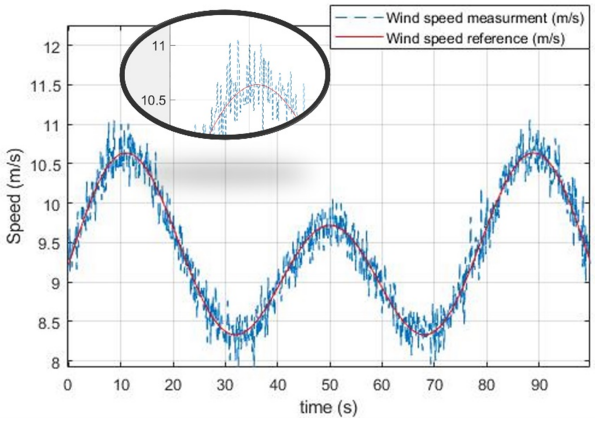

Figure 4.23: Wind speed measurement

3. Design invariant controller G_{c1} with customer-defined damping ratio ζ and undamped natural frequency ω_n to achieve control performance specifications. Where $G_{c1} = \frac{G}{1-G}$ and $G = \frac{{\omega_n}^2}{s^2+2\omega_n s+{\omega_n}^2}$.

Remark 8: Theoretically, the larger parameters k_0, k_1 can realize more efficient U-inverter and improved disturbance estimation performance. However, the system output noise level will also be increased by the increasing value of k_0 and k_1. Accordingly, the parameters k_0 and k_1 should be adjusted from small to large until the control performance specifications are meted. It also should be noticed that k_1 needs to be larger than k_0 to ensure the U-inverter converges faster than the nonlinear DOB because this DOB requires the information from U-controller's output to estimate the disturbance.

4.3.5 Control of wind energy conversion system (WECS)

The WECS model can be referred to (2.54) in Chapter 2.4.2, and its parameters can be referred to Table 2.1. The turbulence intensity is 10% and the mean value of wind speed v in this experiment is 9m/s [64]. This simulation experiment introduces the wind speed sensor error because of its inevitable disturbances. Accordingly, the speed sensor error is chosen as a 10 Hz white noise, with the value from -0.5 to 0.5. Figure 4.23 shows the wind speed with and without sensor error. The block framework of this control system is given in Figure 4.24.

According to the design framework presented in Chapter 4.3.4, the parameter in U-inverter is: $k_1 = 1000$ and in the nonlinear observer is $k_2 = 500$. To assure a fast-tracking performance without overshooting, the damping ratio and undamped natural frequency are chosen as $\zeta = 1$ and $\omega_n = 10$ for invariant controller design as $G_{c1} = \frac{1}{0.01s^2+0.2s}$. To test the robustness of the proposed control method, a disturbance d is introduced and defined as:

$$d = \left\{ \begin{array}{l} 2\sin\left(\frac{t}{4}\right)\ 0 \le t < 16\pi \\ 0.7\sin(t)\ 16\pi \le t < 100 \end{array} \right\} \tag{4.61}$$

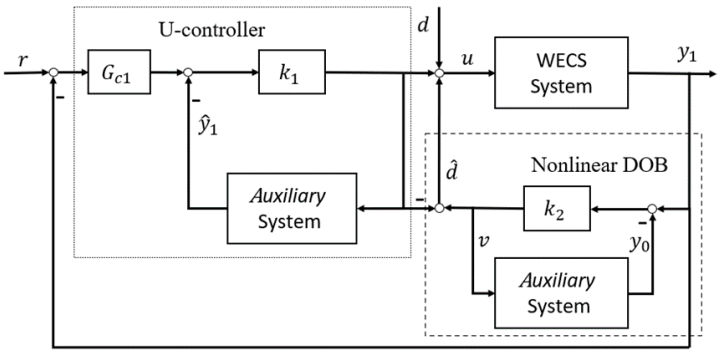

Figure 4.24: Block framework of WECS with improved UDOBC

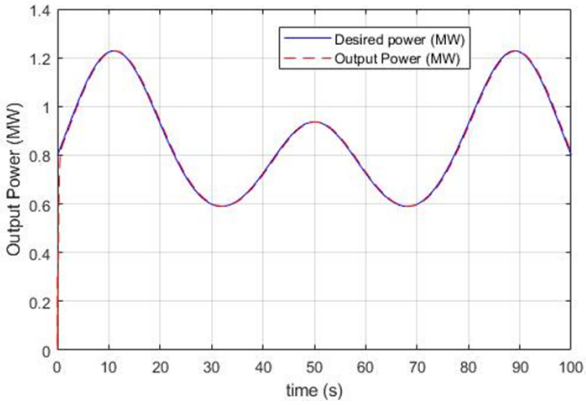

Figure 4.25: System output power

Additionally, modelling errors are considered in this simulation experiment with $J_t = -0.9J_t$, $K_t = 2K_t$, and $T_a = -4T_a$. Therefore, WECS system in (2.54) changed to:

$$\dot{P_g}T_g - P_g\dot{T_g} = \frac{5T_a}{0.1J_t}{T_g}^2 - \frac{3K_t}{J_t}P_gT_g - \frac{1}{0.2J_t}{T_g}^3 \tag{4.62}$$

The simulation results can be observed below. From Figure 4.25, the proposed DOBUC method has good tracking performance; the tracking error rate is less than 1% (compared to peak output power) from Figure 4.26. Obviously, the NDOB shows efficacy in the observation of both system disturbance and modelling errors from Figure 4.27, and the controller output is smooth without chattering from Figure 4.28.

4.4 Summary

Firstly, this chapter presents a novel disturbance-observer-based U-control method inspired by the frequency-domain DOBC structure. This novel DOB applies to linear and nonlinear control systems with invertible controlled plants/processes. With the demonstration of the WECS simula-

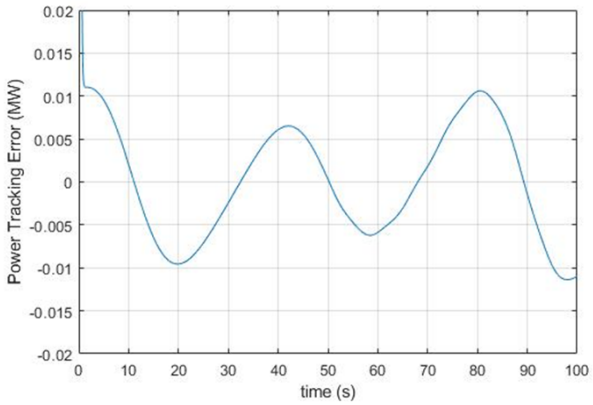

Figure 4.26: Tracking error

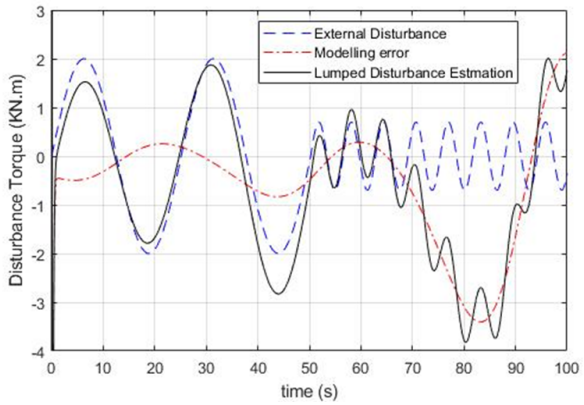

Figure 4.27: Disturbance observer result

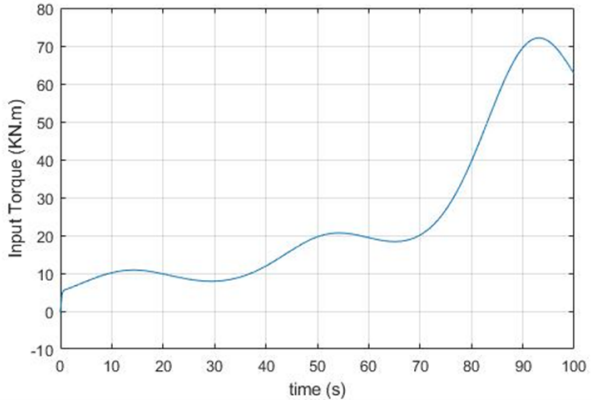

Figure 4.28: System input total torque

tion tests, the U-control method has considered the full complex nonlinear dynamics, and the proposed DOB can observe all system input disturbance and modelling uncertainties. Different from the time-domain NDOBC, the proposed UDOB can integrate all lumped disturbances into the control input channel and perform compensation design, which provides convenience and new ideas for the research of robust control systems combined with other mature control methods. However, subject to the characteristics of UM dynamic inversion algorithm, this proposed DOB can only be applied to a type of invertible and bounded plants/processes. For systems that are unbounded or complex inversion (large computation), the performance of the proposed DOB will be critically restricted. In summary, for systems with a higher order that meet the mentioned assumptions, it is more convenient to use DOBUC; for systems that do not meet the assumptions or the inversion process requires large computation, the classic NDOBC is more efficient.
Secondly, This study proposes a novel improved DOBUC framework for linear/nonlinear systems. It removes the restriction of the current state feedback U-control systems that request observable or measurable state variables. The proposed U-inverter provides a robust dynamic inversion of the control plant so that it makes the U-control inherit robustness throughout the control system operation. It should be noted that this DOBUC requires the controlled input/output system being minimum-phase, which should take care of applications. At the same time, integrating all lumped disturbances into the control input channel also means that the allocation of input disturbance compensation will become a challenge for the multiple input multiple outputs (MIMO) systems, how to efficiently allocate disturbance compensation in MIMO systems and taking up applications to practical systems for the bench tests are the next research direction.

CHAPTER 5

U-MODEL BASED SLIDING MODE CONTROL

Plant modelling has played a very critical role in model-based control system design. In general, there are two main important considerations for model utility and control system, 1) Approximation capabilities in terms of accuracy and conciseness. 2) Control-oriented structure for control system formation and calculation.

Regarding the first concern, in practice, even for academic research, seldom models have an accurate representation of real plants, therefore model-based control system design should take internal uncertainty and external disturbance like system error into consideration [70]. Sliding mode control [82] (SMC) has been effectively used to deal with uncertainties in way of a variable structure system, that is, a control system involving discontinuous control actions. Sliding mode control has developed in various sliding manifolds such as the integral sliding mode control approach [40], second-order sliding mode control approach [24], super-twist sliding mode control approach [119], and adaptive sliding mode control approach [59]. SMC method is a special kind of non-linear control with the characteristics of control discontinuity, even though the switching characteristics of the control system structure change with time. In summary, the advantages of the SMC method are that firstly the dynamic behaviour of the system may be tailored by the particular choice of the switching function [82] and secondly even if the system has external disturbances and uncertain parameters, the sliding mode control method can still keep system stability and have strong robustness.

For the second concern, the key idea used in this study is U-model based control method, the U-control method in short. which has been introduced and studied well in Chapter 2.1.3. Generally, the U-control approach can save the computation of the control system design procedure by avoiding nonlinear system modelling linearization processing. However, U-model based dynamic inversion is very sensitive to internal uncertainties as well as controlled performance. In this

case, reducing the U-control method's sensitivity to uncertainty, that is, improving its robustness is a hot research issue. Meanwhile, continuous time (CT) U-control system design is less attended [129]. This is because it is difficult the solution of CT dynamic inversion with high-order derivative terms of controlled system input and output. Consequently, this study takes these two challenges to try a solution for CT U-model based robust control system design, that is, in form of combined U-control method's computation saving capacity and SMC method's strong robustness.

Accordingly, the main contribution of this study is justified with

1. Proposal of a new U-SMC framework integrating U-control and SMC method, which accommodates both control-oriented model structure and strong robustness against imperfect model representation

2. Proposal of a new U-model based double sliding mode control (UDSMC) control method, improved U-SMC method, firstly treating system dynamics as unknown disturbance, further reducing the dependence of control algorithms on system information.

3. Computational experiments by Simulink to bench test the developed control system design procedure. In addition, the exemplary case study provides potential readers/users with a routine for their ad hoc research expansion and applications.

The rest of the study is organized as follows: Chapter 5.1 introduces the basic principles and concepts of the SMC method. Chapter 5.2 presents the U-SMC system design framework and design procedures, and its control performance is demonstrated by simulation experiments. Based on Chapter 5.2, Chapter 5.3 proposes a U-model based double sliding mode control (UDSMC) method and takes simulation experiments to illustrate and demonstrate the findings of the studies. Chapter 5.4 draws the conclusion and future work of this study.

5.1 Introduction of sliding mode control

5.1.1 Basic principles and design methods

Sliding mode control (SMC) theory originated in the former Soviet Union in the late 1950s and was led by Emelyanov [27] and Utkin [97] to solve the problem with a special type of variable structure (discontinuous control system). Because of its special advantages of robustness to system disturbances and uncertain parameters, it has been widely researched by scholars. The main idea of sliding mode control is to drive the system state to the designed sliding surface and maintain it through the action of the control method. The main difference between SMC and other control methods is the SMC's system structure is purposely changed according to the state of the system, which is forced to move according to a predetermined trajectory. Accordingly, SMC has been widely used to solve some complex engineering control problems, such as motor system control [100], robot [13] and UAV control [67], etc. However, sliding mode variable structure

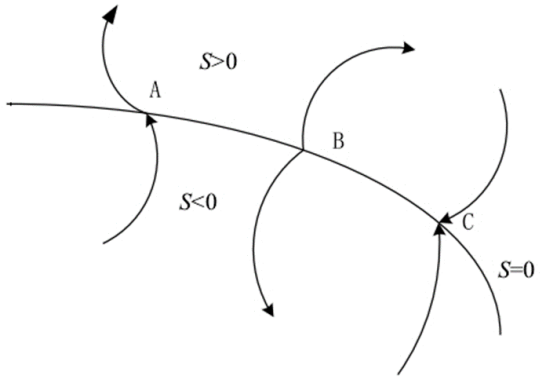

Figure 5.1: Three kinds of points on the sliding switching surface

control has an obvious disadvantage in addition to the above advantages, which is the chattering problem of the control law [4, 25]. Due to the existence of switching time lag, system inertia, and spatial switching lag, the controlled objects of the system produce chattering. Chattering may make the system unstable and other hazards, which affects its practical application. Therefore, it is of great significance to suppress the chattering of the system and increase the engineering application of sliding mode control.

The two main stages of sliding mode control [97] are: 1) reaching stage: the system state is driven by any initial state and reaches the switching manifold within a limited time (expected sliding mode); 2) sliding mode stage: the system state is sliding on the surface and keeps the trajectory of the system on the sliding surface. There are two main steps [97] corresponding to these two stages, which are: 1) The selection of the switching manifold, that is, the sliding mode surface $s(x)$: select a group of switching manifolds with specified ideal dynamic characteristics (sliding surface). 2) controller design: forming a discontinuous control strategy to ensure the limited time accessibility of switching manifolds. The controller can be local or global, depending on the specific control requirements.

5.1.2 Basic concepts and mathematical description

Consider a nonlinear system, which can be expressed as:

$$\dot{x} = f(x) + \Delta f(x) + [B(x) + \Delta B(x)]\, u \tag{5.1}$$

where $\Delta f(x)$ and $\Delta B(x)$ are system uncertainies. Then sliding mode surface function can be designed based on the system as $\sigma(x)$ and $\sigma(x) = 0$ is called the switching surface, which can divide the state space into $\sigma > 0$ and $\sigma < 0$. As shown in Figure 5.1, the points on the switching surface can be divided into three types, namely: A (normal point), B (start point), and C (end point) respectively. Among them, only point C has a special meaning for sliding mode motion.

After determining the switching function, the control law can be defined:

$$u = \left\{ \begin{array}{ll} u^+(x), & \sigma(x) > 0 \\ u^-(x), & \sigma(x) < 0 \end{array} \right\} \tag{5.2}$$

where $u^+(x) \neq u^-(x)$ and SMC needs to meet three requirements:

1. The sliding mode exists, that is, the above formula (5.2) holds.
2. Satisfying the accessibility condition, the movement points other than the switching surface $\sigma(x) = 0$ can reach the switching surface within a limited time.
3. Ensure the stability of sliding mode movement

The existence of the sliding mode is a prerequisite for the application of sliding mode control. The goal of reaching the condition is to ensure that the system state is at any position, and the control strategy forces them to approach and reach the sliding mode surface, that is, their trajectory is in the sliding mode area. Therefore, the sliding mode control needs to meet two conditions:

$$\lim_{\sigma \to 0^+} \dot{\sigma} < 0 \qquad \lim_{\sigma \to 0^-} \dot{\sigma} > 0 \tag{5.3}$$

Equation (5.3) indicates that in the near zone of the switching surface $\sigma(x) = 0$, the system state reaches the switching surface within a limited time. Equation (5.4) is therefore equivalent to:

$$\dot{\sigma}\sigma < 0 \tag{5.4}$$

5.1.3 Invariance of sliding mode control

Consider the system described in (5.1) and let the switching function $\sigma = \sigma(x)$, therefore, its derivative is

$$\dot{\sigma} = \frac{\partial \sigma}{\partial x}(f + \Delta f + (B + \Delta B)u) \tag{5.5}$$

When the system reaching the sliding surface, $\sigma = \dot{\sigma} = 0$, therefore, the equivalent control is:

$$u_{eq} = -\left(\frac{\partial \sigma}{\partial x}(B + \Delta B)\right)^{-1} \frac{\partial \sigma}{\partial x}(f + \Delta f) \tag{5.6}$$

Bring equation (5.6) into equation (5.1):

$$\dot{x} = f + \Delta f - (B + \Delta B)\left(\frac{\partial \sigma}{\partial x}(B + \Delta B)\right)^{-1} \frac{\partial \sigma}{\partial x}(f + \Delta f) \tag{5.7}$$

Let $\Delta f = Bk_1$ and $\Delta B = Bk_2$, equation (5.7) can be converted into:

$$\begin{aligned} \dot{x} &= f + Bk_1 - (B + Bk_2)\left(\frac{\partial \sigma}{\partial x}(B + Bk_2)\right)^{-1} \frac{\partial \sigma}{\partial x}(f + Bk_1) \\ &= f + Bk_1 - B(I + k_2)(I + k_2)^{-1}\left(\frac{\partial \sigma}{\partial x}B\right)^{-1} \frac{\partial \sigma}{\partial x}(f + Bk_1) \\ &= \left(I - B\left(\frac{\partial \sigma}{\partial x}B\right)^{-1} \frac{\partial \sigma}{\partial x}\right) f + B\left(\frac{\partial \sigma}{\partial x}B\right)^{-1} \end{aligned} \tag{5.8}$$

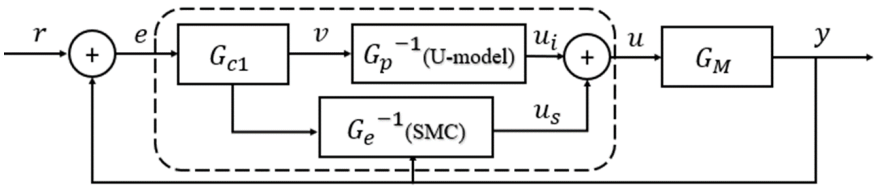

Figure 5.2: U-SMC system framework

It can be seen from (5.8) that the uncertainty and parameter changes of the system have no impact on the sliding mode system, this property is called the invariance ability.

5.2 Sliding mode enhanced U-control (U-SMC)

5.2.1 U-SMC and its design procedure

Due to these two main problems (controlled plant inaccuracy and system disturbance) that will greatly impact U-control performance in Chapter 2.1.3, this Chapter combines the U-control method and SMC method to enhance the robustness of U-control.

From Figure 5.2, G_M is the actual plant model which could be a linear or nonlinear dynamics model and contains uncertain system coefficients. r is the reference, which is the desired output of the control system, and e is the difference (error) between the output y and the reference r. G_{c1} is a linear invariant controller which can be designed by $G_{c1} = \frac{G}{1-G}$ while $G_P^{-1}G_p = 1$ based on Chapter 2.1.3. G_e^{-1}(SMC) model is the core part of this U-SMC system, which can compensate for the inversion error of the plant model G_M. Same to U-control, the U-SMC framework is also applicable to both uncertain linear and nonlinear structures as long as ideal dynamic inverse G_P^{-1} exists. In general, the U-SMC system design procedure has two separate steps:

1. Design ideal U-control system Assume the ideal plant model G_P is stable and bounded, and its inverse G_P^{-1} exists. Design a U-control system based on 2.1.3. Replace the ideal plant model G_P in the U-control system with the actual plant model G_M. Accordingly, the system can be described as below, which is the same to (2.15):

$$\left(F, U\left(G_{c1}, G_P^{-1}\right), G_M\right) \tag{5.9}$$

2. Design compensated plant inverter G_e^{-1} Assume the plant model G_M is bounded, and its ideal inverse G_P^{-1} exists. From Figure 5.2., the U-SMC controller which is shown in the dashed has three parts: the invariant controller G_{c1}, the ideal plant's dynamic inverter G_P^{-1} and the compensated plant inversion G_e^{-1}. To facilitate the design of G_e^{-1}, system (5.9) can be converted into:

$$\left(F, U\left\{G_{c1}, (G_P^{-1}, G_e^{-1})\right\}, G_M\right) \tag{5.10}$$

where $\{G_{c1},(G_P^{-1},G_e^{-1})\}$ is defined as U-SMC controller. Determine $\left(G_P^{-1}+G_e^{-1}\right)$ to work out the controller output u, which is the control input to the plant G_M. The eventual goal is to make plant output equal to the invariant controller output: $v = y$, that is, reaching $\left(G_P^{-1}+G_e^{-1}\right)\ G_M = 1$ under the proper dynamic inversion.

‘

5.2.2 Compensated plant inverter G_e^{-1} design procedure

Consider a general SISO CT state space model as:

$$\left\{\begin{array}{c} \dot{X} = F(X,u) \\ y = H(X) \end{array}\right\} \tag{5.11}$$

where $u, y \in R$, $X \in R^n$, $F \in R^n$ is a smooth mapping to represent the input to the state, and $H \in R$ is a smooth mapping to drive the states to the outputs. In this study, assume that there are no unstable zero dynamics (i.e., the model is reversible) and that the state X can be obtained through measurement or observation. Expand this model (5.11) into a multi-layer polynormal expression as follows:

$$\left\{\begin{array}{c} \dot{x}_1 = f_1(x_1,x_2,\ldots,x_{n-1},x_n) \\ \dot{x}_2 = f_2(x_1,x_2,\ldots,x_{n-1},x_n) \\ \vdots \\ \dot{x}_{n-1} = f_2(x_1,x_2,\ldots,x_{n-1},x_n) \\ \dot{x}_n = f_n(x_1,x_2,\ldots,x_{n-1},x_n) + g(x_1,x_2,\ldots,x_n)u + d \\ y = x_1 \end{array}\right\} \tag{5.12}$$

where d is the control interference and $|d| < \bar{d}$. When reaching $\left(G_P^{-1}+G_e^{-1}\right)\ G_M = 1$, the plant output equals the invariant controller output, that is, $y = v$. Therefore, the desired input–output tracking error compensated dynamics for the controlled system (5.12) can be defined as output tracking error $e = x_1 - x_d$, where x_d is the user-designed invariant controller output. From the designing procedure of the dynamic inverterG_P^{-1}, it is known that the direct relationship between u and y has been found after $m\,(m \le n)$ times differentiating the state variables in the output equation. Therefore, based on [27], the error equations are designed as:

$$\left\{\begin{array}{l} e_1 = x_1 - x_d \\ e_2 = \dot{e_1} = \dot{x_1} - \dot{x} \\ e_3 = \dot{e_2} = \ddot{x}_1 - \ddot{x}_d \\ \vdots \\ e_m = \dot{e}_{m-1} = {x_1}^{(m-1)} - {x_d}^{(m-1)} \end{array}\right\} \tag{5.13}$$

Where ${x_1}^{(m-1)}$ and ${x_d}^{(m-1)}$ are the $(m-1)$th order derivative of the plant output x_1 and desired output x_d. Specifically, the sliding surface function can be therefore defined by:

$$\sigma = c_1 e_1 + c_2 e_2 + \ldots + c_{m-1} e_{m-1} + e_m \tag{5.14}$$

From equation (5.14), the derivative of the sliding surface is

$$\begin{aligned}\dot{\sigma} &= c_1\dot{e}_1 + c_2\dot{e}_2 + \ldots + c_{m-1}\dot{e}_{m-1} + \dot{e}_m \\ &= c_1(\dot{x}_1 - \dot{x_d}) + c_2(\ddot{x}_2 - \ddot{x}_d) + \ldots + \left({x_1}^{(m)} - {x_d}^{(m)}\right)\end{aligned} \tag{5.15}$$

Where $c_i \in R^+, i \in R^+$. is the bandwidth sliding surface function coefficient. Same as the U-model stare space expression, replace the highest order derivative of the desired output ${x_d}^{(m)}$ with v, in this case, the other orders derivatives of the desired output ${x_d}^{(i)}(0 < i < m)$ can be expressed by the $(m-i)$ times integral operation of v, that is, ${x_d}^{(i)} = v\left(\frac{1}{s}\right)^{m-i}$, where $\frac{1}{s}$ is the Laplace transform of integration. In this case, error equations system (5.14) and sliding surface (5.15) can be converted into:

$$\left\{\begin{array}{l} e_1 = x_1 - v\left(\frac{1}{s}\right)^m \\ e_2 = \dot{e_1} = \dot{x_1} - v\left(\frac{1}{s}\right)^{m-1} \\ \vdots \\ e_m = \dot{e}_{m-1} = {x_1}^{(m-1)} - v\left(\frac{1}{s}\right) \end{array}\right. \tag{5.16}$$

$$\begin{aligned}\dot{\sigma} &= c_1\left(\dot{x}_1 - v\left(\frac{1}{s}\right)^{m-1}\right) + c_2\left(\ddot{x}_2 - \left(\frac{1}{s}\right)^{m-2}\right) + \ldots + \left({x_1}^{(m)} - v\right) \\ &= \sum_{i=1}^{m-1}\left(c_i{x_1}^{(i)} - v\left(\frac{1}{s}\right)^{m-i}\right) + \left({x_1}^{(m)} - v\right)\end{aligned} \tag{5.17}$$

However, in the actual calculation process, direct calculation of ${x_1}^{(m)}$ can be complicated, therefore, continuously differentiating the lower order derivates of ${x_1}^{(i)}$ and replace its first order derivates items with corresponding items in equation (5.12) until $i = m$. Therefore, the first $(m-2)$ times differentiating operation does not have x_n items and the expression of a series of derivatives of x_1 are:

$$\left\{\begin{array}{l} \dot{x}_1 = f_1(x_1, x_2, \ldots, x_{n-1}) = F_1(x_1, x_2, \ldots, x_{n-1}) \\ \ddot{x}_1 = \dot{F}_1 = \frac{\partial F_1}{\partial x_1}f_1 + \frac{\partial F_1}{\partial x_2}f_2 + \ldots + \frac{\partial F_1}{\partial x_{n-1}}f_{n-1} = F_2(x_1, x_2, \ldots, x_{n-1}) \\ \vdots \\ {x_1}^{(m)} = \frac{\partial F_{m-1}}{\partial x_1}f_1 + \frac{\partial F_{m-1}}{\partial x_2}f_2 + \ldots + \frac{\partial F_{m-1}}{\partial x_{n-1}}f_{n-1} + \frac{\partial F_{m-1}}{\partial x_n}(f_n + gu + d) \end{array}\right. \tag{5.18}$$

In this case, equation (5.17) can be expanded to:

$$\begin{aligned}\dot{\sigma} &= \sum_{i=1}^{m-1}\left(c_i{x_1}^{(i)} - v\left(\frac{1}{s}\right)^{m-i}\right) + \left({x_1}^{(m)} - v\right) \\ &= \sum_{i=1}^{m-1} c_i\left(F_i - v\left(\frac{1}{s}\right)^{m-i}\right) + \left(\frac{\partial F_{m-1}}{\partial x_1}f_1 + \frac{\partial F_{m-1}}{\partial x_2}f_2 + \ldots + \frac{\partial F_{m-1}}{\partial x_n}(f_n + gu + d) - v\right)\end{aligned} \tag{5.19}$$

Let $\dot{\sigma} = 0$, the equivalent controller output and switching controller output are

$$u_{eq} = -\left(\frac{\partial F_{m-1}}{\partial x_n}g\right)^{-1}\left(\sum_{i=1}^{m-1} c_i\left(F_i - v\left(\frac{1}{s}\right)^{m-i}\right) + \left(\frac{\partial F_{m-1}}{\partial x_1}f_1 + \frac{\partial F_{m-1}}{\partial x_2}f_2 + \ldots + \frac{\partial F_{m-1}}{\partial x_n}f_n - v\right)\right) \tag{5.20}$$

$$u_{sw} = -\left(\frac{\partial F_{m-1}}{\partial x_n} g\right)^{-1} (\varepsilon sgn(\sigma) + k\sigma),\ \varepsilon > 0, k > 0 \tag{5.21}$$

Therefore, $u = u_{eq} + u_{sw}$ Bring controller output u_s into sliding surface (5.19), it has:

$$\dot{\sigma} = -\varepsilon sgn(\sigma) - k\sigma + \frac{\partial F_{m-1}}{\partial x_n} d \tag{5.22}$$

Let $\varepsilon = \bar{d} + \rho,\ \rho > 0$. The Lyapunov function can be defined as $V = \frac{1}{2}\sigma^2$, then:

$$\begin{aligned} \dot{V} = \sigma\dot{\sigma} &= \sigma\left(-\left(\bar{d} + \rho\right) sgn(\sigma) - k\sigma + \frac{\partial F_{m-1}}{\partial x_n} d\right) \\ &= -\left(\bar{d} + \rho\right)|\sigma| - k\sigma^2 + \sigma\frac{\partial F_{m-1}}{\partial x_n} d \\ &\le -\rho|\sigma| - k\sigma^2 \le 0 \end{aligned} \tag{5.23}$$

Therefore, when $t \to \infty$, $\sigma = 0$. When $\sigma = 0$, equation (5.23) can be converted into:

$$e_m = -c_1 e_1 - c_2 e_2 - \ldots - c_{m-1} e_{m-1} \tag{5.24}$$

Let $A = \begin{bmatrix} 0 & 1 & \ldots & 0 \\ \vdots & \vdots & \ddots & \vdots \\ 0 & \ldots & \ldots & 1 \\ -c_1 & -c_2 & \ldots & -c_{m-1} \end{bmatrix}$, where A is Hurwitz. Let $E_1 = \begin{bmatrix} e_1 & e_2 & \ldots & e_{m-1} \end{bmatrix}^T$, then equation (5.24) can be rewrite as:

$$\dot{E}_1 = AE_1 \tag{5.25}$$

Consider $Q = Q^T > 0$. Due to A is Hurwitz, there will be a Lyapunov function:

$$A^T P + PA = -Q \tag{5.26}$$

The solution of equation (5.26) is $P = P^T > 0$. Based on equation (5.25), consider the Lyapunov function: $V_1 = E_1^T P E_1$, then:

$$\begin{aligned} \dot{V}_1 &= \dot{E}_1^T P E_1 + E_1^T P \dot{E}_1 \\ &= (AE_1)^T P E_1 + E_1^T (AE_1) \\ &= E_1^T A^T P E_1 + E_1^T P A E_1 = E_1^T \left(A^T P + PA\right) E_1 \\ &= -E_1^T Q E_1 \le -\lambda_{min}(Q)\|E_1\| \le 0 \end{aligned} \tag{5.27}$$

Where $\lambda_{min}(Q)$ is the smallest eigenvalue of the positive definite matrix Q. From $\dot{V}_1 \le 0$, it has $e_1 \to 0, e_2 \to 0, \ldots, e_{m-1} \to 0$. From equation (5.24), $e_m \to 0$. Based on error equations (5.13) and $e_i (i > 0) \to 0$, ${x_1}^{(i)} \to {x_d}^{(i)}$ will be established. In this case, the plant output y equals the designed invariant controller output v, that is, $\left(G_P^{-1} + G_e^{-1}\right) G_M = 1$ reached. Additionally, A is a Hurwitz matrix, which means the real part of the eigenvalue of the matrix A is negative, that is, $Re[\lambda_i] < 0$.

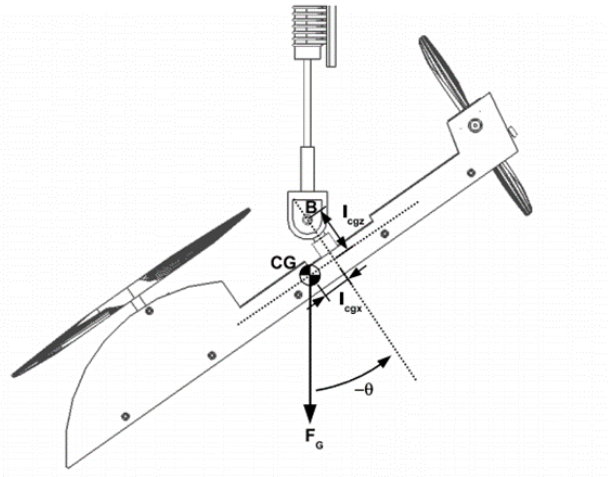

Figure 5.3: Simplified pitch model of the helicopter [75]

5.2.3 Simulation demonstrations

In this part, a simplified helicopter pitch dynamics model is selected to test the U-SMC method. The invariable controller G_{c1}, ideal plant inverter G_P^{-1}, and compensated plant inverter G_e^{-1} will be designed step by step according to Chapter 5.2.1 to 5.2.2. Then three experiments are arranged to demonstrate the consistency of the U-SMC method under the ideal error-free model, the model with uncertainty, and plus system noise based on the previous uncertain plant.

1. **Simplified helicopter pitch dynamic model**
   The schematic diagram of the helicopter [75] is shown in Figure 5.3. The nonlinear model of the pitch dynamics of the simplified helicopter is described by the following equation:

$$\ddot{\theta} I_{yy} + m_{hel} g l_{cgx} cos\theta + m_{hel} g l_{cgz} sin\vartheta + F_{vM} \dot{\theta} \tag{5.28}$$

   This simplified helicopter model has two degrees of freedom in the vertical direction with only one actuator: propeller lifting power. Let $\theta = x_1$, $\dot{\theta} = x_2$, convert nonlinear system (5.28) into state space expression:

$$\left\{ \begin{array}{l} \dot{x}_1 = x_2 \\ \dot{x}_2 = \frac{1}{I_{yy}} \left(-m_{hel} l_{cgx} g cos(x_1) - m_{hel} l_{cgz} g sin(x_1) - F_{vM} x_2 + u \right) \end{array} \right) \tag{5.29}$$

   where x_1 is the pitch angle θ and x_2 represents the pitch rate ω; I_{yy} is the second moment around the y-axis; m_{hel} is the mass of the helicopter; l_{cgx} and l_{cgz} are displacements from the centre point of mass (GC in 5.3) relative to the rotation joint B shown in Figure 5.3; F_{vM} is the pitch damping; u is the control torque exerted by the main blade of the helicopter around the y-axis;

2. **Invariant controller G_{c1} design**

   In order to make the system has no overshoot, therefore, system (5.29) should be a critical damping system that returns the system to equilibrium (desired reference) as fast as possible without overshooting. With reference to the U-SMC system design procedure proposed in Chapter 5.2.1, this study chooses system damping ratio $\zeta = 1$ and natural frequency $\omega_n = 5$. Accordingly, the desired closed-loop system gain is assigned with the:

$$\frac{Y(S)}{R(S)} = G(S) = \frac{25}{s^2 + 10s + 25} \tag{5.30}$$

   From Chapter 2.1.3, the invariant controller G_{c1} with a unit constant plant in a feedback control system is determined by taking the inverse of the closed loop transfer function (5.30) as below:

$$G_{c1} = \frac{G}{1-G} = \frac{25}{s^2 + 10s} \tag{5.31}$$

3. **Ideal inverter G_P^{-1} design**

   According to the ideal plant dynamic inverter G_P^{-1} design procedure in Chapter 2.2.2, continue to take the derivative to then it can be found:

$$\ddot{y} = \dot{x_2} = \frac{1}{I_{yy}}\left(-m_{hel}l_{cgx}gcos(x_1) - m_{hel}l_{cgz}gsin(x_1) - F_{vM}x_2 + u\right) \tag{5.32}$$

   Then the system (5.32) can be rewritten into U-model expression:

$$\left\{ \begin{array}{l} \ddot{y} = \lambda_0 + \lambda_1 u \\ \lambda_0 = \frac{1}{I_{yy}}\left(-m_{hel}l_{cgx}gcos(x_1) - m_{hel}l_{cgz}gsin(x_1) - F_{vM}x_2\right) \\ \lambda_1 = \frac{1}{I_{yy}} \end{array} \right) \tag{5.33}$$

   Let $\ddot{y}$ be replaced with v, then the inverter G_P^{-1} is designed as

$$u_i = \frac{v - \lambda_0}{\lambda_1} \tag{5.34}$$

4. **Compensated inverter G_e^{-1} design**

   Based on Chapter 5.2.1 and 5.2.2, the error equations are designed as:

$$\left\{ \begin{array}{c} e_1 = x_1 - v\left(\frac{1}{s}\right)^2 \\ e_2 = \dot{e_1} = \dot{x}_1 \ - v\frac{1}{s} \end{array} \right) \tag{5.35}$$

   The sliding function for the system (5.29) is:

$$\sigma = ce_1 + e_2 \tag{5.36}$$

   From equation (5.35) and (5.36), we have:

$$\begin{aligned} \dot{\sigma} = \ & c\dot{e_1} + \dot{e_2} = c\left(\dot{x}_1 - v\frac{1}{s}\right) + (\dot{x}_2 - v) \\ & = c\left(x_2 - v\frac{1}{s}\right) + \left(\frac{1}{I_{yy}}\left(-m_{hel}l_{cgx}gcos(x_1) - m_{hel}l_{cgz}gsin(x_1) - F_{vM}x_2\right) + \frac{u}{I_{yy}} - v\right) \end{aligned} \tag{5.37}$$

Parameter	Value	Unit
I_{yy}	0.0283	kgm^2
m_{hel}	0.9941	kg
l_{cgx}	0.0134	m
l_{cgz}	0.0289	m
F_{vM}	0.0041	Nm/rad/s
g	9.81	m/s^2

Table 5.1: Parameters for the helicopter characteristics

Bring U-model expression (5.33) into (5.57), it can be converted into:

$$\begin{aligned} \dot{\sigma} &= c\left(x_2 - v\frac{1}{s}\right) + (\lambda_0 + \lambda_1 u - v) \\ u_{eq} &= \frac{v - c\left(x_2 - v\frac{1}{s}\right) - \lambda_0}{\lambda_1} \\ u_{sw} &= -(\varepsilon sgn(\sigma) + k\sigma) \end{aligned} \tag{5.38}$$

Assume there is no disturbance first, let $\rho = 0.1$, $c = 10$ and $\varepsilon = \bar{d} + \rho = 0.1$. In order to keep the sliding rate [82], let $k = 1$, then the output of the compensated inverter G_e^{-1} is:

$$\begin{aligned} u_s &= u_{eq} + u_{sw} - u_i \\ &= \frac{v - 10\left(x_2 - v\frac{1}{s}\right) - \lambda_0}{\lambda_1} - \frac{v - \lambda_0}{\lambda_1} - (sgn(\sigma) + \sigma) \\ &= \frac{-10\left(x_2 - v\frac{1}{s}\right)}{\lambda_1} - (sgn(\sigma) + \sigma) \end{aligned} \tag{5.39}$$

To avoid system chattering, the switching operation should not be held if the system dynamic sliding inside the boundary $\xi \in R^+$. When the system dynamic is outside the boundary ξ, the switching function is defined by:

$$sat(\sigma) = \begin{cases} sgn(\sigma) & |\sigma| \geq \xi \\ \frac{\sigma}{\xi} & |\sigma| < \xi \end{cases} \tag{5.40}$$

For more precise convergence and assuming this system has no disturbance or uncertainty at the starter, ξ should be small. Let $\xi = 0.05$, then the compensated inverter G_e^{-1} is shown:

$$u_s = \frac{-10\left(x_2 - v\frac{1}{s}\right)}{\lambda_1} - (sat(\sigma) + \sigma) \tag{5.41}$$

The experiment modelling parameters are shown in Table 5.1. Here are the three simulation experiments demonstrating the efficiency of the proposed U-SMC method:

1. **Experiment 1**

   The first experiment assumes the helicopter system is perfectly modelled and free of distur-

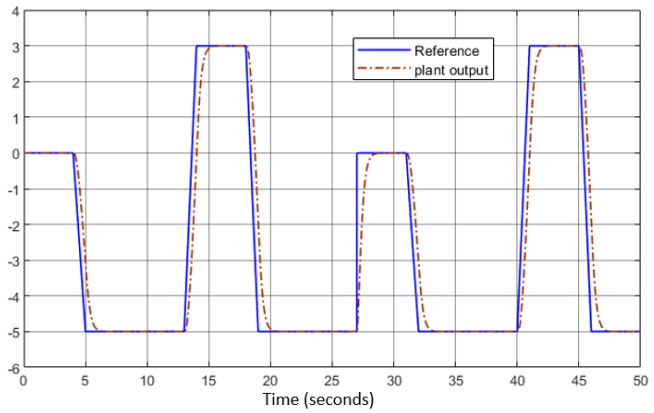

Figure 5.4: U-SMC system output and reference in Experiment 1

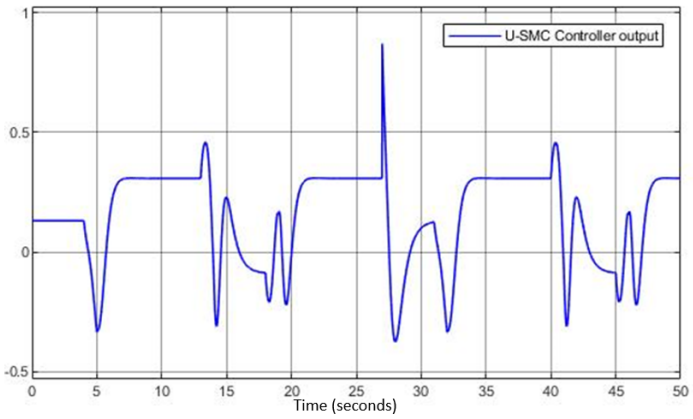

Figure 5.5: U-SMC controller output in Experiment 1

bances. In this case, the model of this system can be described with specific parameters:

$$\left\{ \begin{array}{l} \ddot{y} = \lambda_0 + \lambda_1 u \\ \lambda_0 = -4.618cos(x_1) - 9.958sin(x_1) - 0.1449x_2 \\ \lambda_1 = \frac{1}{0.0283} \end{array} \right\} \tag{5.42}$$

Figure 5.4 shows the tracking results of the ideal simplified helicopter model controlled by the U-SMC method. Figure 5.5 shows controller output. Figure 5.6 shows the compensated inverter output. It is clear that when the system is free of disturbance and uncertainties, only the U-controller is in charge of the whole system. The output of the U-SMC compensated inverter is zero, which means this inverter is not activated.

2. **Experiment 2**
In practical control system operation, a perfectly matched model will cost much. Therefore,

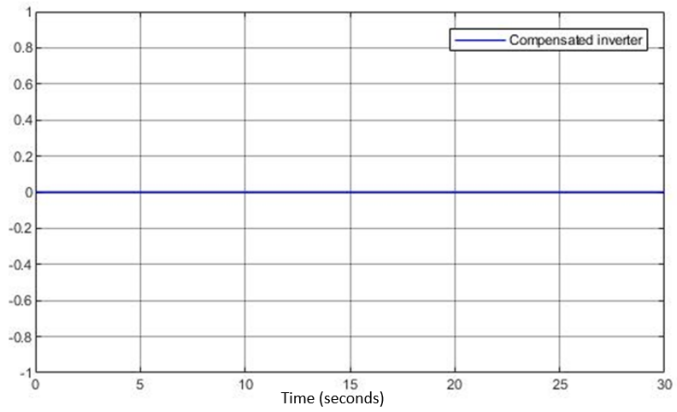

Figure 5.6: U-SMC compensated inverter output in Experiment 1

to accommodate such inaccuracies, system (5.29) is therefore changed into:

$$\left\{ \begin{array}{l} \dot{x}_1 = \Phi x_2 \\ \dot{x}_2 = \frac{1}{I_{yy}}\left(-m_{hel} l_{cgx} g cos(x_1) - m_{hel} l_{cgz} g sin(x_1) - F_{vM} x_2 + u\right) \end{array} \right) \tag{5.43}$$

Where Φ is the system uncertain coefficient and its amplitude changes from 0.5 to 1 with a rate of 1Hz. Figure 5.7 shows its variation curve. Φ is chosen randomly changed within its boundary, that is, the uncertain system will deviate by up to 50 % from the perfectly matched system. To avoid chattering, ξ should be larger than before. Let $\xi = 0.1$, then the switching function is shown:

$$sat(\sigma) = \left\{ \begin{array}{ll} sgn(\sigma) & |\sigma| \geq 0.1 \\ 10\sigma & |\sigma| < 0.1 \end{array} \right. \tag{5.44}$$

Figure 5.8 shows the tracking results of the ideal simplified helicopter model with internal

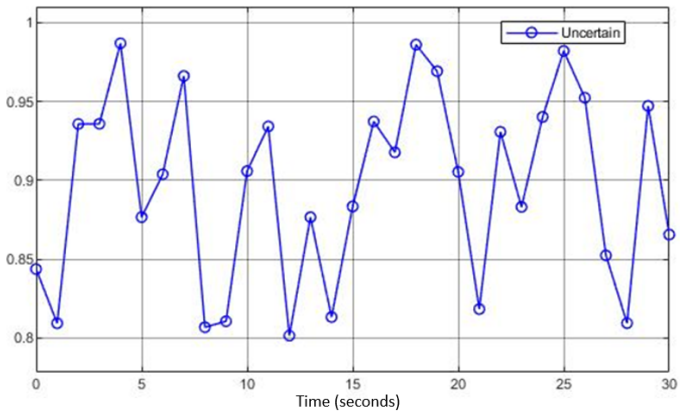

Figure 5.7: System uncertain coefficient

uncertainty controlled by the U-SMC method. Figure 5.9 shows the controller output.

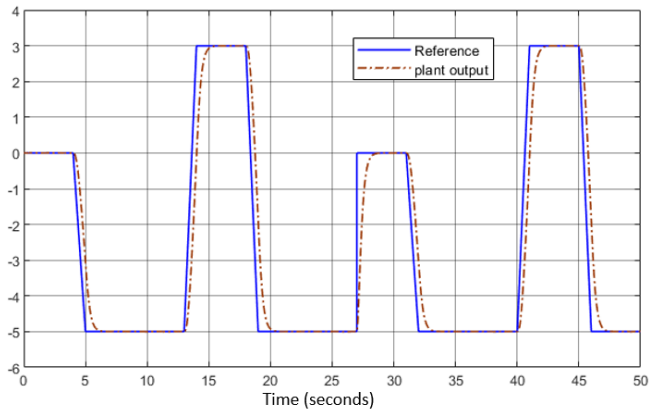

Figure 5.8: U-SMC system output and reference in Experiment 2

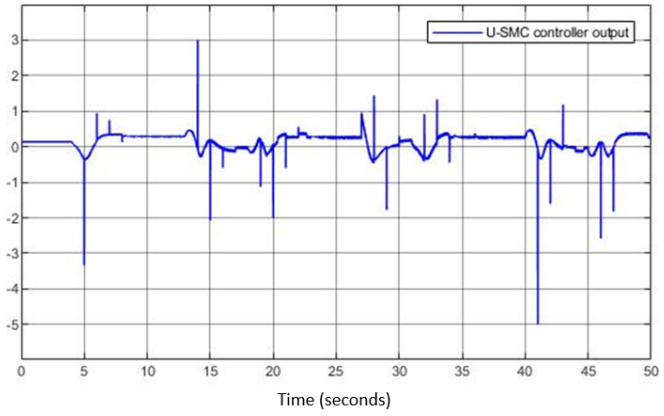

Figure 5.9: U-SMC controller output in Experiment 2

Figure 5.10 shows the compensated inverter output. It is clear that when system internal uncertainty affects the system, the system output can still track the desired reference well and the U-SMC compensated inverter is activated to improve the system's robustness.

3. **Experiment 3**

Consider a more complex and practical control situation to test the proposed control method: the system contains both modelling errors (internal uncertainties) and control system input noise (external disturbances). Therefore, to accommodate such inaccuracies and disturbances, system (5.29) is therefore changed into:

$$\left\{ \begin{array}{l} \dot{x}_1 = \Phi x_2 \\ \dot{x}_2 = \frac{1}{I_{yy}}\left(-m_{hel} l_{cgx} g cos(x_1) - m_{hel} l_{cgz} g sin(x_1) - F_{vM} x_2 + (u+d)\right) \end{array} \right\} \tag{5.45}$$

Where d is system noise/disturbance added into the control input channel. Φ changes the same as it in the system (5.43) from 0.5 to 1 with 1Hz variation frequency. d changes from 0 to 0.3 with 10Hz. Figure 5.11 shows the system noise/disturbance variation curve. Φ and

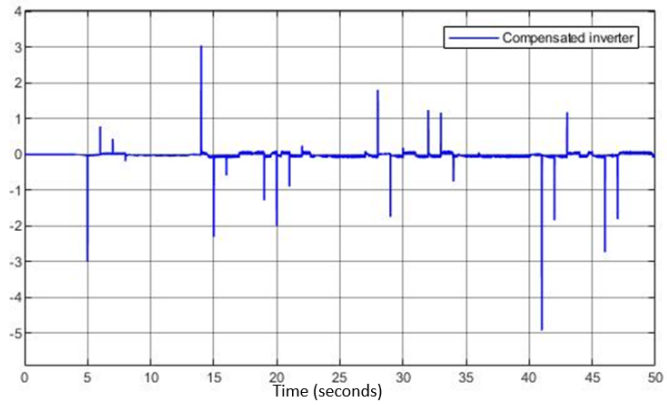

Figure 5.10: U-SMC compensated inverter output in Experiment 2

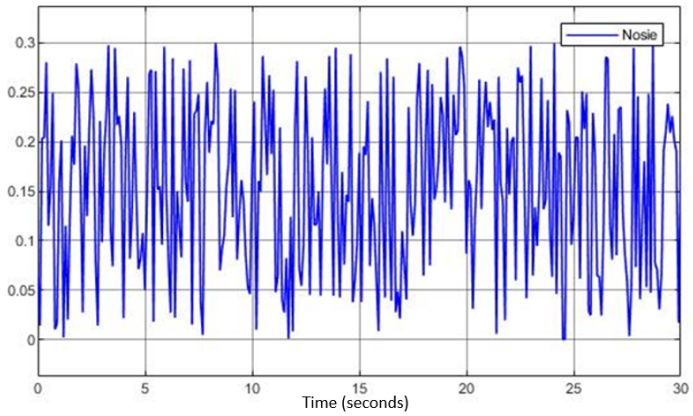

Figure 5.11: System control input noise/disturbance

d are randomly changed within their boundaries. In this system, based on the U-controller output of a perfectly matched plant which is shown in Figure 5.5, it is clear that the power of this controller output is small (less than 1), system noise/disturbance will therefore greatly affect system stability and control performance. Same as the boundary coefficient design for the system (5.43), to avoid chattering, $\xi = 0.1$ is chosen in Experiment 3. Figure 5.12 shows the tracking results with the desired reference of the ideal simplified helicopter model with both internal uncertainties and external system disturbance controlled by the U-SMC method. Figure 5.13 shows the controller output. Figure 5.14 shows the compensated inverter output. It is clear that when system internal uncertainty and external system disturbance affect the system, the U-SMC system output can still track the desired reference well and the U-SMC compensated inverter is activated to improve the system's robustness. It should be noticed the reason for the chattering in U-SMC controller output is to counter the impact of high-frequency noise interference in 5.13.

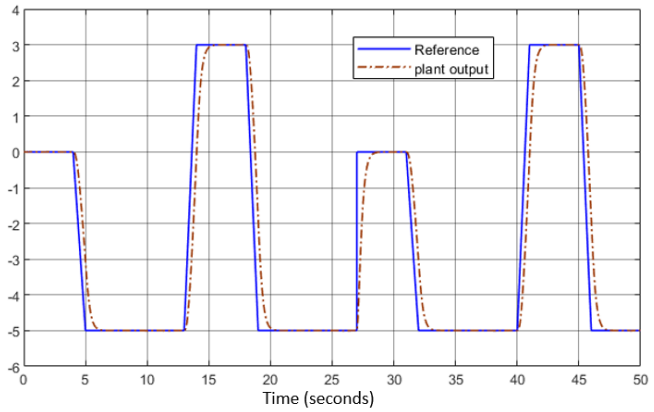

Figure 5.12: U-SMC system output and reference in Experiment 3

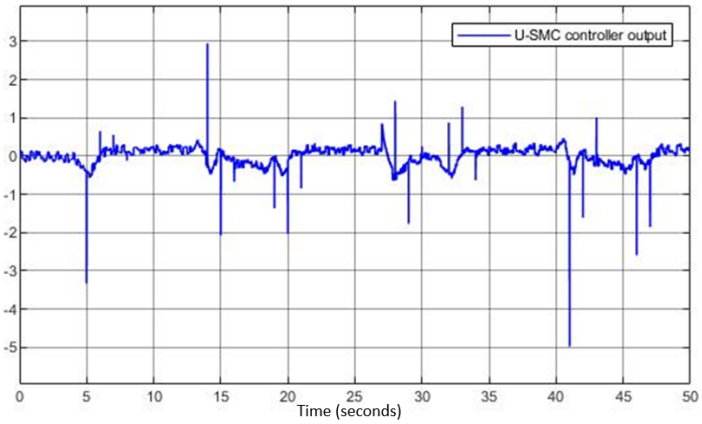

Figure 5.13: U-SMC controller output in Experiment 3

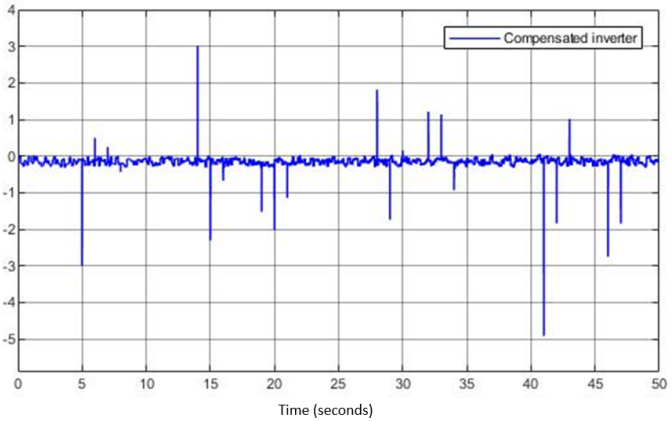

Figure 5.14: U-SMC compensated inverter output in Experiment 3

5.3 U-model based double sliding control

5.3.1 Problem statement

Dynamic inversion (DI), particularly the DI in terms of nonlinear expressions [85] in control system design, is one of the kernel issues, which many approaches have taken plant nonlinearity cancellation into a controllable equivalent linear dynamic by feedback linearisations [44, 104], and then design the corresponding control system. Although the DI concept provides concise control system design frameworks, the idealized assumption of the model perfectly matched has been challenging for applications and academic research. Consequently, this has motivated various methods to improve the robustness of DI. Adaptive approaches [62] are surely options for the solutions, but these are not the interest in the study. Accordingly, this study will focus on the robust approaches in dealing with model uncertainties/disturbances and the induced problems in the formulations of NDI-based control system design.

Incremental NDI (INDI) [94], this technique does not use required input to control the system. Alternatively, it takes the required change in the input. Therefore, the INDI only uses a small part of the model in DI, so it is more able to cope with model inaccuracies and more robust than NDI. Two commonly shared characteristics with NDI and INDI are feedback linearization and limited with affine nonlinear models. Sliding Mode Control based NDI (SMCNDI) [103], which proposes an incremental nonlinear dynamic inversion driven by sliding mode disturbance observers with application to a quadrotor fault tolerant control problem. Eigenvalue Assignment based NDI (EANDI) [105], it is not necessary to convert the nonlinear state space models into linear equivalent expressions by feedback linearisation prior to designing the control systems. The approach also claims able to cope with non-affine and non-minimum phase systems if the eigenvalues of error dynamics are properly selected to keep the desired dynamics stable. However, it is still an approach canceling nonlinearities instead of both cancellations of dynamics and nonlinearities.

U-control succeeded from the NDI control system design methods, has been proposed to cover the two essential tasks, establishing a universal NDI platform to remove the pre-requirement of the state feedback linearisation and configuring the control system framework to decompose the whole NDI for the solution of controller output into two parallel DIs that is DI of control system performance to form an external linear feedback control loop and DI of the plant to cancel both the plant dynamics and nonlinearities into a unite constant. The perfectly matched model is the foundation for U-control, however, this assumption should be removed for practical applications. Chapter 5.2 used sliding mode to enhance the robustness of the U-control method and increase its independence to modelling accuracy. In the U-SMC system, the sliding mode is used to design the compensated inverter to cancel the effect of system uncertainties and disturbances to the U-control system, therefore improving the U-control system's robustness. This study tries another way to combine the U-control and SMC methods by using the sliding mode to design the DI for

the controlled plant to establish a general robust U-control framework. Without the continuous and tedious differentiation process to find the relationship between the system input and output, the sliding mode can provide and calculate the DI directly. Accordingly, the major contributions of this study:

1. Propose a DSMC scheme to establish a robust dynamic inverter to cancel the plant nonlinearities and dynamics, which removes the request for a plant nominal model and eliminates chattering in classical SMC design. Lyapunov stability is used twice for respectively determining the switching control and equivalent control in the SM Inverter (SMI).

2. Establish a UDSM control (UDSMC) system design platform and present bench tests with computational experiments to validate the analytical results and function block connections.

5.3.2 model-mismatched U-control system structure

To accommodate mismatched plant model and external disturbance, Figure 5.15 proposes a model mismatched U-control system structure, expressed functionally below,

$$\sum = \left(F, G_{c1}, G_P^{-1}, G_M\right) \Leftrightarrow \sum = \left(F, G_{c1}, C\left(G_P^{-1}, G_M\right)\right) \Leftrightarrow \sum = (F, G_{c1}, I_n) \tag{5.46}$$

where F presents the U-control system structure, G_{c1} is a linear invariant controller to specify the external loop control performance, $C()$ is gain for a closed-loop containing G_P^{-1} and G_M, and G_P^{-1} is the nominal dynamic inversion for the controlled plant model G_M that aims to cancel the system dynamics and nonlinearities.

To still achieve the similar control target as described in stage 1 (model matched U-control) in Chapter 2.1.3, different from the conventional U-control system design, the critical technical challenge is how to obtain an inner closed-loop system $C(G_P^{-1}, G_M) = I_n$ with I_n being a nth order identity matrix. As sliding mode control (SMC) has strong robustness in performance, fast response, and conciseness in design, this study presents a scheme using SMC for DI, called SM inverter (SMI) in brief.

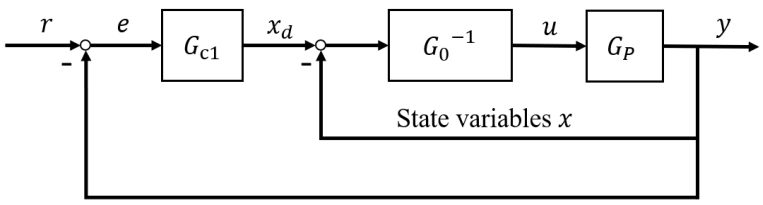

Figure 5.15: Model mismatched U-control system framework

5.3.3 U-model based double sliding control

This Chapter presents a scheme using SMC to derive a robust dynamic inverter G_P^{-1} to achieve $C(G_P^{-1}, G_M) = I_n$. A widely used SMC approach [111] is referred to formulate the dynamic inverter with $u = u_{eq} + u_{sw}$, which is a prototype of combing equivalent input u_{eq} and switching input u_{sw}. Once the sliding surface is determined, then the sliding mode inverter (SMI) can be obtained in a revised SMC formulation. Accordingly, this study proposes a double sliding mode control (DSMC) method, a global SM band with interval δ to drive errors into and remain in the stable interval, a local SM line to attract the error within the stable interval toward zero exponentially monotonically. Figure 5.16 shows the double sliding surface against the classical one, where the yellow plus orange curve is classical SMC and the yellow plus green curve is DMSC. The DMSC design procedure is explained below.

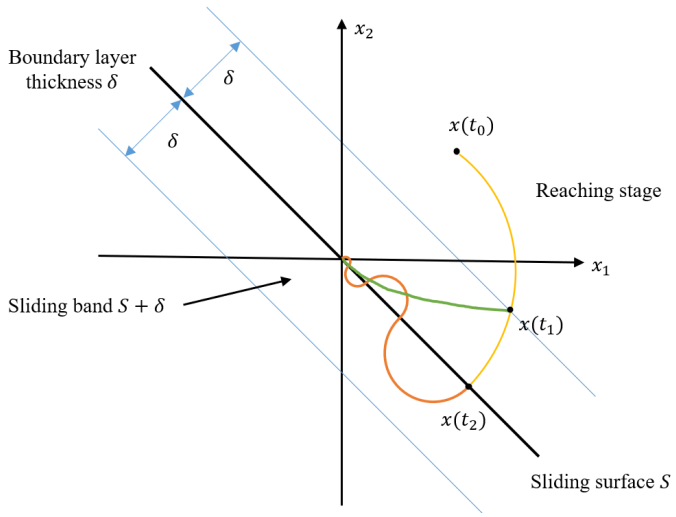

Figure 5.16: Sliding stage comparison of system states

1. Design a global sliding surface σ_g to specify the considered system having desired performance once the system remains in the sliding mode. Realistically a small interval (boundary) δ is assigned for the distance to the classical sliding surface σ. So that σ_g presents a sliding band surface with thickness δ. For a nth order dynamic plant, define a $(n-1)$th order of state tracking error vector as

$$E = X - X_d = \left[\begin{array}{cccc} e_1 = x_1 - x_d & e_2 = \dot{x_1} - \dot{x}_d & \cdots & e_{m-1} = {x_1}^{(n-1)} - {x_d}^{(n-1)} \end{array} \right]^T \tag{5.47}$$

where ${x_1}^{(i)}$ and ${x_d}^{(i)}$ are the ith order derivatives of the plant model state x_1 and desired state x_d, respectively. Then set up a classical sliding surface function σ [111] in form of

$$\sigma = c_1 e_1 + c_2 e_2 + \ldots + c_{m-2} e_{m-2} + e_{m-1} \tag{5.48}$$

where coefficient vector $C = \begin{bmatrix} c_1 & c_2 & \cdots & c_{m-2} \end{bmatrix} \in R^+$ is chosen in terms of Hurwitz stable. Then the global sliding surface with the boundary δ in the sliding mode interval is designed as

$$\sigma_g = \sigma + \delta_1, \;\; 0 \le |\delta_1| \le |\delta| \tag{5.49}$$

2. Design a switching controller u_{sw} to drive the system states to the sliding surface (interval/band) in finite time and keep the system state motion on the surface thereafter. Assign a Lyapunov function $V_g = \frac{1}{2}(\sigma_g)^2 = \frac{1}{2}(\sigma + \delta_1)^2$ and the corresponding derivative is given by $\dot{V}_g = \dot{\sigma_g}\sigma_g = \dot{\sigma}(\sigma + \delta_1)$. Let $\dot{\sigma} = f_g + u_{sw}$, where f_g represents all the neglected bounded terms in classical SMC design. Then the derivative of the Lyapunov function gives

$$\dot{V}_g = \dot{\sigma}(\sigma + \delta_1) = \big(f_g + u_{sw}\big)(\sigma + \delta_1) \tag{5.50}$$

To satisfy $\dot{V}_g \le 0$ for stability, choose

$$u_{sw} = -k_g sgn(\sigma + \delta_1) \tag{5.51}$$

where $k_g \in R^+ > \big|f_g\big|$ is a positive gain of the design choice and $sgn()$ is the sign function.

3. Design a local sliding surface σ_l. Then design an equivalent controller u_{eq} with the condition of driving the system state motion towards $\dot{\sigma_l} = 0$ and $\sigma_l = 0$ asymptotically. For the local sliding surface, assign it as the classical Hurwitz stable manifold, that is, $\sigma_l = \sigma$. Assign a Lyapunov function $V_l = \frac{1}{2}(\sigma)^2$ and the corresponding derivative is given by $\dot{V}_l = \dot{\sigma}\sigma$. Let

$$\dot{\sigma} = f_l + u_{eq} = k_2\sigma + u_{eq} \tag{5.52}$$

where f_l represents all neglected bounded terms in classical SMC design. Let the matching condition of $f_l = k_2\sigma$ satisfied, where k_2 is a bounded unknown tangent factor of σ. To derive the equivalent controller u_{eq} satisfying the Lyapunov stability conditions of $\dot{V} = 0$ and $V_l = 0$, expand the derivative of the Lyapunov function as

$$\dot{V}_l = \dot{\sigma}\sigma = \big(f_l + u_{eq}\big)\sigma = \big(k_2\sigma + u_{eq}\big)\sigma \tag{5.53}$$

To satisfy $\dot{V}_l \le 0$, choose

$$u_{eq} = -k_l\sigma, \;\; k_l \in R^+ > |k_2| \tag{5.54}$$

4. Finally, the Double SM controller is formulated as $u = u_{eq} + u_{sw}$

Figure 5.17 shows the control system structure to facilitate the explanation of the design procedure. Assume the plant is BIBO and its inverse exists, the DSMC is globally stable, and force $C(G_P^{-1}, G_M) = I_n$. The DSMC design procedure actually is a process of proof. The first Lyapunov stability used in the second step is to force the state vector X to converge to the sliding band $\sigma_g = \sigma + \delta_1, \;\; 0 \le |\delta_1| \le |\delta|$ by switching control. The second Lyapunov stability used in the third

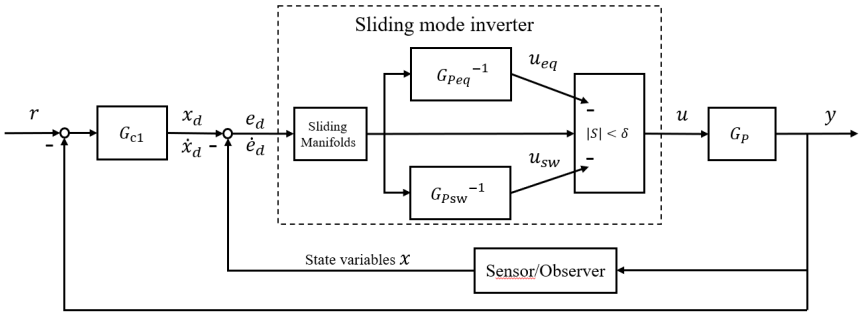

Figure 5.17: UDSMC system design framework

step is to force the state vector X in the sliding band to converge asymptotically to the final sliding surface $\sigma_l = \sigma = 0$ by continuous equivalent control. If $C(G_P^{-1}, G_M) = I_n$ asymptotically and the linear invariant controller G_{c1} is Hurwitz stable, the U-control system is Hurwitz stable because of $G = \frac{C_{c1}}{1+C_{c1}}$.

5.3.4 Simulation demonstrations

In this part, a simplified helicopter pitch dynamics model is selected to test the UDSMC method. The invariable controller G_{c1}, sliding mode inverter will be designed step by step according to Chapter 5.3.3. Then two experiments are arranged to demonstrate the consistency of the UDSMC method under 1) the plant model with uncertainty, and 2) the model plant plus system noise based on the previous uncertain plant.

1. **The simplified helicopter pitch dynamic model**
   The simplified helicopter pitch dynamic model is the same as Chapter 5.2.3:

$$\left\{ \begin{array}{l} \dot{x}_1 = x_2 \\ \dot{x}_2 = \frac{1}{I_{yy}}\left(-m_{hel} l_{cgx} g cos(x_1) - m_{hel} l_{cgz} g sin(x_1) - F_{vM} x_2 + u\right) \end{array} \right) \tag{5.55}$$

   where x_1 is the pitch angle θ and x_2 represents the pitch rate ω; I_{yy} is the second moment around the y-axis; m_{hel} is the mass of the helicopter; l_{cgx} and l_{cgz} are displacements from the centre point of mass (GC in 5.3) relative to the rotation joint B shown in Figure 5.3; F_{vM} is the pitch damping; u is the control torque exerted by the main blade of the helicopter around the y-axis;

2. **Invariant controller G_{c1} design**
   In order to make the system has no overshoot, therefore, system (5.55) should be a critical damping system that returns the system to equilibrium (desired reference) as fast as possible without overshooting. With reference to the UDSMC system design procedure

proposed in Chapter 5.3.3, this study chooses system damping ratio $\zeta = 1$ and natural frequency $\omega_n = 5$. Accordingly, the desired closed-loop system gain is assigned with the:

$$\frac{Y(S)}{R(S)} = G(S) = \frac{25}{s^2 + 10s + 25} \tag{5.56}$$

From Chapter 2.1.3, the invariant controller G_{c1} with a unit constant plant in a feedback control system is determined by taking the inverse of the closed loop transfer function (5.30) as below:

$$G_{c1} = \frac{G}{1-G} = \frac{25}{s^2 + 10s} \tag{5.57}$$

3. **Sliding mode inverter design**
   According to the sliding mode inverter design procedure in Chapter 5.3.3, the sliding surface function can be designed as:

$$\sigma = ce_1 + e_2 = ce_1 + \dot{e}_1 \tag{5.58}$$

Then the global and local sliding surface with the boundary δ in the sliding mode interval is designed as

$$\begin{aligned} \sigma_g &= \sigma + \delta_1, \;\; 0 \le |\delta_1| \le |\delta| \\ \sigma_l &= \sigma \end{aligned} \tag{5.59}$$

Assign a Lyapunov function $V_g = \frac{1}{2}\left(\sigma_g\right)^2 = \frac{1}{2}(\sigma + \delta_1)^2$ and $V_l = \frac{1}{2}(\sigma)^2$, their corresponding derivatives are given by $\dot{V}_g = \dot{\sigma_g}\sigma_g = \dot{\sigma}(\sigma + \delta_1)$ and $\dot{V}_l = \dot{\sigma}\sigma$. Let $\dot{\sigma} = f_g + u_{sw}$, where f_g represents all the neglected bounded terms in classical SMC design. Then the derivative of the Lyapunov function gives

$$\begin{aligned} \dot{V}_g &= \dot{\sigma}(\sigma + \delta_1) = \left(f_g + u_{sw}\right)(\sigma + \delta_1) \\ \dot{V}_l &= \dot{\sigma}\sigma = \left(f_l + u_{eq}\right)\sigma = \left(k_2\sigma + u_{eq}\right)\sigma \end{aligned} \tag{5.60}$$

To satisfy $\dot{V}_g \le 0$ and $\dot{V}_l \le 0$ for stability, choose

$$\begin{aligned} u_{sw} &= -k_g sgn(\sigma + \delta_1), \;\; k_g \in R^+ > \left|f_g\right| \\ u_{eq} &= -k_l\sigma, \;\; k_l \in R^+ > |k_2| \end{aligned} \tag{5.61}$$

where $f_g = \frac{1}{I_{yy}}\left(-m_{hel}l_{cgx}gcos(x_1) - m_{hel}l_{cgz}gsin(x_1) - F_{vM}x_2\right)$ according to system (5.55).

The experiment modelling parameters are the same as Table 5.1. The UDSMC design coefficients are listed in Table 5.2. Here are the two simulation experiments demonstrating the efficiency of the proposed UDSMC method:

1. **Experiment 1**
   In practical control system operation, a perfectly matched model will cost much or even be

Coefficient	Value
c	10
k_g	3
k_l	3
δ	1

Table 5.2: Parameters for UDSMC

unimplementable. Therefore, to accommodate such inaccuracies, system (5.55) is therefore changed into:

$$\left\{ \begin{array}{l} \dot{x}_1 = \Phi x_2 \\ \dot{x}_2 = \frac{1}{I_{yy}}\left(-m_{hel} l_{cgx} g cos(x_1) - m_{hel} l_{cgz} g sin(x_1) - F_{vM} x_2 + u\right) \end{array} \right) \tag{5.62}$$

Where Φ is the system uncertain coefficient and its amplitude changes from 0.5 to 1 with a rate of 1Hz. Figure 5.18 shows its variation curve. Φ is chosen randomly changed within its boundary, that is, the uncertain system will deviate by up to 50 % from the perfectly matched system. Figure 5.19 shows the tracking results with reference of the ideal

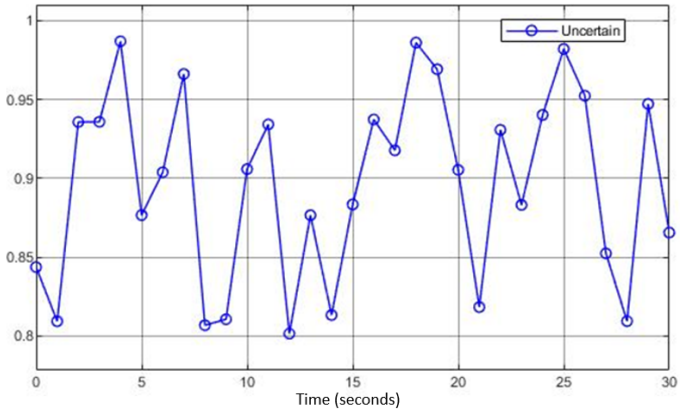

Figure 5.18: System uncertain coefficient

simplified helicopter model with internal uncertainty controlled by the UDSMC method. Figure 5.20 shows the controller output. Figure 5.21 shows the tracking error. It is clear that when system internal uncertainty affects the system, the UDSMC system output can still track the desired reference well.

2. **Experiment 2**

   Consider a more complex and practical control situation to test the proposed control method: the system contains both modelling errors (internal uncertainties) and control system input noise (external disturbances). Therefore, to accommodate such inaccuracies

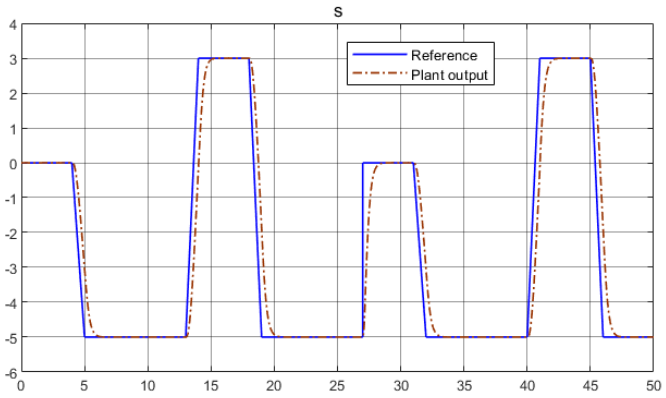

Figure 5.19: UDSMC system output and reference in Experiment 1

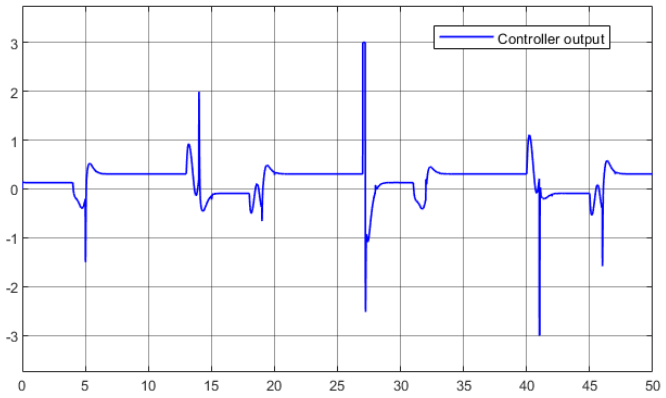

Figure 5.20: UDSMC controller output in Experiment 1

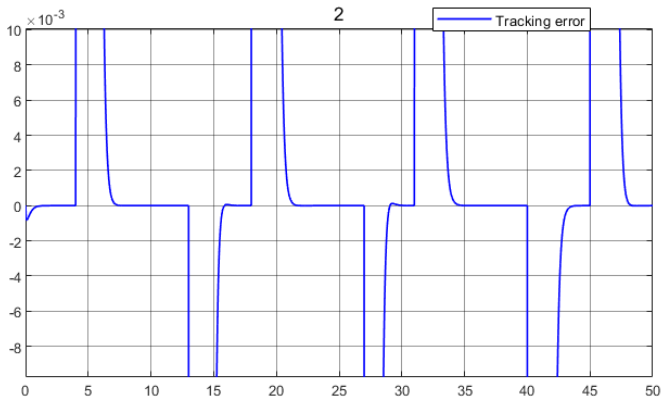

Figure 5.21: UDSMC system output tracking error in Experiment 1

and disturbances, system (5.55) is therefore changed into:

$$\left\{ \begin{array}{l} \dot{x}_1 = \Phi x_2 \\ \dot{x}_2 = \frac{1}{I_{yy}}\left(-m_{hel} l_{cgx} g cos(x_1) - m_{hel} l_{cgz} g sin(x_1) - F_{vM} x_2 + (u+d)\right) \end{array} \right\} \tag{5.63}$$

where d is system noise/disturbance added into the control input channel. Φ changes the same as it in the system (5.62) from 0.5 to 1 with 1Hz variation frequency. d changes from 0 to 0.3 with 10Hz. Figure 5.22 shows the system noise/disturbance variation curve. Φ and

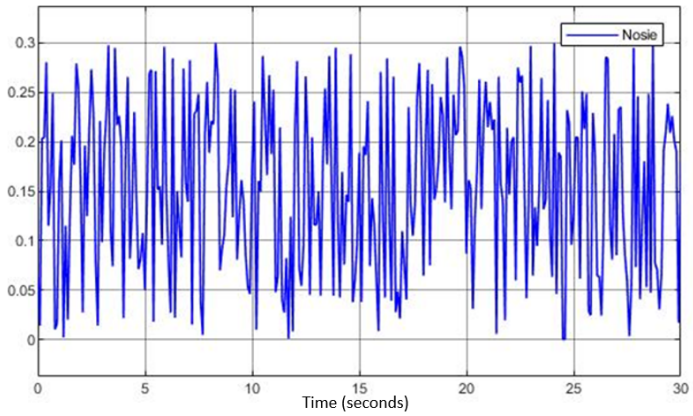

Figure 5.22: System control input noise/disturbance

d are randomly changed within their boundaries. In this system, based on the UDSMC output in experiment 1 which is shown in Figure 5.20, it is clear that the average power of this controller output is small (less than 1), system noise/disturbance will therefore greatly affect system stability and control performance. Figure 5.23 shows the tracking results with the desired reference of the ideal simplified helicopter model with both internal uncertainties and external system disturbance controlled by the UDSMC method. Figure 5.24 shows the controller output. Figure 5.25 shows the UDSMC output tracking error. It is clear that when system internal uncertainty and external system disturbance affect the system, the UDSMC system output can still track the desired reference well and serious chattering problems are not observed from the UDSMC controller output considering the impact of high-frequency noise disturbance in 5.24. Although the tracking error in experiment 2 is greater than that in experiment 1, it is acceptable. In summary, these two experiments demonstrate that the proposed UDSMC method can improve the robustness of the U-control method under system uncertainties and external disturbances.

5.4 Summary

This study firstly introduces a new sliding mode enhanced U-control method (U-SMC) for the nonlinear systems, which shows a strong stable ability to control uncertain and disturbing

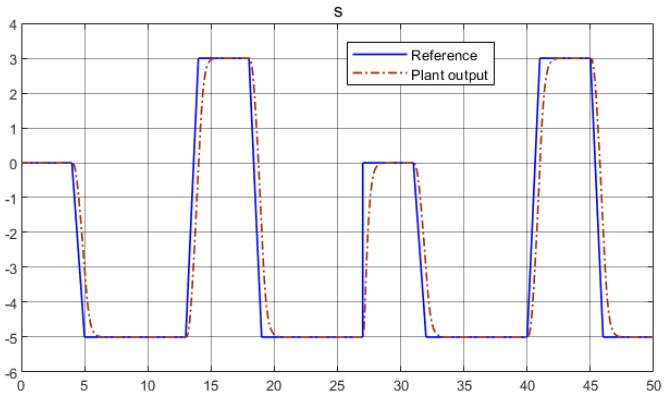

Figure 5.23: UDSMC system output and reference in Experiment 2

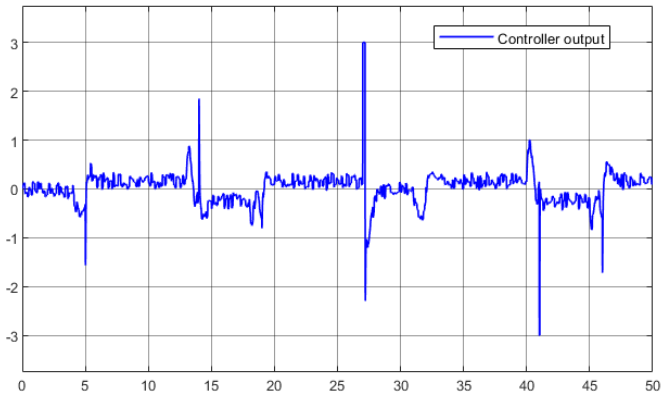

Figure 5.24: UDSMC controller output in Experiment 2

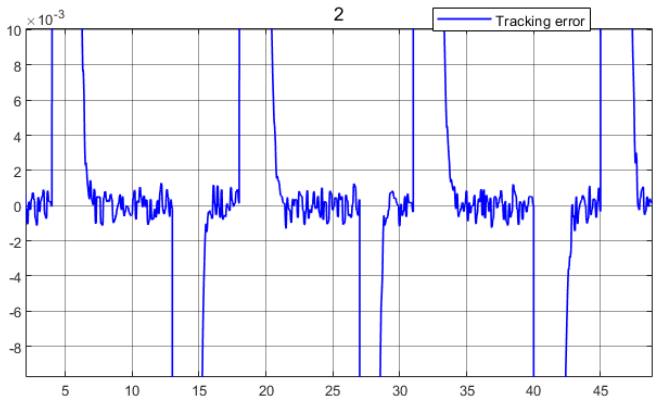

Figure 5.25: UDSMC system output tracking error in Experiment 2

plants. The overall scheme is based on the U-control structure wherein its dynamic inverter is compensated by robust sliding mode control (SMC). This work is able to combine the strong robustness of the SMC method and the control-oriented nature of the U-control to provide a comprehensive uncertain system control scheme, therefore, it is expected to prove clearly useful for practical control applications. Secondly, against classical NDI, based on the idea of U-SMC, this study attempts to treat all system dynamics as unknown disturbances and uses a sliding mode control algorithm to directly design the dynamic inversion to cancel the system's complex nonlinearities. This UDSMC not only reduces the design complexity of the control system but also reduces the system information requirements (only the order and error of the controlled plant need to be known). The effectiveness of these proposed SMC-enhanced U-control methods has been verified by simulation experiments. Based on the experiment results, the use of the sliding band in the UDSMC method can effectively compress the chattering problem without affecting the control performance from Figures (5.9 5.20) and (5.13 5.24).

For future work, firstly, the proposed method should be further tested and analyzed to show their comparative advantages and disadvantages. The proposed U-SMC and UDSMC methods are only for SISO systems, therefore, these proposed schemes should be expanded to multiple input and multiple outputs (MIMO) systems, especially underactuated and overactuated systems. Secondly, state observers should be considered sooner or later because full system state variables are not always easily measured in most practical modern control engineering systems. At the same time, it is also interesting to apply the proposed methods to real-time control systems.

CHAPTER 6

U-CONTROL BASED TRAJECTORY TRACKING CONTROL OF QUADROTOR

6.1 Introduction

The quadrotor has the advantages of Vertical Take-Off and Landing (VTOL) aircraft along with a smaller size, more payload capability, greater hover stability, and greater manoeuvrability. Compared with conventional aircraft, quadrotor UAVs have a simpler mechanical structure and easier take-off conditions. Nowadays, particularly in academia and the industry, along with the research and development communities, there has been a growth of interest in UAVs [5, 81, 95]. Probably, the feasibility of effectively performing various tasks with a wide range of applications like courier delivery, spraying of pesticides, aerial photography, surveying and mapping, wildfire surveillance, search and rescue missions, and several others, could have whetted this popularity [81]. Besides the endurance, cost, and size of the unmanned aircraft being highly attractive, the possibility of keeping human pilots out of danger (human capacity or aircraft failure) could be a matter of high concern [5]. Nevertheless, in the case of practical flight missions, there could be the risk of the stability of the aircraft being degraded sensitively by obstacles in the air, sudden changes of command, and turbulent changes in weather conditions. Hence, in the flight process, it is crucial to have a flight controller design that could provide the aircraft with robust and accurate control.

As a result of the quadrotor structures with the existing six-state outputs, which include the angles and the robot positions in such a manner that there would be only four rotors available for control inputs, the quadrotor UAV is known as an underactuated system. The rotational and transitional movements of the quadrotor are made possible by the speed variations of the rotors. Overall, the basic control target of the quadrotors involves the control of the altitude and the

attitude for the quadrotor to continue holding the same position in the specified location [60]. There could be several issues of challenges in the control of the UAVs, such as disturbances from the atmosphere and input constraints, nonlinear components, time-varying states and delays, unmodelled dynamics, the uncertainty of the parameters, underactuation, coupled states, open-loop instability, and the MIMO structure [57, 106]. Thus, for the control of the quadrotors several control schemes have been applied. The literature reported the outcomes of the methods that were non-adaptive like the state feedback [7], Proportional–Integral–Derivative (PID) [93], and the Linear-Quadratic-Regulator (LQR) [63].

Nonetheless, robust and adaptive methods of control would display a better control performance because quadrotor system dynamics are nonlinear in addition to being time-varying. Sliding Mode Control (SMC) is a conventional method of control for dealing with bounded external disturbances, nonlinearities, the properties of time variations, and other uncertainties [85]. Zheng and Xiong [109] developed an integrated approach to quadrotor attitude and position tracking control, in which the dynamics model is divided into underactuated and fully actuated subsystems. To compensate for faults in quadrotor motor actuators, the SMC observer applies linear parameter changes [10]. While in the case of quadrotor systems that are underactuated and uncertain, it is proposed to have a system for tracking and stability control according to the technique of the SMC [46]. Nevertheless, in the pertinent paper, a fully actuated dynamic model of the quadrotor was not considered suitable for our application. Initially, the continuous-time quadrotor dynamic model was converted to a discrete-time model [108]. Later, to control the tracking and stability of the modified quadrotor model, a discrete SMC was proposed. Mofid and Mobayen [66] studied the efficiency of adaptive SMC under uncertain model parameters, Lyapunov's proof method also exhibits its finite-time stability. The proposed method is evaluated by simulation.

Nonetheless, many issues still remain to be resolved in quadrotor control. Most of the existing quadrotor controllers are designed based on a simplified dynamic model that ignores its complex nonlinearities and disturbances. Among them, the decoupling problem caused by the complex transformation between the frame systems is important, which directly increases the design difficulty of the quadrotor position controller [107, 114]. [56] proposed a nonlinear decoupling controller using surface control and disturbance observer, but the radical term that appears in the denominator of the decoupling algorithm will undoubtedly limit its application. [107] improves the decoupling method based on [56] to achieve position tracking, which reduces the trigonometric computation, but it has the same problem as [56], the radical item will limit its application. [33] only decouples yaw dynamics from other dynamics. [45] proposed a fuzzy logic controller to decouple the position and attitude of the quadrotor, but the design of its inner loop attitude controller ignored nonlinear dynamics.

Additionally, the majority of the early works have evaluated control methods through simulations [19, 28, 29, 43, 67], only certain works could establish real-time control on quadrotors

[29, 38, 69]. There are significant differences between real-time experiments and simulations. In most simulation studies, the control signal is usually considered to be the torque or force produced by the rotor. Therefore, rotors with dynamic models are ignored. Furthermore, aerodynamic perturbations, matrix asymmetry of the moment of inertia, mass imbalance, and effects of wind and eddy currents, besides the air friction and that between the air and the drone were also neglected. In addition to all the above factors, another crucial aspect is the measurement of velocity sensor noise.

Considering the above real-time experimental results, the experimental test of QBall2 by Quanser in [29] has a spherical outer protective shell, its diameter is about twice the length of the quadrotor. While protecting the fuselage, this kind of protective shell will also increase its mass, which will increase the moment generated when the quadrotor's attitude changes and result in affecting the stability design of the control system as well as its test of the anti-disturbance ability of the flight controller. The quadrotor in [69] is mounted on a passive mechanical suspension to reduce the effect of rotor vibration, and at the same time limit the small angular changes of the aircraft. [38] requires a large amount of actual flight data to train reinforcement learning models, which is therefore time and computationally expensive. In this study, a MIMO-ESO is designed to estimate the disturbance and unmeasured velocities. The Lyapunov analysis is used to prove the convergence boundary of ESO estimated error. For tracking a time-varying trajectory of the quadrotor stably, the Double Sliding Mode Control (DSMC) based inverter (for robustness and nonlinear dynamic cancellation) and a U-controller (for the control performance specification) are included in the control system. The Lyapunov analysis proved the stability of the proposed control system, and the Hurwitz stability theory was applied to designing the related sliding manifolds coefficients. The control efficiency is tested and evaluated by real-time experimental Parrot Minidrone.

Summarily, the major contributions of this chapter are:

1. To the authors' knowledge, this is the first study to apply the U-control method to a real-time application (quadrotor control).

2. Proposing a quadrotor decoupling algorithm, using an indirect control strategy (position control by controlling the angle) turns the original underactuated system into a fully actuated system. This decoupling algorithm is implemented by the DSMC method, which avoids the square root calculation [56, 107].

3. Based on Lyapunov analysis, presenting a MIMO-ESO for unmeasured velocities estimation and a robust framework for flight control of quadrotors based on the ESO UDSMC method.

4. Expand the SISO implementation and application of the UDSMI [122] into MIMO systems with obvious progression in integrating SISO UDSMC and MIMO UDSMC plus decoupling algorithm.

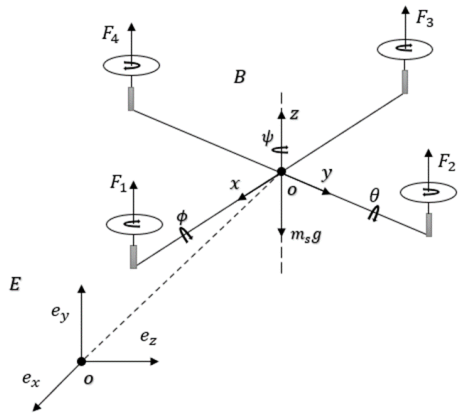

Figure 6.1: Quadrotor aircraft framework

5. Comparative experimental studies with the built-in PID controller (come from the product) and SMC method (advanced control algorithm) are involved to show the efficiency of the proposed controller.

The remaining portion of this chapter has been arranged as follows. Chapter 6.2 introduces the dynamical model of the quadrotor and control problems for follow-up development. In Chapter 6.3, the MIMO-ESO is derived to estimate the unmeasured quadrotor's velocities. Chapter 6.4 presents the UDSMC method first, then comes with its quadrotor flight controller design procedures, coefficients designed principle, and stability analysis. Also, it proposes a new decoupling algorithm for the quadrotor flight operation. Chapter 6.5 presents the experimental bench tests, which show the experimental setup procedure, design parameters of the involved control methods, and experiment results to compare to demonstrate the efficiency of the proposed control system. Chapter 6.6 concludes the study.

6.2 Dynamic description and problem statement

6.2.1 Quadrotor Dynamic model

This study considers and tests followed quadrotor motion control: 1) Roll and pitch control: which changes the output power of the neighbouring motors to tilt; 2) Horizontal movement control, the roll or pitch of the vehicle will generate a horizontal component of the rotor lift, thereby realizing the horizontal movement of the quadrotor; 3) Vertical movement control: increase or decrease the output power of all motors by the same account; 4) Hover Control: make the output power of all motors the same and the lifting force they generate is equal to the gravity [5]. Figure 6.1 shows the quadrotor framework and its dynamical model which is established by the body-frame $B(Oxyz)$ and the earth-frame $E(Oxyz)$. In quadrotor position control, the compensation of the

rotation is necessary and obtained from the rotation matrix $R: E \rightarrow B$:

$$\begin{aligned} R &= R(\phi,\theta,\psi) = R(z,\psi)R(y,\theta)R(x,\phi) \\ R(z,\psi) &= \begin{bmatrix} cos\ \psi & -\sin\psi & 0 \\ \sin\psi & cos\ \psi & 0 \\ 0 & 0 & 1 \end{bmatrix} \\ R(y,\theta) &= \begin{bmatrix} cos\ \theta & 0 & \sin\theta \\ 0 & 1 & 0 \\ -\sin\theta & 0 & cos\ \theta \end{bmatrix} \\ R(x,\phi) &= \begin{bmatrix} 1 & 0 & 0 \\ 0 & cos\ \phi & -\sin\phi \\ 0 & \sin\phi & cos\ \phi \end{bmatrix} \end{aligned} \tag{6.1}$$

where roll ϕ, pitch θ and yaw ψ angles are quadrotor orientations in the body frames. Then it comes from (6.1):

$$R = \begin{bmatrix} C_\psi C_\theta & C_\psi S_\theta S_\phi - S_\psi C_\phi & C_\psi S_\theta C_\phi + S_\psi S_\phi \\ S_\psi C_\theta & S_\psi S_\theta S_\phi + C_\psi C_\phi & S_\psi S_\theta C_\phi - C_\psi S_\phi \\ -S_\theta & C_\theta S_\phi & C_\theta C_\phi \end{bmatrix} \tag{6.2}$$

where S denotes $sin(*)$ and C denotes $cos(*)$. The translational kinematic equations are attained by:

$$v_e = R \cdot v_b \tag{6.3}$$

where $v_e = [u_0,\ v_0,\ w_0]^T$ and $v_b = [u_b,\ v_b,\ w_b]^T$ are quadrotor's linear velocities in the earth-frame E(Oxyz) and body-frame B(Oxyz), respectively. This study considers the following assumptions to simplify the dynamics modelling complexity [5]:

1. The structure of the quadrotor is rigid and symmetrical.
2. The propeller that produces lift is rigid.
3. The air drag forces are proportional to the propellers' speed.

Under these assumptions, the quadrotor flight dynamics can be presented by the flight dynamics of a rigid body under the aerodynamic forces and moments generated by the rotation of the propeller. Then the translational motions and rotational motions kinetic equations of the quadrotor can be described as:

$$\left\{ \begin{array}{l} m_s\ddot{P} = F_f + F_d + F_g \\ J\ddot{\Theta} = -\dot{\Theta} \times \left(J\dot{\Theta}\right) + \Gamma_f - \Gamma_a - \Gamma_g \end{array} \right) \tag{6.4}$$

where m_s is the total mass of the quadrotor; vector $P = [x,\ y,\ z]^T$ presents the quadrotor position; $F_f\ = R_{j,3}\sum_{i=1}^{4} F_i = R_{j,3}K_p\omega_i^2$ presents the composition of forces generated by all rotors with $R_{j,3}$ being the third column of the rotation matrix R in (6.2) and K_p being a coefficient related

to the square of the angular rotor speed ω_i^2, which can be determined by static thrust tests [3]. $F_d = diag(-K_1,-K_2,-K_3)\dot{P}$ presents the composition of the drag forces along (X,Y,Z) axis with K_i $(i=1,2,3)$ being positive translation air drag coefficients. $F_g = [0,0,-m_s g]^T$ presents the gravity force acting on the centre of mass with g being gravitational acceleration. Euler angles vector $\Theta = \left[\phi,\theta,\psi\right]^T$ donates quadrotor orientation. $J = diag\left(I_x,\ I_y,I_z\right)\ \in R^{3\times3}$ is a positive definite symmetric inertia matrix of the quadrotor with I_i $(i=x,y,z)$ being the inertial moment in the body-frame $B(Oxyz)$. $\Gamma_a = diag\left(K_{ax},K_{ay},K_{az}\right)\dot{\Theta}$ presents the composition of aerodynamic resistance torque with K_{ax}, $K_{ay,}$ and K_{az} being the coefficients of aerodynamic resistance. Γ_f is the moment generated by the rotation of the propeller for the quadrotor's fixed frame and Γ_g is the composition of torques due to the gyroscopic effects [3], these forces are described by:

$$\Gamma_f = \begin{pmatrix} l(F_3-F_1) \\ l(F_2-F_4) \\ \omega_1^2-\omega_2^2+\omega_3^2-\omega_4^2 \end{pmatrix} = \begin{pmatrix} lK_p\left(\omega_3^2-\omega_1^2\right) \\ lK_p\left(\omega_4^2-\omega_2^2\right) \\ \omega_1^2-\omega_2^2+\omega_3^2-\omega_4^2 \end{pmatrix} \tag{6.5}$$

$$\Gamma_g = \sum_{i=1}^{4} J_r \begin{pmatrix} 0 \\ 0 \\ (-1)^{i+1}\omega_i \end{pmatrix} \dot{\Theta} \tag{6.6}$$

where l is the length between the centre of mass of the quadrotor and the axis of rotation of the propeller, J_r is the rotor inertia along the z-axis. The angular velocities $[p,\ q,\ r]^T$ in the body frame can be obtained by transforming the angular velocity $\left[\dot{\phi},\ \dot{\theta},\ \dot{\psi}\right]^T$ in the inertial frame as:

$$\begin{pmatrix} p \\ q \\ r \end{pmatrix} = \begin{pmatrix} 1 & 0 & -\sin\theta \\ 0 & \cos\phi & \cos\theta\sin\phi \\ 0 & -\sin\phi & \cos\phi\cos\theta \end{pmatrix} \begin{pmatrix} \dot{\phi} \\ \dot{\theta} \\ \dot{\psi} \end{pmatrix} \tag{6.7}$$

Therefore, the mathematical dynamics of a quadrotor can be established by:

$$\begin{cases} \ddot{x} = \frac{1}{m_s}\left(cos\ \psi\sin\theta cos\ \phi + \sin\phi\sin\psi\ \right)u_1 - \frac{1}{m_s}K_1\dot{x} \\ \ddot{y} = \frac{1}{m_s}\left(\sin\psi\sin\theta cos\ \phi - cos\ \psi\sin\phi\right)u_1 - \frac{1}{m_s}K_2\dot{y} \\ \ddot{z} = \frac{1}{m_s}\left(cos\ \theta cos\ \phi\right)u_1 - g - \frac{1}{m_s}K_3\dot{z} \end{cases} \tag{6.8}$$

$$\begin{cases} \ddot{\phi} = \frac{l}{I_x}\left[\left(I_y-I_z\right)qr - K_{ax}p - J_r q\Omega_r + u_2\right] \\ \ddot{\theta} = \frac{l}{I_y}\left[(I_z-I_x)pr - K_{ay}q + J_r p\Omega_r + u_3\right] \\ \ddot{\psi} = \frac{1}{I_z}\left[\left(I_x-I_y\right)pq - K_{az}r + u_4\right] \end{cases} \tag{6.9}$$

where $\Omega_r = \omega_1-\omega_2+\omega_3-\omega_4$ presents the total rotor angular velocity, u_1 represents the total thrust acting on the body in the z-axis, u_2 represents the roll torque and u_3 represent the pitch torques; u_4 represents the yaw torque. Rewrite them by the angular velocities as follows:

$$\begin{bmatrix} u_1 \\ u_2 \\ u_3 \\ u_4 \end{bmatrix} = \begin{bmatrix} K_p & K_p & K_p & K_p \\ -lK_p & 0 & lK_p & 0 \\ 0 & lK_p & 0 & -lK_p \\ 1 & -1 & 1 & -1 \end{bmatrix} \begin{bmatrix} \omega_1^2 \\ \omega_2^2 \\ \omega_3^2 \\ \omega_4^2 \end{bmatrix} \tag{6.10}$$

Let us introduce the following notations for simplicity:

$$\begin{aligned} X_1 = P, X_2 = \dot{P}, X_4 = \Theta, X_5 = \dot{\Theta}, F = \left(F_f + F_g\right)/m_s \\ f_2(X_2) = F_d/m_s = (diag(-K_1, -K_2, -K_3)X_2)/m_s \\ f_5(X_5) = J^{-1}\left(-\dot{\Theta} \times \left(J\dot{\Theta}\right) - \Gamma_a - \Gamma_g\right) \end{aligned} \tag{6.11}$$

Then the original translational and rotational models of the quadrotor (6.8) and (6.9) can be converted into

$$\left\{ \begin{array}{l} \dot{X}_1 = X_2 \\ \dot{X}_2 = f_2(X_2) + F + d_2 \\ \dot{X}_4 = X_5 \\ \dot{X}_5 = f_5(X_5) + J^{-1}\Gamma_f + d_5 \end{array} \right) \tag{6.12}$$

where d_2 and d_5 present lumped disturbances absorbing the uncertainties and external disturbances in the translational and rotational subsystems, respectively, where the uncertainties consist of inaccurate parameters, unmodelled unknown nonlinearities, etc and the disturbances include unpredictable environmental variables, sensor measurement noise, etc. The introduction of lumped disturbances can describe the quadrotor model more accurately, which will facilitate the design of MIMO-ESO and controllers.

6.2.2 Problem statement

According to the dynamical model from (6.8) and (6.9), the quadrotor control system can be separated into a fully actuated subsystem composed of ϕ, θ and ψ and an underactuated subsystem composed of x,y and z. However, in the attitude control of the quadrotor, the changes of the pitch angle θ and roll angle ϕ will cause the drone to tilt so that the lift force of the rotor generates a horizontal component, and then the horizontal movement can be realized. In this case, this study will directly use u_1 to control the quadrotor altitude z, and incidentally realize the x, y position tracking of the quadrotor by controlling the pitch θ and roll ϕ angle. Therefore, the new subsystems implemented by the decoupling algorithm will be separated into a fully actuated subsystem composed of z and ψ and an underactuated subsystem composed of x, y, ϕ, and θ.

Denote by $[x_d, y_d, z_d]^T$ and $\left[\phi_d, \theta_d, \psi_d\right]^T$, the desired positions and attitude angles respectively. The central control problem considered in this study is to design a robust tracking control system including a decoupling algorithm, position, and attitude control algorithms to ensure that the quadrotor can follow the desired position and attitude trajectories asymptotically and stably despite the modelling errors and unknown external system disturbances. In other words, the control strategy proposed in this study should ensure the position tracking errors ($e_x = x_d - x$, $e_y = y_d - y$, $e_z = z_d - z$) and the attitude tracking errors ($\phi_x = \phi_d - \phi$, $\theta_y = \theta_d - \theta$, $\psi_z = \psi_d - \psi$) converge to zero.

6.3 ESO design and analysis

This Chapter introduces the specific MIMO-ESO design process for translational and rotational subsystems. This MIMO-ESO provides not only the quadrotor's velocities but also disturbance estimation. According to the ESO design [39], it is necessary to assume d_2 and d_5 are continuously differentiable and their derivatives h_3 and h_6 are bounded. Introduce $X_3 = d_2$ and $X_6 = d_5$ for additional state variables, then convert the original translational and rotational models of the quadrotor (6.12) into:

$$\left\{ \begin{array}{l} \dot{X}_1 = X_2 \\ \dot{X}_2 = f_2(X_2) + F + X_3 \\ \dot{X}_3 = h_3 \end{array} \right) \qquad \left\{ \begin{array}{l} \dot{X}_4 = X_5 \\ \dot{X}_5 = f_5(X_5) + J^{-1}\Gamma_f + X_6 \\ \dot{X}_6 = h_6 \end{array} \right) \tag{6.13}$$

With the definition of $X_T = \begin{bmatrix} X_1 & X_2 & X_3 \end{bmatrix}^T$ and $X_R = \begin{bmatrix} X_4 & X_5 & X_6 \end{bmatrix}^T$, system (6.13) can be covert into:

$$\left\{ \begin{array}{l} \dot{X}_T = AX_T + F_1(X_T) + L_2F + \Delta_T \\ \dot{X}_R = AX_R + F_2(X_R) + L_2\left(J^{-1}\Gamma_f\right) + \Delta_R \end{array} \right) \tag{6.14}$$

where $A = \begin{bmatrix} 0 & I_3 & 0 \\ 0 & 0 & I_3 \\ 0 & 0 & 0 \end{bmatrix}$, $F_1(X_T) = [0,\, f_2(X_2), 0]^T$, $F_2(X_R) = [0,\, f_5(X_5), 0]^T$, $\Delta_T = [0,\, 0,\, h_3]^T$, $\Delta_R = [0,\, 0,\, h_6]^T$ and $L_2 = [0, I_3, 0]^T$. I_i presents an $i \times i, i \in R^+$ identity matrix, and 0 is a zero vector with proper dimensions. Therefore, the MIMO-ESO design based on dynamic modelling information in (6.11) is:

$$\left\{ \begin{array}{l} \dot{\hat{X}}_T = A\hat{X}_T + F_1\left(\hat{X}_T\right) + L_2F + \beta_1\left(X_1 - \hat{X}_1\right) \\ \dot{\hat{X}}_R = A\hat{X}_R + F_2\left(\hat{X}_R\right) + L_2\left(J^{-1}\Gamma_f\right) + \beta_2\left(X_4 - \hat{X}_4\right) \end{array} \right) \tag{6.15}$$

where $\hat{X}_T = \begin{bmatrix} \hat{X}_1 & \hat{X}_2 & \hat{X}_3 \end{bmatrix}^T$ and $\hat{X}_R = \begin{bmatrix} \hat{X}_4 & \hat{X}_5 & \hat{X}_6 \end{bmatrix}^T$ are the estimated state variable matrix, $F_1\left(\hat{X}_T\right) = \begin{bmatrix} 0 & f_2\left(\hat{X}_2\right) & 0 \end{bmatrix}^T$, $F_2\left(\hat{X}_R\right) = \begin{bmatrix} 0 & f_5\left(\hat{X}_5\right) & 0 \end{bmatrix}^T$. β_1 and β_2 are the observer gain matrices with $\beta_1 = \begin{bmatrix} 3\omega_1 \cdot I_3 & 3\omega_1^2 \cdot I_3 & \omega_1^3 \cdot I_3 \end{bmatrix}^T$ and $\beta_2 = \begin{bmatrix} 3\omega_2 \cdot I_3 & 3\omega_2^2 \cdot I_3 & \omega_2^3 \cdot I_3 \end{bmatrix}^T$. The parameters $\omega_1, \omega_2 \in R^+$ are the only tuning parameters presenting the observer bandwidths. Then introduce the estimation errors as $X_T = X_T - \hat{X}_T = \begin{bmatrix} X_1 & X_2 & X_3 \end{bmatrix}^T$ and $X_R = X_R - \hat{X}_R = \begin{bmatrix} X_4 & X_5 & X_6 \end{bmatrix}^T$, respectively. Their scaled estimation errors are defined as $Q_T = \begin{bmatrix} Q_1 & Q_2 & Q_3 \end{bmatrix}^T = \begin{bmatrix} X_1 & X_2/\omega_1 & X_3/\omega_1^2 \end{bmatrix}^T$ and $Q_R = \begin{bmatrix} Q_4 & Q_5 & Q_6 \end{bmatrix}^T = \begin{bmatrix} X_4 & X_5/\omega_2 & X_6/\omega_2^2 \end{bmatrix}^T$. Thus, the scaled estimation errors are:

$$\left\{ \begin{array}{l} \dot{Q}_T = \omega_1 \cdot A_1Q_T + L_2\left(f_2(X_2) - f_2\left(\hat{X}_2\right)\right) \cdot \omega_1^{-1} + L_3h_3 \cdot \omega_1^{-2} \\ \dot{Q}_R = \omega_1 \cdot A_1Q_R + L_2\left(f_5(X_5) - f_5\left(\hat{X}_5\right)\right) \cdot \omega_2^{-1} + L_3h_6 \cdot \omega_2^{-2} \end{array} \right) \tag{6.16}$$

with $A_1 = \begin{bmatrix} -3\cdot I_3 & I_3 & 0 \\ -3\cdot I_3 & 0 & I_3 \\ -I_3 & 0 & 0 \end{bmatrix}$ and $L_3 = \begin{bmatrix} 0 & 0 & I_3 \end{bmatrix}^T$.

Assumption 1. The derivatives of the lumped disturbances satisfy $\|h_3\| \le \varepsilon_1$ and $\|h_6\| \le \varepsilon_2$ with $\varepsilon_1, \varepsilon_3 > 0$. Functions f_2 and f_5 belong to C^2 (with 2 continuous derivatives) and are globally Lipschitz with respect to X_2 and X_5 with $c_1, c_2 \in R^+$, that is,

$$\begin{cases} \left\| f_2(X_2) - f_2(\hat{X}_2) \right\| \le c_1 \left\| X_2 - \hat{X}_2 \right\| = c_1\omega_1 \|Q_2\| \le c_1\omega_1 \|Q_T\| \\ \left\| f_5(X_5) - f_5(\hat{X}_5) \right\| \le c_2 \left\| X_5 - \hat{X}_5 \right\| = c_2\omega_2 \|Q_5\| \le c_2\omega_2 |Q_R| \end{cases} \tag{6.17}$$

Remark 1. Since A_1 is the Hurwitz matrix in (6.16), there exists a positive definite matrix P satisfying $A_1^T P + P A_1 = -I_9$. Select observer bandwidth $\omega_1 > 2c_1|PL_2|$ for translational subsystem and substituting A_1 into the above equation, it comes $P = \begin{bmatrix} I_3 & -0.5I_3 & -I_3 \\ -0.5I_3 & 0 & -0.5I_3 \\ -I_3 & -0.5I_3 & 4I_3 \end{bmatrix}$. Then choose the following Lyapunov candidate function:

$$V(Q_T) = Q_T^T P Q_T \tag{6.18}$$

Substituting (6.16) and (6.17) into the time derivative of $V(Q_T)$, it has

$$\begin{aligned} \dot{V}(Q_T) =& \dot{Q}_T^T P Q_T + Q_T^T P \dot{Q}_T \\ =& \omega_1 Q_T^T A_1^T P Q_T + \left(\frac{L_2\left(f_2(X_2) - f_2(\hat{X}_2)\right)}{\omega_1} \right)^T P Q_T + \left(\frac{L_3 h_3}{\omega_1^2} \right)^T P Q_T \\ &+ \omega_1 Q_T^T P A_1 Q_T + Q_T^T P \frac{L_2\left(f_2(X_2) - f_2(\hat{X}_2)\right)}{\omega_1} + Q_T^T P L_3 \frac{L_3 h_3}{\omega_1^2} \\ =& \omega_1 Q_T^T \left(A_1^T P + P A_1 \right) Q_T + \left(\frac{L_2\left(f_2(X_2) - f_2(\hat{X}_2)\right)}{\omega_1} \right)^T P Q_T \\ &+ \left(\frac{L_3 h_3}{\omega_1^2} \right)^T P Q_T + \omega_1 Q_T^T P A_1 Q_T + Q_T^T P \frac{L_2\left(f_2(X_2) - f_2(\hat{X}_2)\right)}{\omega_1} + Q_T^T P L_3 \frac{L_3 h_3}{\omega_1^2} \end{aligned} \tag{6.19}$$

According to **Remark 1**, P is a symmetric positive definite matrix, it comes from (6.19) that

$$\begin{aligned} \left(\frac{L_2\left(f_2(X_2) - f_2(\hat{X}_2)\right)}{\omega_1} \right)^T P Q_T &= Q_T^T P \frac{L_2\left(f_2(X_2) - f_2(\hat{X}_2)\right)}{\omega_1} \\ \left(\frac{L_3 h_3}{\omega_1^2} \right)^T P Q_T &= Q_T^T P \frac{L_3 h_3}{\omega_1^2} \end{aligned} \tag{6.20}$$

Substituting (6.20) into (6.19), we have

$$\begin{aligned}\dot{V}(Q_T) =&\omega_1 Q_T^T(-I_9)Q_T + 2Q_T^T P\frac{L_2\big(f_2(X_2)-f_2(\hat{X}_2)\big)}{\omega_1} + 2Q_T^T P\frac{L_3 h_3}{\omega_1^2}\\ \leq& -\omega_1\|Q_T\|^2 + 2Q_T^T P\frac{L_2(c_1\omega_1\|Q_T\|)}{\omega_1} + 2Q_T^T P\frac{L_3\cdot\varepsilon_1}{\omega_1^2}\\ \leq& -\omega_1\|Q_T\|^2 + \frac{2c_1\omega_1\|Q_T\|\cdot\|PL_2\|\cdot\|Q_T\|}{\omega_1} + \frac{2\varepsilon_1\|Q_T\|\cdot\|PL_3\|}{\omega_1^2}\\ =& -(\omega_1 - 2c_1\|PL_2\|)\|Q_T\|^2 - \left(\frac{-2\varepsilon_1\|PL_3\|}{\omega_1^2}\right)\|Q_T\|\\ =& -\|Q_T\|\left((\omega_1 - 2c_1\|PL_2\|)\|Q_T\| - \frac{2\varepsilon_1\|PL_3\|}{\omega_1^2}\right)\end{aligned} \tag{6.21}$$

Therefore, the designed MIMO-ESO is stable, and the estimation error will be bounded with $\|Q_T\| \leq \frac{2\varepsilon_1\|PL_3\|}{(\omega_1-2c_1\|PL_2\|)\omega_1^2}$ after a finite time, that is, the estimated velocity variable $\hat{X}_2$ can track the real velocity precisely. According to **Remark 1**, $\omega_1 > 2c_1|PL_2|$ means a sufficiently large ω_1 can reduce the upper bound of the estimation error.

Remark 2. The stability proof for rotational subsystems is the same as for translational subsystems from (6.18) to (6.19). The observer bandwidth in the rotational subsystem is selected as $\omega_2 > 2c_2|PL_2|$, therefore $\dot{V}(Q_R) \leq -|Q_R|\big((\omega_2 - 2c_2|PL_2|)\cdot|Q_R| - 2\varepsilon_2|PL_3|\cdot\omega_2^{-2}\big)$, the upper bound for estimation error in rotational subsystem is $|Q_R| \leq \frac{2\varepsilon_2|PL_3|}{(\omega_2-2c_2|PL_2|)\omega_2^2}$ and inversely proportional to the value of the bandwidth.

Remark 3. The larger observer bandwidth ω_1 and ω_2 can reduce the estimation error but may lead to high-frequency oscillation due to the high-gain integration, which will reduce the robustness of the MIMO-ESO and the whole control system. Therefore, designers should consider an appropriate compromise/ trade-off between the estimation quality and the system robustness.

6.4 Controller design and analysis

To accomplish this position and attitude control system, a decoupling algorithm and robust UDSMC method are presented in this section. Figure 6.2 shows the quadrotor control framework, where IMU is the internal measurement unit, providing basic motion and rotation information of the quadrotor aircraft, and UDSMC is U-model based double sliding controller module.

6.4.1 Decoupling algorithm

Assume system (6.8) is fully actuated and convert it into

$$\left\{\begin{array}{l}\ddot{x} = u_x - \frac{1}{m_s}K_1\dot{x}\\ \ddot{y} = u_y - \frac{1}{m_s}K_2\dot{y}\\ \ddot{z} = u_z - g - \frac{1}{m_s}K_3\dot{z}\end{array}\right. \tag{6.22}$$

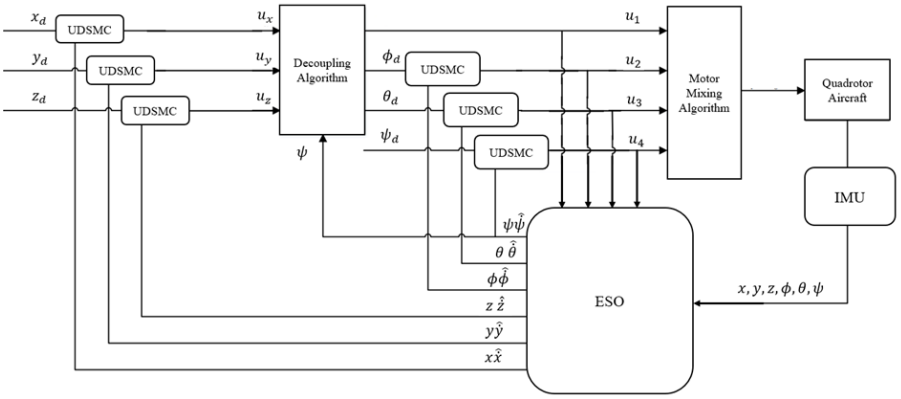

Figure 6.2: The quadrotor control framework

where u_x, u_y and u_z are assumed position controllers shown as:

$$\left\{ \begin{array}{l} u_x = \frac{u_1}{m_s}\left(cos\ \psi \sin\theta cos\ \phi + \sin\phi \sin\psi\ \right) \\ u_y = \frac{u_1}{m_s}\left(\sin\psi \sin\theta cos\ \phi - cos\ \psi \sin\phi\right) \\ u_z = \frac{u_1}{m_s}\left(cos\ \theta cos\ \phi\right) \end{array} \right. \tag{6.23}$$

By squaring both sides of the above equations (6.23), it comes:

$$\frac{u_1}{m_s} = \sqrt{u_x^2 + u_y^2 + u_z^2} = \frac{u_z}{cos\ \theta cos\ \phi} \tag{6.24}$$

Therefore, the desired roll and pitch angles (ϕ_d, θ_d) can be calculated by:

$$\phi_d = \arcsin\left(m_s \frac{u_x sin\psi - u_y cos\psi}{u_1}\right) \tag{6.25}$$

$$\theta_d = \arctan\left(\frac{u_x cos\psi + u_y sin\psi}{u_z}\right) \tag{6.26}$$

Remark 4. It should be noticed that the roll, pitch, and yaw angles (ϕ, θ, ψ) are bounded and meet the satisfaction of $\phi, \theta \in (-\pi/2, \pi/2)$ and $\psi \in (-\pi, \pi)$, which are necessarily considered avoiding the singularity problems in the aerodynamic and controller design [3].

Assuming the body of the quadrotor is rigid, the position controllers for x and y are designed by using the UDSMC method. According to the UDSMC design procedures in Chapter 5.3.2, the sliding manifolds and their derivatives are defined as

$$\begin{array}{c} S_P = C_P e_P + \dot{\hat{e}}_P,\ \ S_{P1} = S_P + \delta_P,\ \ S_{P2} = S_P \\ \dot{S}_{P1} = f_P + U_{Psw},\ \ \dot{S}_{P2} = K_P + U_{Peq} \end{array} \tag{6.27}$$

where $S_P = \left[S_x, S_y, S_z\right]^T$, $S_{P1} = \left[S_{x1}, S_{y1}, S_{z1}\right]^T$, C_P is designed positive definite diagonal matric, $e_P = \left[e_x, e_y, e_z\right]^T = [x - x_d, y - y_d, z - z_d]^T$, $\delta_P = \left[\delta_x, \delta_y, \delta_z\right]^T$, $f_P = \left[f_x, f_y, f_z\right]^T$ with $f_x = c_x \dot{\hat{e}}_x -$

$\frac{1}{m_s}K_1\dot{\hat{x}}$, $f_y = c_y\dot{\hat{e}}_y - \frac{1}{m_s}K_2\dot{\hat{y}}$ and $f_z = c_z\dot{\hat{e}}_z - g - \frac{1}{m_s}K_3\dot{\hat{z}}$. K_P is bounded unknown tangent matrices of S_P. The corresponding position controllers are designed as:

$$U_P = -K_{P1}sgn(S_{P1}) - K_{P2}S_{P2} \tag{6.28}$$

where K_{P1} and K_{P2} are designed positive definite diagonal matrices, $U_P = U_{Psw} + U_{Peq}$, $sgn(S_{P1}) = \left[sgn(S_{x1}), sgn\left(S_{y1}\right), sgn(S_{z1})\right]^T$. Assuming a Lyapunov function $V_P = \frac{1}{2}S_{P1}^T S_{P1} + \frac{1}{2}S_{P2}^T S_{P2}$, its corresponding derivative is:

$$\begin{aligned}\dot{V}_P =& \frac{1}{2}\dot{S}_{P1}^T S_{P1} + \frac{1}{2}\dot{S}_{P2}^T S_{P2} + \frac{1}{2}S_{P1}^T\dot{S}_{P1} + \frac{1}{2}S_{P2}^T\dot{S}_{P2} \\ &\leq S_{P1}^T\dot{S}_{P1} + S_{P2}^T\dot{S}_{P2} \\ &= S_{P1}^T(f_P - K_{P1}sgn(S_{P1})) + S_{P2}^T(K_P - K_{P2}S_{P2}) \\ &\leq -\|S_{P1}\|(K_{P1} - f_P) - \|S_{P2}\|(K_{P2} - K_P)\end{aligned} \tag{6.29}$$

To satisfy $\dot{V}_P < 0$ for horizontal position control stability, it comes $K_{P1} - f_P > 0$ and $K_{P2} - K_P > 0$, therefore

$$K_{P1} > \|f_P\|, \;\; K_{P2} > \|K_P\| \tag{6.30}$$

Remark 5. This study divides the control system into two main subsystems: a fully actuated subsystem composed of $z$and ψ and an underactuated subsystem composed of x,θ and y,ϕ. According to Figure 6.1, for a given reference positions x_d and y_d, this study first converts system (6.14) into a fully actuated control system, and its position controllers are designed respectively by using the UDSMC method. Then the desired angles reference for positions control are calculated through the decoupling system accordingly. Next, the design steps of the subsequent fully actuated and underactuated controller will be introduced in detail.

6.4.2 Uncoupled/fully actuated subsystem controller

The fully actuated subsystem controller is designed by the UDSMC method to ensure the altitude variables z and yaw angle ψ can converge to their desired values z_d and ψ_d. Additionally, assuming that the structure of the quadrotor is rigid and symmetrical, therefore, the sliding manifolds are designed as

$$\begin{aligned}&S_F = C_F e_F + \dot{\hat{e}}_F, \;\; S_{F1} = S_F + \delta_F, \;\; S_{F2} = S_F \\ &\dot{S}_{F1} = f_F + f_{FU}U_{Fsw}, \;\; \dot{S}_{F2} = K_F + f_{FU}U_{Feq}\end{aligned} \tag{6.31}$$

where $S_F = [S_1, S_4]^T$ are sliding manifolds for fully actuated subsystem, $S_{F1} = \left[S_{g1}, S_{g4}\right]^T$, $C_F = diag\left(c_z, c_\psi\right)$ is designed positive definite diagonal matric, $e_F = \left[e_z, e_\psi\right]^T = \left[z - z_d, \psi - \psi_d\right]^T$, $\delta_F = \left[\delta_z, \delta_\psi\right]^T$, $f_F = \left[f_{g1}, f_{g4}\right]^T$ with $f_{g1} = c_z\dot{\hat{e}}_z - g - \frac{1}{m_s}K_3\dot{\hat{z}} - \ddot{z}_d$ and $f_{g4} = c_\psi\dot{\hat{e}}_\psi + pq\frac{I_x - I_y}{I_z} - \frac{k_6}{I_z}r - \ddot{\psi}_d$. $f_{FU} = diag(f_{u1}, f_{u4})$ with $f_u1 = 1$ and $f_{u4} = \frac{C}{I_z}$; K_F is bounded unknown tangent matrices of

S_F. $U_{Fsw} = [u_{1sw}, u_{4sw}]^T$ is the switching controller and $U_{Feq} = \left[u_{1eq}, u_{4eq}\right]^T$ is the equivalent controller. The corresponding controllers for this fully actuated subsystem are designed as:

$$U_F = -K_{F1} sgn(S_{F1}) - K_{F2} S_{F2} \tag{6.32}$$

where K_{F1} and K_{F2} are designed positive definite diagonal matrices, $U_F = [u_1, u_4]^T = U_{Fsw} + U_{Feq}$, $sgn(S_{F1}) = \left[sgn\left(S_{g1}\right), sgn\left(S_{g4}\right)\right]^T$. Assuming a Lyapunov function $V_F = \frac{1}{2} S_{F1}^T S_{F1} + \frac{1}{2} S_{F2}^T S_{F2}$, its corresponding derivative is:

$$\begin{aligned} \dot{V}_F =& \frac{1}{2} \dot{S}_{F1}^T S_{F1} + \frac{1}{2} \dot{S}_{F2}^T S_{F2} + \frac{1}{2} S_{F1}^T \dot{S}_{F1} + \frac{1}{2} S_{F2}^T \dot{S}_{F2} \\ \leq & S_{F1}^T \dot{S}_{F1} + S_{F2}^T \dot{S}_{F2} \\ = & S_{F1}^T (f_F - f_{FU}(K_{F1} sgn(S_{F1}))) + S_{P2}^T (K_F - f_{FU}(K_{F2} S_{F2})) \\ \leq & - \| S_{F1} \| \left(f_{FU} K_{F1} - f_F \right) - \| S_{F2} \| \left(f_{FU} K_{F2} - K_F \right) \end{aligned} \tag{6.33}$$

To satisfy $\dot{V}_F < 0$ for altitude control and yaw angle control stability, it comes $f_{FU} K_{F1} - f_F > 0$ and $f_{FU} K_{F2} - K_F > 0$, therefore

$$K_{F1} > \| f_F \| f_{FU}^{-1}, \quad K_{P2} > \| K_F \| f_{FU}^{-1} \tag{6.34}$$

Remark 6. The relationship between u_z and u_1 is $u_z = \frac{u_1 cos\ \theta cos\ \phi}{m_s}$. Therefore, the design of u_1 can be converted into the design of u_z according to (6.24).

6.4.3 Coupled/underactuated subsystem controller

Underactuated subsystem controller is also designed by the UDSMC method to maintain the horizontal position variables $[x, y]$ and pitch and roll angles variables $[\ \phi, \theta\ ]$ can converge to their desired values $[x_d,\ y_d]$ and $\left[\phi_d, \theta_d\right]$ with only two control inputs u_2 and u_3. Accordingly, the sliding manifolds are designed as

$$\begin{aligned} S_{UN} &= C_{UN1} e_{UN1} + C_{UN2} \dot{e}_{UN1} + C_{UN3} e_{UN2} + C_{UN4} \dot{e}_{UN2} \\ S_{UN1} &= S_{UN} + \delta_{UN}, \quad S_{UN2} = S_{UN} \\ \dot{S}_{UN1} &= f_{UN} + f_{UNU} U_{UNsw}, \ \ \dot{S}_{UN2} = K_{UN} + f_{UNU} U_{UNeq} \end{aligned} \tag{6.35}$$

where $S_{UN} = [S_2, S_3]^T$ are sliding manifolds for fully actuated subsystem, $S_{UN1} = \left[S_{g2}, S_{g3}\right]^T$; $C_{UN1} = diag(c_1, c_5)$, $C_{UN2} = diag(c_2, c_6)$, $C_{UN3} = diag(c_3, c_7)$, $C_{UN4} = diag(c_4, c_8)$ are designed positive definite diagonal matrices, $e_{UN1} = \left[e_x, e_y\right]^T = [x - x_d, y - y_d]^T$, $e_{UN2} = \left[e_\theta, e_\phi\right]^T = \left[\theta - \theta_d, \phi - \phi_d\right]^T$, $\delta_{UN} = [\delta_2, \delta_3]^T$, $f_{UN} = \left[f_{g2}, f_{g3}\right]^T$ with $f_{g2} = c_1 \ddot{e}_y + c_2 \dot{\hat{e}}_y + c_3 \left(\hat{q} \hat{r} \frac{I_y - I_z}{I_x} + \frac{J_r}{I_x} \hat{q} \Omega_r - \frac{k_4 l}{I_x} \hat{p} \right) - \ddot{\phi}_d + c_4 \dot{\hat{e}}_\phi$ and $f_{g3} = c_5 \ddot{\hat{e}}_x + c_6 \dot{\hat{e}}_x + c_7 \left(\hat{p} \hat{r} \frac{I_z - I_x}{I_y} - \frac{J_r}{I_y} \hat{p} \Omega_r - \frac{k_5 l}{I_y} \hat{q} \right) - \ddot{\theta}_d + c_8 \dot{\hat{e}}_\theta$; $f_{UNU} = diag(f_{u2}, f_{u3})$ with $f_{u2} = \frac{c_3 l}{I_x}$ and $f_{u3} = \frac{c_7 l}{I_y}$; K_{UN} is bounded unknown tangent matrices of S_{UN}. $U_{UNeq} = \left[u_{2eq}, u_{3eq}\right]^T$ is the switching controller and $U_{UNeq} = \left[u_{2eq}, u_{3eq}\right]^T$ is the equivalent controller. The corresponding controllers for this fully actuated subsystem are designed as

$$U_{UN} = -K_{UN1} sgn(S_{UN1}) - K_{UN2} S_{UN2} \tag{6.36}$$

where K_{UN1} and K_{UN2} are designed positive definite diagonal matrices, $U_{UN} = [u_2, u_3]^T = U_{UNsw} + U_{UNeq}$, $sgn(S_{UN1}) = \left[sgn\left(S_{g2}\right), sgn\left(S_{g3}\right)\right]^T$. Assuming a Lyapunov function $V_{UN} = [V_2, V_3]^T = \frac{1}{2}S_{UN1}^T S_{UN1} + \frac{1}{2}S_{UN2}^T S_{UN2}$, its corresponding derivative is:

$$\begin{aligned}\dot{V}_{UN} =& \frac{1}{2}\dot{S}_{UN1}^T S_{UN1} + \frac{1}{2}\dot{S}_{UN2}^T S_{UN2} + \frac{1}{2}S_{UN1}^T \dot{S}_{UN1} + \frac{1}{2}S_{UN2}^T \dot{S}_{UN2} \\ \leq& S_{UN1}^T \dot{S}_{UN1} + S_{UN2}^T \dot{S}_{UN2} \\ =& S_{UN1}^T (f_{UN} - f_{UNU}(K_{UN1} sgn(S_{UN1}))) + S_{UN2}^T (K_{UN} - f_{UNU}(K_{UN2} S_{UN2})) \\ \leq& -\|S_{UN1}\|(f_{UNU}K_{UN1} - f_{UN}) - \|S_{UN2}\|(f_{UNU}K_{UN2} - K_{UN})\end{aligned} \tag{6.37}$$

To satisfy $\dot{V}_2 < 0$ for x position and roll angle control stability and $\dot{V}_3 < 0$ for y position and pitch angle control stability, it comes $f_{UNU}K_{UN1} - f_{UN} > 0$ and $f_{UNU}K_{UN2} - K_{UN} > 0$, therefore

$$K_{UN1} > \|f_{UN}\| f_{UNU}^{-1}, \quad K_{UN2} > \|K_{UN}\| f_{UNU}^{-1} \tag{6.38}$$

6.4.4 The sliding manifolds coefficients

Let the sliding manifold S_2 and its derivative equal to zero:

$$S_{UN} = C_{UN1}e_{UN1} + C_{UN2}\dot{\hat{e}}_{UN1} + C_{UN3}e_{UN2} + C_{UN4}\dot{\hat{e}}_{UN2} = 0 \tag{6.39}$$

$$\dot{S}_{UN} = C_{UN1}\dot{\hat{e}}_{UN1} + C_{UN2}\ddot{\hat{e}}_{UN1} + C_{UN3}\dot{\hat{e}}_{UN2} + C_{UN4}\ddot{\hat{e}}_{UN2} = 0 \tag{6.40}$$

From (6.40), it has

$$\ddot{\hat{e}}_{UN2} = -C_{UN4}^{-1}\left(C_{UN1}\dot{\hat{e}}_{UN1} + C_{UN2}\ddot{\hat{e}}_{UN1} + C_{UN3}\dot{\hat{e}}_{UN2}\right) \tag{6.41}$$

From (6.39), it has

$$\dot{\hat{e}}_{UN1} = -C_{UN2}^{-1}\left(C_{UN1}e_{UN1} + C_{UN3}e_{UN2} + C_{UN4}\dot{\hat{e}}_{UN2}\right) \tag{6.42}$$

Substituting (6.42) into (6.41), it comes,

$$\begin{aligned}\ddot{\hat{e}}_{UN2} =& -C_{UN4}^{-1}\left(C_{UN1}\left(-C_{UN2}^{-1}\left(C_{UN1}e_{UN1} + C_{UN3}e_{UN2} + C_{UN4}\dot{\hat{e}}_{UN2}\right)\right)\right) \\ & - C_{UN4}^{-1}\left(C_{UN2}\ddot{\hat{e}}_{UN1} + C_{UN3}\dot{\hat{e}}_{UN2}\right) \\ =& C_{UN4}^{-1}C_{UN1}C_{UN2}^{-1}\left(C_{UN1}e_{UN1} + C_{UN3}e_{UN2} + C_{UN4}\dot{\hat{e}}_{UN2}\right) \\ & - C_{UN4}^{-1}C_{UN2}\ddot{\hat{e}}_{UN1} - C_{UN4}^{-1}C_{UN3}\dot{\hat{e}}_{UN2} \\ =& C_{UN4}^{-1}C_{UN1}C_{UN2}^{-1}C_{UN1}e_{UN1} + C_{UN4}^{-1}C_{UN1}C_{UN2}^{-1}C_{UN3}e_{UN2} \\ & + \left(C_{UN4}^{-1}C_{UN1}C_{UN2}^{-1}C_{UN4} - C_{UN4}^{-1}C_{UN3}\right)\dot{\hat{e}}_{UN2} - C_{UN4}^{-1}C_{UN2}\ddot{\hat{e}}_{UN1}\end{aligned} \tag{6.43}$$

Let $Y_1 = e_{UN2}$, $Y_2 = \dot{Y}_1 = \dot{\hat{e}}_{UN2}$ and $Y_3 = e_{UN1}$. The cascaded form is obtained as:

$$\begin{aligned}\dot{Y}_1 =& Y_2 \\ \dot{Y}_2 =& C_{UN4}^{-1}C_{UN1}C_{UN2}^{-1}C_{UN1}e_{UN1} + C_{UN4}^{-1}C_{UN1}C_{UN2}^{-1}C_{UN3}e_{UN2} \\ & + \left(C_{UN4}^{-1}C_{UN1}C_{UN2}^{-1}C_{UN4} - C_{UN4}^{-1}C_{UN3}\right)\dot{\hat{e}}_{UN2} - C_{UN4}^{-1}C_{UN2}\ddot{\hat{e}}_{UN1} \\ \dot{Y}_3 =& -C_{UN2}^{-1}C_{UN1}e_{UN1} - C_{UN2}^{-1}C_{UN3}e_{UN2} - C_{UN2}^{-1}C_{UN4}\dot{\hat{e}}_{UN2}\end{aligned} \tag{6.44}$$

When the system state variables approach their equilibrium points, that is, $e_{UN2} \to 0$, $\dot{e}_{UN2} \to 0$, $e_{UN1} \to 0$, thus, $Y_1 \to 0$, $Y_2 \to 0$, $Y_3 \to 0$. After the linearization operation around the equilibrium points, it comes

$$\ddot{e}_{UN1} = He_{UN2} + N \tag{6.45}$$

where $H = diag\left(\begin{bmatrix} u_1 cos\ \psi cos\ \phi/m_s & -u_1 cos\ \psi/m_s \end{bmatrix}\right)$, $e_{UN2} = \begin{bmatrix} \theta - \theta_d & \phi - \phi_d \end{bmatrix}^T$, $N = \begin{bmatrix} u_1 \sin\phi \sin\psi/m_s - K_1\dot{\hat{x}}/m_s - \ddot{x}_d & u_1 \sin\psi \sin\theta cos\ \phi/m_s - K_2\dot{\hat{y}}/m_s - \ddot{y}_d \end{bmatrix}^T$. Then substitute (6.45) into (6.44) and use Y_1, Y_2, Y_3 to replace the related items, the new cascaded form is obtained after organization as:

$$\begin{aligned}
\dot{Y}_1 =& Y_2 \\
\dot{Y}_2 =& \left(C_{UN4}^{-1} C_{UN1} C_{UN2}^{-1} C_{UN3} - C_{UN4}^{-1} C_{UN2} H\right) Y_1 \\
&+ \left(C_{UN4}^{-1} C_{UN1} C_{UN2}^{-1} C_{UN4} - C_{UN4}^{-1} C_{UN3}\right) Y_2 \\
&+ C_{UN4}^{-1} C_{UN1} C_{UN2}^{-1} C_{UN1} Y_3 - C_{UN4}^{-1} C_{UN2} N \\
\dot{Y}_3 =& -C_{UN2}^{-1} C_{UN3} Y_1 - C_{UN2}^{-1} C_{UN4} Y_2 - C_{UN2}^{-1} C_{UN1} Y_3
\end{aligned} \tag{6.46}$$

Let $Y = [Y_1, Y_2, Y_3]^T$, its derivative matrix form is $\dot{Y} = A_2 Y$, where

$$A_2 = \begin{bmatrix} A_{11} & A_{12} & A_{13} \\ A_{21} & A_{22} & A_{23} \\ A_{31} & A_{32} & A_{33} \end{bmatrix} \tag{6.47}$$

The matrix A_2 is Hurwitz and the system states will be asymptotically approaching their equilibrium points. Assuming $C_{UN4}^{-1} \neq 0$ and $C_{UN2}^{-1} \neq 0$, the parameters in (6.46) are obtained from (6.47):

$$\begin{aligned}
A_{11} = A_{13} = 0,\ A_{12} = I_2 \\
A_{21} = C_{UN4}^{-1} C_{UN1} C_{UN2}^{-1} C_{UN3} - C_{UN4}^{-1} C_{UN2} H \\
A_{22} = C_{UN4}^{-1} C_{UN1} C_{UN2}^{-1} C_{UN4} - C_{UN4}^{-1} C_{UN3} \\
A_{23} = C_{UN4}^{-1} C_{UN1} C_{UN2}^{-1} C_{UN1} \\
A_{31} = -C_{UN2}^{-1} C_{UN3},\ A_{32} = -C_{UN2}^{-1} C_{UN4},\ A_{33} = -C_{UN2}^{-1} C_{UN1}
\end{aligned} \tag{6.48}$$

Let $|\lambda \cdot I_6 - A| = 0$, that is,

$$\begin{vmatrix} \lambda \cdot I_2 & -I_2 & 0 \\ A_{21} & \lambda \cdot I_2 - A_{22} & A_{23} \\ A_{31} & A_{32} & \lambda \cdot I_2 - A_{33} \end{vmatrix} = 0 \tag{6.49}$$

Determinant (6.49) can be calculated as:

$$(\lambda \cdot I_2)^3 - (A_{22} + A_{33})(\lambda \cdot I_2)^2 + (A_{33}A_{22} - A_{21} - A_{32}A_{23})(\lambda \cdot I_2) + (A_{33}A_{21} - A_{31}A_{23}) = 0 \tag{6.50}$$

Let the characteristic equation be $(\lambda \cdot I_2 + 2I_2)^3 = 0$, after the comparison of this equation with (6.50), it has:

$$\left\{ \begin{array}{l} -(A_{22} + A_{33}) = 6I_2 \\ A_{33}A_{22} - A_{21} - A_{32}A_{23} = 12I_2 \\ A_{33}A_{21} - A_{31}A_{23} = 8I_2 \end{array} \right\} \tag{6.51}$$

After organization, Let $c_4 = c_8 = 1$, then the other coefficients are: $c_1 = \frac{8m_s}{u_1 cos\ \phi cos\ \psi}$, $c_2 = \frac{12m_s}{u_1 cos\ \phi cos\ \psi}$, $c_3 = 6$, $c_5 = -\frac{8m_s}{cos\ \psi u_1}$, $c_6 = -\frac{12m_s}{cos\ \psi u_1}$, $c_7 = 6$.

6.5 Experimental Studies

The proposed ESO UDSMC based quadrotor control system has been tested by the Parrot Mambo Minidrone position tracking experiment. In order to evaluate the real-time position and attitude tracking of the performance of the quadrotor under the UDSMC method, its experiment results will be compared with the PID controller and sliding mode controller. The PID controller is the original built-in controller of the Parrot Minidrone and has been adjusted by the manufacturer for optimum performance.

6.5.1 Experiment Setup

The Parrot Mambo Minidrone, which is shown in Figure 6.3, is equipped with a 6-DOF inertial measurement unit (3-axis accelerometer and 3-axis gyroscope), an ultrasound sensor and pressure sensors that can detect the quadrotor's altitude, a pressure sensor, a 60FPS camera with a resolution of 120x160 pixels. The support package provided by MATLAB/Simulink can connect with Parrot Mambo Minidrone via Bluetooth 4.0, and access the mini drone's internal sensor data, and deploy the control algorithm in real-time, the output of which will be sent back to MATLAB/Simulink and displayed on it. The sampling time of the mini drone control system is $T = 0.005s$, the position $[x,\ y,\ z]'$ and the attitude $\left[\phi, \theta, \psi\right]'$ of the mini drone are estimated by the built-in sensor fusion algorithm based on Kalman filter; the linear velocity $[u,\ v,\ w]'$ and angular velocity $[p,\ q,\ r]'$ are calculated/estimated by ESO. The simulation package is performed on MATLAB/Simulink 2021a.

6.5.2 Experiment Parameters

The initial position for quadrotor experiments is [0, 0, 0] m. Table 6.1 lists the variable values of Parrot Minidrone and Table 6.2 shows the UDSMC design parameters. The invariant controller in the outer loop is designed as $G_{c1} = \frac{1}{0.01s^2 + 0.2s}$. The parameters of the PID controller are design as $K_P = diag$[0.1, −0.1, 0.8, 0.003, 0.0024, 0.004], $K_I = diag$[0.1, −0.1, 0.24, 0.006, 0.048, 0.002] and $K_D = diag$[−0.2, 0.2, 0.5, 0.00012, 0.000096, 0.00012] for $\left[x,\ y,\ z, \phi, \theta, \psi\right]'$. The sliding mode con-

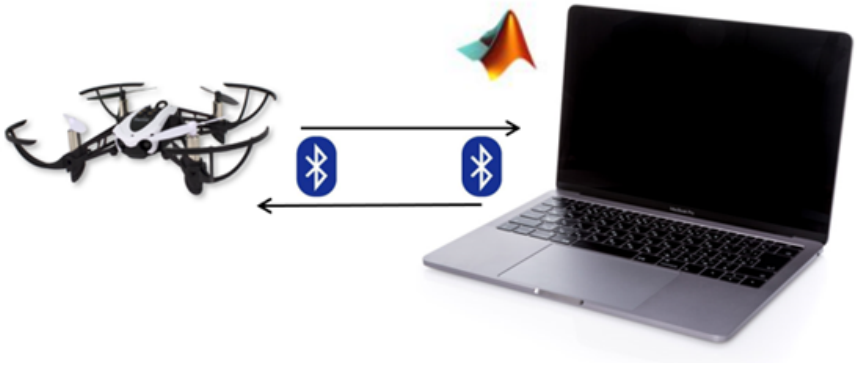

Figure 6.3: Parrot Minidrone experimental platform

Variables	Values	Units
m_s	0.063	kg
l	0.108m	m
g	9.81	m/s^2
J_r	0.1021×10^{-6}	m^2
I_x	5.85×10^{-5}	m^2
I_y	7.17×10^{-5}	m^2
I_z	1×10^{-4}	m^2

Table 6.1: Parrot Minidrone parameters

troller design is followed by [118]. The sliding manifolds are designed as

$$\left\{\begin{array}{l} s_1 = c_z(z_d - z) + (\dot{z}_d - \dot{z}) \\ s_2 = c_\psi\left(\psi_d - \psi\right) + \left(\dot{\psi}_d - \dot{\psi}\right) \\ s_3 = c_1(\dot{x}_d - \dot{x}) + c_2(x_d - x) + c_3\left(\dot{\theta}_d - \dot{\theta}\right) + c_4(\theta_d - \theta) \\ s_4 = c_5(\dot{y}_d - \dot{y}) + c_6(y_d - y) + c_7\left(\dot{\phi}_d - \dot{\phi}\right) + c_8\left(\phi_d - \phi\right) \end{array}\right\} \tag{6.52}$$

and its controllers are designed as

$$\left\{\begin{array}{l} u_1 = m_s \frac{c_z(\dot{z}_d - \dot{z}) + \ddot{z}_d + g + \varepsilon_1 sgn(s_1) + \eta_1 s_1}{cos\phi cos\theta} \\ u_2 = \frac{I_x}{l}\left(\frac{c_5}{c_7}(\ddot{y}_d - \ddot{y}) + \frac{c_6}{c_7}(\dot{y}_d - \dot{y}) + \ddot{\phi}_d + \frac{c_8}{c_7}\left(\dot{\phi}_d - \dot{\phi}\right) + \frac{1}{c_7}\left(\varepsilon_4 sgn(s_4) + \eta_4 s_4\right)\right) \\ u_3 = \frac{I_y}{l}\left(\frac{c_1}{c_3}(\ddot{x}_d - \ddot{x}) + \frac{c_2}{c_3}(\dot{x}_d - \dot{x}) + \ddot{\theta}_d + \frac{c_4}{c_3}\left(\dot{\theta}_d - \dot{\theta}\right) + \frac{1}{c_3}\left(\varepsilon_3 sgn(s_3) + \eta_3 s_3\right)\right) \\ u_4 = I_z\left(c_\psi\left(\dot{\psi}_d - \dot{\psi}\right) + \ddot{\psi}_d + \varepsilon_2 sgn(s_2) + \eta_2 s_2\right) \end{array}\right\} \tag{6.53}$$

The coefficients for SMC design are listed in Table 6.3

6.5.3 Experiment Results

In this experiment, the sampling time of the sensor and flight control system in the quadrotor is 5ms, which means that every 5 milliseconds, the Parrot quadrotor reads and processes sensor

$\omega_i (i = 1,2)$	15
$\delta_i (i = P,F,UN)$	$[0.8, 0.8]^T$
C_P	$diag(0.5, 0.6, 0)$
$K_{Pi} (i = 1,2)$	$diag(-4, 6, 0)$
C_F	$diag(3.6, 5, 0)$
K_{F1}	$diag(4, 0.01)$
K_{F2}	$diag(3, 0.008)$
C_{UN1}	$diag\left(8m_s/\, u_1 cos\, \phi cos\, \psi, -8m_s/cos\, \psi u_1\right)$
C_{UN2}	$diag\left(12m_s/\, u_1 cos\, \phi cos\, \psi, -12m_s/cos\, \psi u_1\right)$
C_{UN3}	$diag(6, 6)$
C_{UN4}	$diag(1, 1)$
C_{UN5}	$diag(0.0002, 0.003)$
C_{UN6}	$diag(0.001, 0.0015)$

Table 6.2: Design coefficients of ESO UDSMC

Variables	Values	Variables	Values
c_z	5	c_ψ	10
ε_1	0.8	ε_2	0.8
η_1	2	η_2	2
c_1	11	c_5	11
c_2	6	c_6	6
c_3	1	c_7	1
c_4	6	c_8	5
ε_3	-0.2	ε_4	0.2
η_3	-1.5	η_4	1.5

Table 6.3: Design coefficients of SMC

data. Compared to the 1ms sampling time in [12] (the latest real-time quadrotor control research), this experiment is more challenging and requires higher-quality controllers. The position-tracking control performance of Parrot Minidrone is tested and evaluated by following the desired linear and spiral path. The quadrotor takes off from the ground, first quickly climbs to a height of 1m, then follows the trajectory from $(0,0,1)$ to $(0,0.5,1)$ to $(1,0.5,1)$, and finally reaches the $(1,1,1)$ position according to the specified linear trajectory at 40 seconds. After this, the quadrotor climbs to a height of 1.5m at a steady speed in 20 seconds, and hovers at a height of 1.5m for 20 seconds. At the same time, during the climbing and hovering process, the aircraft makes a circular motion with a radius of 30cm. The trajectory of the quadrotor is calculated by IMU data, and the IMU has been calibrated by professional technician with 3 cameras (in x,y,z axis) in indoor environment.

The practical trajectory of the Parrot Minidrone is shown in Figure 6.4 and Figure 6.5. Further analysis of the tracking results are shown in Table 6.4, which shows the practical position tracking results of the quadrotor in each axis. To compare the tracking results for these three controllers numerically, the RMS values of the tracking errors are introduced as $e_{RMS} = \sqrt{\frac{1}{n}\left(e_1^2 + e_2^2 + \ldots + e_n^2\right)}$ with n being the total sampling size, the results are shown in Table

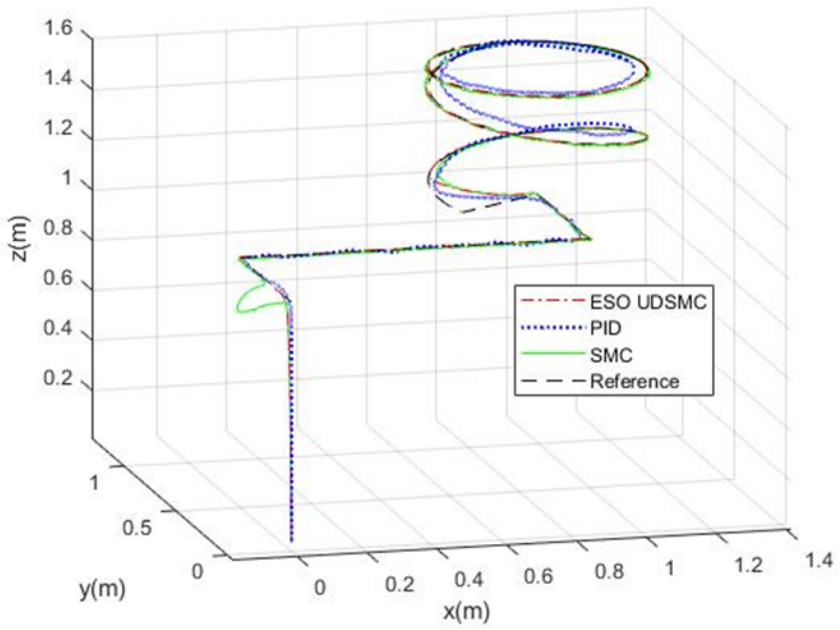

Figure 6.4: Actual flight and desired trajectory in 3-D space

e_{RMS}	PID	ESO UDSMC	SMC
x(m)	0.0827	0.0302	0.0376
y(m)	0.0780	0.0114	0.0218
z(m)	0.0679	0.0674	0.0691

Table 6.4: RMS results for trajectory tracking

6.4. Intuitively, From Table 6.4 and Figure 6.4, both the proposed ESO UDSM controller and the built-in PID controller can drive the quadrotor tracking the desired trajectory. And a more stable trajectory, less tracking error, and faster response speed with the proposed controller than the PID controller in each channel can be observed. This shows that the proposed control algorithm is superior to the control algorithm that comes with the Parrot Minidrone product. Meanwhile, from Table 6.4, the proposed UDSMC is only slightly better than SMC, but UDSMC does not exhibit a large overshoot in the XY axis (from Figures 6.6(a) 6.6(b) 6.6(c) 6.6(d)) and less chattering in the Z axis (from Figures 6.6(e)). This shows that the proposed algorithm still has certain advantages compared with advanced control algorithms.

Figure 6.7 presents the control inputs for involved three controllers and the RMS ($u_{RMS} = \sqrt{\frac{1}{n}\left(u_1^2+u_2^2+\ldots+u_n^2\right)}$) results are shown in Table 6.5. The huge difference in control input chattering can be clearly observed in Figure 6.7. From Table 6.5, frequent switching function triggers make large control input energy of SMC. Compared with PID, the proposed UDMSC has a larger control input energy, but is within the acceptable range. Therefore, considering the superior control performance of the proposed controller, although it has obvious fluctuations and higher

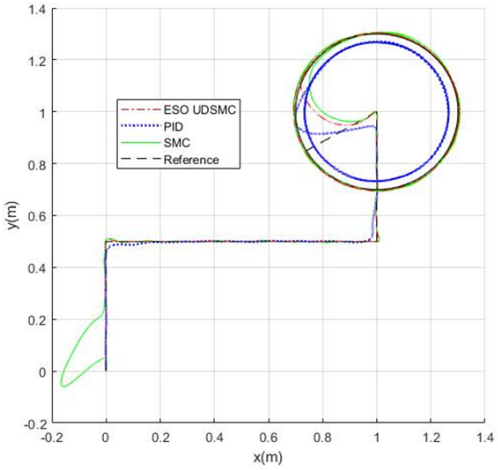

Figure 6.5: Actual flight and desired trajectory in horizontal plane

Channel	PID	UDSMC	SMC
Pitch control torque (Nm)	1.5748×10^{-6}	2.4246×10^{-5}	3.5199×10^{-4}
Roll control torque (Nm)	1.7226×10^{-5}	3.0336×10^{-5}	3.5850×10^{-4}
Yaw control torque (Nm)	2.3294×10^{-5}	1.3768×10^{-5}	0.0011
Altitude control thrust (N)	0.6189	0.6223	0.6749

Table 6.5: RMS results for control inputs

control input energy, the implementation of ESO UDMSC on the quadrotor can be successful. It should be noted that the performance of the built-in PID controller could be improved after careful tuning. However, this is very empirical and the original parameters for the PID controller are not changed in this experiment. From Figure 6.7, the chattering problems appear in both UDSMC and SMC in this experiment because of the frequent switching operations due to the long sampling time. The saturation function can reduce chattering but may result in a decrease in the robustness and tracking performance. Although these advanced control algorithms can achieve better control performance, however, in real-time applications, considering the computational cost, hardware sampling time, and unpredictable changes in external environmental factors, PID is still a mature controller that cannot be completely replaced.

6.6 Summary

This study proposes a robust control strategy for quadrotor trajectory tracking based on the ESO UDSMC method. Compared with the built-in PID and SMC-based flight control system of the Parrot Minidrone, the proposed control strategy not only achieves the fast response of the quadrotor control system but also guarantees flight stability and efficient desired flight trajectories tracking performance without offline identification of the quadrotor dynamic system.

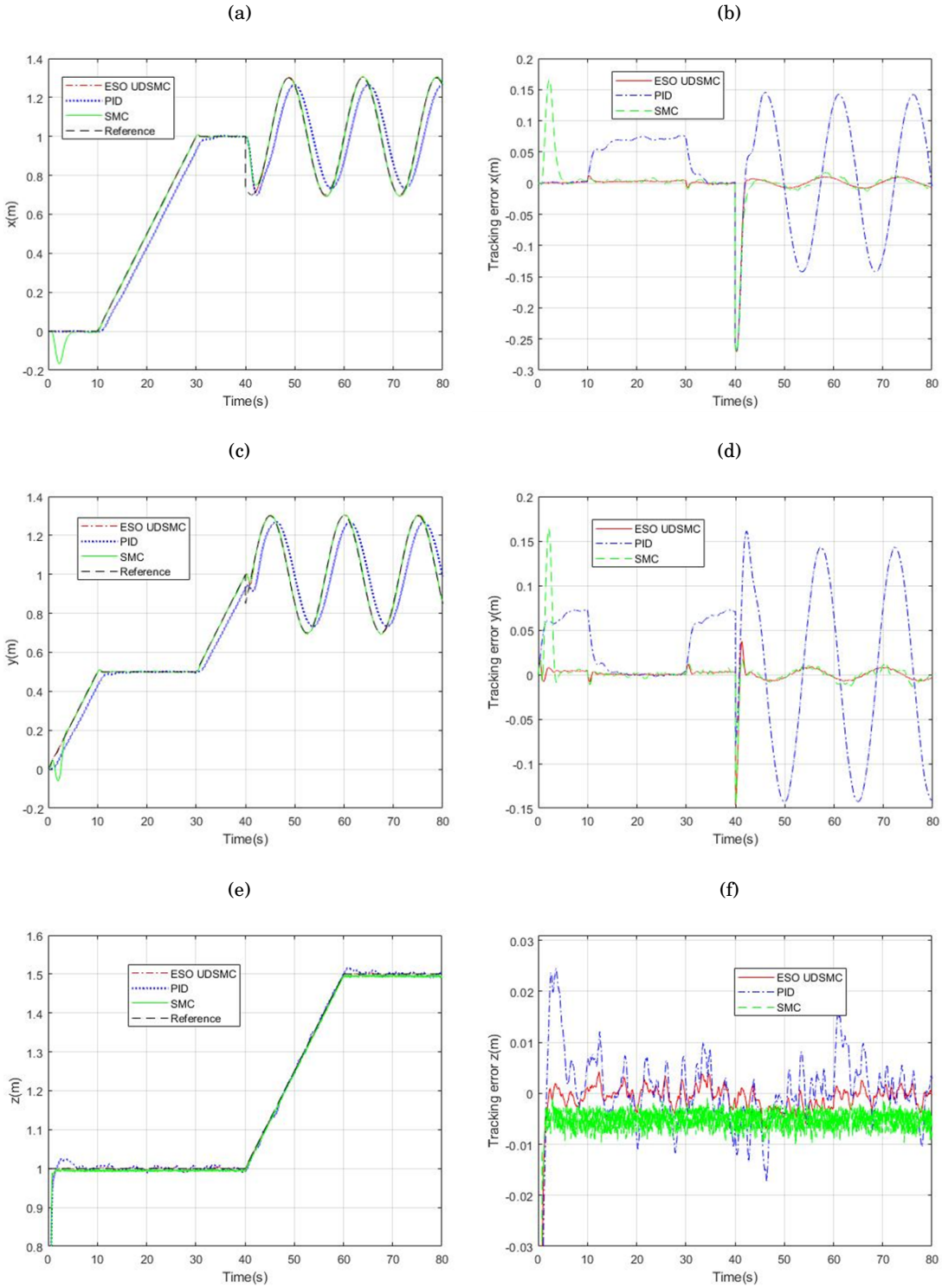

Figure 6.6: Actual trajectory tracking results: (a) x position tracking; (b) x position tracking error; (c) y position tracking; (d) y position tracking error; (e) z position tracking; (f) z position tracking error

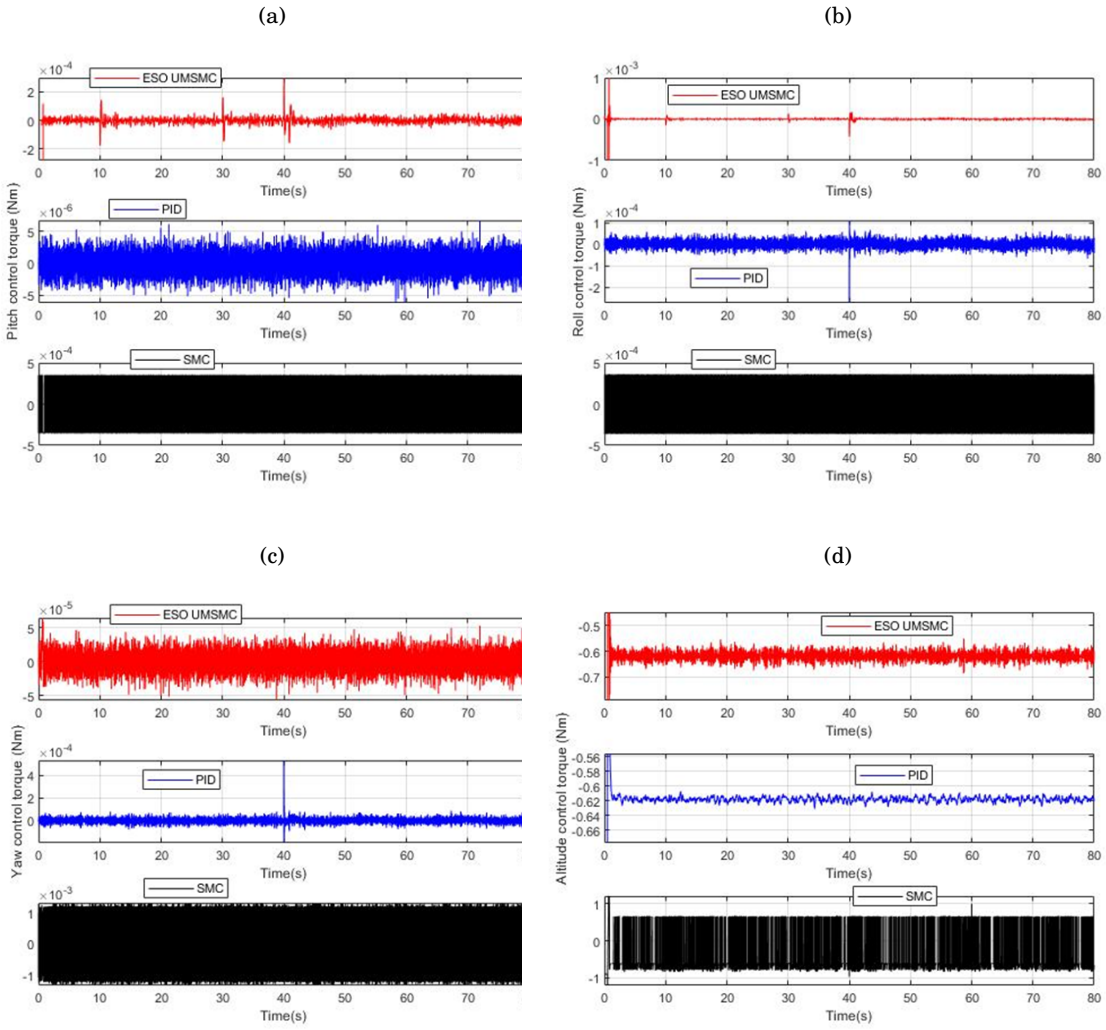

Figure 6.7: control torque inputs results: (a) Actual pitch control torque; (b) Actual roll control torque; (c) Actual yaw control torque; (d) Actual altitude control input

At the same time, the 5ms system sampling time also makes the designed control system have a large room for improvement with advanced computational algorithms for most quadrotors.

However, because of the small size, lightweight, and low motor torque of the Parrot Minidrone quadrotor used in the experiment, which cannot conduct flight tests in long-distance flights or complex environments. Also, this experiment does not involve variable load and unpredictable wind disturbance (indoor experiment). One of the future works will evaluate the proposed controller for stable flight under unknown wind disturbances. It is believed that with the improvement of UAV hardware support, the proposed quadrotor control system can reach better control performance.

CHAPTER 7

CONCLUSIONS

7.1 Conclusions

The overall goal of this PhD research is to develop the classical U-model control algorithm to increase its robustness and dependence on accurate modelling by combining it with other robust control method structures or techniques. In this study, a generic continuous-time U-model based dynamic inversion algorithm is proposed. Based on this technique, a generic continuous-time U-control is introduced as the basic control method and framework. The U-control system includes two loops: the inner loop realizes U-model based inverter, aiming to cancel the dynamics and nonlinearities of the controlled plant; the outer loop can therefore design an invariant controller according to user-defined control performance to meet their requirements. These two loops demonstrate the versatility and compatibility of the U-control system and the feasibility of further expanding it into advanced control algorithms. The proposed U model design framework has therefore become the basis for subsequent research.

By introducing IMC into the U-control framework, compared with the traditional TDF-IMC, UTDF-IMC can improve the robustness of the U-control algorithm while completely separating the robustness and control performance of the control system for independent design. Such a control system design framework is more convenient for achieving stable control and meeting the performance needs of customers. UTDF-IMC is simple in design and only needs U-model based inverter and two low-pass filters. The simulation results based on PMSM verify the effectiveness of the proposed algorithm. It is worth noting that UTDF-IMC adopts the method of error suppression to improve the robustness of the U-control, which means that the error cannot be eliminated but reduced to a small level.

Different from using error suppression in UTDF-IMC, the system's robustness is improved

by error compensation in DOBUC. The frequency-domain DOBC has been studied for many years, but because of the limitation of the classical inversion algorithm, it has not been effectively applied in nonlinear control. This study combines U-dynamic inversion and frequency-domain DOBC, which not only expands the application range of traditional DOBC but also improves the robustness of the U-control method by compensating errors in the input channel. Furthermore, the proposed DOUBC is extended to an input-output-based control algorithm, which reduces the need for system state variables information in control system design while maintaining its robustness and convenient control performance design characteristics. However, the proposed DOBUC algorithm is only oriented to SISO systems, which is its critical limitation.

The use of sliding mode to enhance U-control robustness is divided into two stages. The U-SMC proposed in the first stage is based on an error compensation strategy, which is designed by introducing a dynamic inverter compensator using the sliding mode technology design on the traditional U-control framework. The proposed UDSMC in the second stage directly use the sliding mode to design the dynamic inverter. Compared with the U-SMC, UDSMC not only significantly reduces the chattering problem of the controller by introducing a sliding band, but also reduces the requirements of the control system state variables information in design (only the order of the controlled plant and the feedback control error). At the same time, this study first attempts to treat the whole dynamics of the system as disturbances, so it is necessary to adjust the controller output gain to meet different control performance indicators during the design process.

Based on the proposed UDSMC, this study extends it to MIMO systems, and introduces MIMO-ESO to estimate the derivative information of system output and feedback errors, and applies it to the design of a quadrotor trajectory tracking control system. This is the first time that the U-control algorithm has been applied to a real-time industry application. Compared with the experimental results of the conventional SMC and built-in PID control systems, the MIMO-ESO enhanced UDSMC control system shows superiority in trajectory tracking performance (faster response and fewer tracking errors) and the controller output chattering is significantly reduced. This successful experiment further illustrated and verified the superiority and potential of the U-control system.

7.2 Proposed further research

As for the algorithm, based on the MIMO-ESO UDSMC, the adaptive UDSMC can be further developed and researched to automatically adjust the controller gain to cope with different controlled plants and control performance specifications. At the same time, the learning-based U-control system algorithm should also be very interesting, because these two algorithms, especially reinforcement learning and UDSMC method both have very low requirements for the model information of the controlled plants, and these methods can be regarded as black box

control methods. Therefore, the development on the basis of model-based reinforcement learning and model-free reinforcement, model-independent reinforcement U-learning is challenging and potential.

In terms of applications, the quadrotor used in this study is Parrot Minidrone, which is a small UAV with a small size and light load. Therefore, it is difficult to cope with complex and extreme environments, so the experiments tested in this study were carried out indoors. The next step of the experimental tests can consider using large UAVs for the long-distance, variable load to implement flight missions in more complex environments such as wind distances to test the effectiveness of the proposed algorithm. At the same time, this research has not covered the design and application of the control algorithm for the over-actuated system, and it can also be a potential research direction.

BIBLIOGRAPHY

[1] I. B. C. AHMED, C. OTHMAN, AND D. SOUDANI, *On the fuzzy adaptative internal model control of the discrete-time nonlinear systems*, in 2017 International Conference on Advanced Systems and Electric Technologies (IC_ASET), IEEE, 2017, pp. 395–400.

[2] N. AHMED, M. CHEN, AND S. SHAO, *Disturbance observer based tracking control of quadrotor with high-order disturbances*, IEEE access, 8 (2020), pp. 8300–8313.

[3] J. AJMERA AND V. SANKARANARAYANAN, *Point-to-point control of a quadrotor: Theory and experiment*, IFAC-PapersOnLine, 49 (2016), pp. 401–406.

[4] A. T. AZAR AND Q. ZHU, *Advances and applications in sliding mode control systems*, Springer, 2015.

[5] L. BESNARD, Y. B. SHTESSEL, AND B. LANDRUM, *Quadrotor vehicle control via sliding mode controller driven by sliding mode disturbance observer*, Journal of the Franklin Institute, 349 (2012), pp. 658–684.

[6] S. A. BILLINGS, *Nonlinear system identification: NARMAX methods in the time, frequency, and spatio-temporal domains*, John Wiley & Sons, 2013.

[7] T. R. BIYANTO, *State feedback controller design by utilizing linear quadratic regulator and backstepping control for uav quadrotor*, (2023).

[8] F. BONASSI AND R. SCATTOLINI, *Recurrent neural network-based internal model control design for stable nonlinear systems*, European Journal of Control, 65 (2022), p. 100632.

[9] M. CHADLI, S. AOUAOUDA, H. R. KARIMI, AND P. SHI, *Robust fault tolerant tracking controller design for a vtol aircraft*, Journal of the Franklin Institute, 350 (2013), pp. 2627–2645.

[10] K. P. B. CHANDRA, H. ALWI, AND C. EDWARDS, *Fault reconstruction for a quadrotor using an lpv sliding mode observer1*, IFAC-PapersOnLine, 48 (2015), pp. 374–379.

[11] J. CHEN, R. SUN, AND B. ZHU, *Disturbance observer-based control for small nonlinear uav systems with transient performance constraint*, Aerospace Science and Technology, 105 (2020), p. 106028.

[12] L. CHEN, Z. LIU, H. GAO, AND G. WANG, *Robust adaptive recursive sliding mode attitude control for a quadrotor with unknown disturbances*, ISA transactions, 122 (2022), pp. 114–125.

[13] L. CHEN, B. YAN, H. WANG, K. SHAO, E. KURNIAWAN, AND G. WANG, *Extreme-learning-machine-based robust integral terminal sliding mode control of bicycle robot*, Control Engineering Practice, 121 (2022), p. 105064.

[14] W. CHEN, *Disturbance observer based control for nonlinear systems*, IEEE/ASME transactions on mechatronics, 9 (2004), pp. 706–710.

[15] W.-H. CHEN, *Nonlinear disturbance observer-enhanced dynamic inversion control of missiles*, Journal of Guidance, Control, and Dynamics, 26 (2003), pp. 161–166.

[16] W.-H. CHEN, D. J. BALLANCE, P. J. GAWTHROP, AND J. O'REILLY, *A nonlinear disturbance observer for robotic manipulators*, IEEE Transactions on industrial Electronics, 47 (2000), pp. 932–938.

[17] W.-H. CHEN, J. YANG, L. GUO, AND S. LI, *Disturbance-observer-based control and related methods—an overview*, IEEE Transactions on industrial electronics, 63 (2015), pp. 1083–1095.

[18] X. CHEN, J. YANG, S. LI, AND Q. LI, *Disturbance observer based multi-variable control of ball mill grinding circuits*, Journal of Process Control, 19 (2009), pp. 1205–1213.

[19] X. CHENG AND Z.-W. LIU, *Robust tracking control of a quadcopter via terminal sliding mode control based on finite-time disturbance observer*, in 2019 14th IEEE Conference on Industrial Electronics and Applications (ICIEA), IEEE, 2019, pp. 1217–1222.

[20] T. ÇIMEN, *Systematic and effective design of nonlinear feedback controllers via the state-dependent riccati equation (sdre) method*, Annual Reviews in control, 34 (2010), pp. 32–51.

[21] V. CIRTOAJE, *A practical unified algorithm of p-imc type*, Processes, 8 (2020), p. 165.

[22] G. CONTE, C. H. MOOG, AND A. M. PERDON, *Algebraic methods for nonlinear control systems*, Springer Science & Business Media, 2007.

[23] S. DING, W.-H. CHEN, K. MEI, AND D. J. MURRAY-SMITH, *Disturbance observer design for nonlinear systems represented by input–output models*, IEEE Transactions on Industrial Electronics, 67 (2019), pp. 1222–1232.

[24] S. DING, W. X. ZHENG, J. SUN, AND J. WANG, *Second-order sliding-mode controller design and its implementation for buck converters*, IEEE Transactions on Industrial Informatics, 14 (2017), pp. 1990–2000.

[25] H. DU, X. YU, M. Z. CHEN, AND S. LI, *Chattering-free discrete-time sliding mode control*, Automatica, 68 (2016), pp. 87–91.

[26] C. G. ECONOMOU, M. MORARI, AND B. O. PALSSON, *Internal model control: Extension to nonlinear system*, Industrial & Engineering Chemistry Process Design and Development, 25 (1986), pp. 403–411.

[27] S. EMELYANOV, *Control of first order delay systems by means of an astatic controller and nonlinear correction*, Autom. Remote Control, 8 (1959), pp. 983–991.

[28] A. ESKANDARPOUR AND I. SHARF, *A constrained error-based mpc for path following of quadrotor with stability analysis*, Nonlinear Dynamics, 99 (2020), pp. 899–918.

[29] R. FALCÓN, H. RÍOS, AND A. DZUL, *Comparative analysis of continuous sliding-modes control strategies for quad-rotor robust tracking*, Control Engineering Practice, 90 (2019), pp. 241–256.

[30] Q. FEI, Y. DENG, H. LI, J. LIU, AND M. SHAO, *Speed ripple minimization of permanent magnet synchronous motor based on model predictive and iterative learning controls*, IEEE Access, 7 (2019), pp. 31791–31800.

[31] P. A. FISHWICK, *Handbook of dynamic system modeling*, CRC Press, 2007.

[32] V. FTHENAKIS AND H. C. KIM, *Land use and electricity generation: A life-cycle analysis*, Renewable and Sustainable Energy Reviews, 13 (2009), pp. 1465–1474.

[33] K. GAMAGEDARA AND T. LEE, *Geometric adaptive controls of a quadrotor unmanned aerial vehicle with decoupled attitude dynamics*, Journal of Dynamic Systems, Measurement, and Control, 144 (2022).

[34] C. E. GARCIA AND M. MORARI, *Internal model control. a unifying review and some new results*, Industrial & Engineering Chemistry Process Design and Development, 21 (1982), pp. 308–323.

[35] X. GENG, Q. ZHU, T. LIU, AND J. NA, *U-model based predictive control for nonlinear processes with input delay*, Journal of Process Control, 75 (2019), pp. 156–170.

[36] T. GEORGE THURUTHEL, Y. ANSARI, E. FALOTICO, AND C. LASCHI, *Control strategies for soft robotic manipulators: A survey*, Soft robotics, 5 (2018), pp. 149–163.

[37] Y. GOHIL AND J. DESAI, *Real-time tracking and fuel monitoring system for vehicle*, International Journal of Trend in Scientific Research and Development, 2 (2018), pp. 544–546.

[38] C. GREATWOOD AND A. G. RICHARDS, *Reinforcement learning and model predictive control for robust embedded quadrotor guidance and control*, Autonomous Robots, 43 (2019), pp. 1681–1693.

[39] B.-Z. GUO AND Z.-L. ZHAO, *On the convergence of an extended state observer for nonlinear systems with uncertainty*, Systems & Control Letters, 60 (2011), pp. 420–430.

[40] M. T. HAMAYUN, C. EDWARDS, H. ALWI, M. T. HAMAYUN, C. EDWARDS, AND H. ALWI, *Integral Sliding Mode Control*, Springer, 2016.

[41] J. D. HAMILTON, *State-space models*, Handbook of econometrics, 4 (1994), pp. 3039–3080.

[42] J. HAN, *From pid to active disturbance rejection control*, IEEE transactions on Industrial Electronics, 56 (2009), pp. 900–906.

[43] H. HASSANI, A. MANSOURI, AND A. AHAITOUF, *Robust autonomous flight for quadrotor uav based on adaptive nonsingular fast terminal sliding mode control*, International Journal of Dynamics and Control, 9 (2021), pp. 619–635.

[44] J. F. HORN, *Non-linear dynamic inversion control design for rotorcraft*, Aerospace, 6 (2019), p. 38.

[45] C. HUANG, *Design of decoupling fuzzy logic controller for quadrotor uav*, in Journal of Physics: Conference Series, vol. 1684, IOP Publishing, 2020, p. 012155.

[46] T. HUANG, D. HUANG, Z. WANG, X. DAI, AND A. SHAH, *Generic adaptive sliding mode control for a quadrotor uav system subject to severe parametric uncertainties and fully unknown external disturbance*, International Journal of Control, Automation and Systems, 19 (2021), pp. 698–711.

[47] N. A. A. HUSSAIN, S. S. A. ALI, M. OVINIS, M. R. ARSHAD, AND U. M. AL-SAGGAF, *Underactuated coupled nonlinear adaptive control synthesis using u-model for multivariable unmanned marine robotics*, IEEE Access, 8 (2019), pp. 1851–1865.

[48] A. ISIDORI, *Nonlinear control systems: an introduction*, Springer, 1985.

[49] S. K. KOMMURI, J. J. RATH, AND K. C. VELUVOLU, *Sliding-mode-based observer–controller structure for fault-resilient control in dc servomotors*, IEEE Transactions on Industrial Electronics, 65 (2017), pp. 918–929.

[50] P. KRISHNAMURTHY, F. KHORRAMI, AND R. S. CHANDRA, *Global high-gain-based observer and backstepping controller for generalized output-feedback canonical form*, IEEE Transactions on Automatic Control, 48 (2003), pp. 2277–2283.

[51] N. KUMAR AND M. VEERACHARY, *Stability region based robust controller design for high-gain boost dc–dc converter*, IEEE Transactions on Industrial Electronics, 68 (2020), pp. 2246–2256.

[52] R. LI, Q. ZHU, J. KIELY, AND W. ZHANG, *Algorithms for u-model-based dynamic inversion (um-dynamic inversion) for continuous time control systems*, Complexity, 2020 (2020), pp. 1–14.

[53] R. LI, Q. ZHU, P. NARAYAN, A. YUE, Y. YAO, AND M. DENG, *U-model-based two-degree-of-freedom internal model control of nonlinear dynamic systems*, Entropy, 23 (2021), p. 169.

[54] S. LI, J. YANG, W.-H. CHEN, AND X. CHEN, *Generalized extended state observer based control for systems with mismatched uncertainties*, IEEE Transactions on Industrial Electronics, 59 (2011), pp. 4792–4802.

[55] S. LI, J. YANG, W.-H. CHEN, AND X.-S. CHEN, *Disturbance observer-based control: methods and applications*, CRC press, 2014.

[56] X. LIN, Y. YU, AND C.-Y. SUN, *A decoupling control for quadrotor uav using dynamic surface control and sliding mode disturbance observer*, Nonlinear Dynamics, 97 (2019), pp. 781–795.

[57] H. LIU, J. XI, AND Y. ZHONG, *Robust attitude stabilization for nonlinear quadrotor systems with uncertainties and delays*, IEEE Transactions on Industrial Electronics, 64 (2017), pp. 5585–5594.

[58] J. LIU, Z. YIN, C. BAI, AND N. DU, *Internal model control of induction motors based on extended state observer*, Journal of Power Electronics, 20 (2020), pp. 163–175.

[59] M. LIU, Z. ZHAO, AND L. HAO, *Prescribed performance model-free adaptive sliding mode control of a shape memory alloy actuated system*, ISA transactions, 123 (2022), pp. 339–345.

[60] R. LÓPEZ-GUTIÉRREZ, A. E. RODRIGUEZ-MATA, S. SALAZAR, I. GONZÁLEZ-HERNÁNDEZ, AND R. LOZANO, *Robust quadrotor control: Attitude and altitude real-time results.*, J. Intell. Robotic Syst., 88 (2017), pp. 299–312.

[61] T. MA, Y. LIU, C. SHIH, AND C. CAO, *Handling of nonlinear systems using filtered high-gain output feedback controller*, International Journal of Robust and Nonlinear Control, 28 (2018), pp. 6070–6086.

[62] W. MACKUNIS, P. M. PATRE, M. K. KAISER, AND W. E. DIXON, *Asymptotic tracking for aircraft via robust and adaptive dynamic inversion methods*, IEEE Transactions on Control Systems Technology, 18 (2010), pp. 1448–1456.

[63] L. MARTINS, C. CARDEIRA, AND P. OLIVEIRA, *Linear quadratic regulator for trajectory tracking of a quadrotor*, IFAC-PapersOnLine, 52 (2019), pp. 176–181.

[64] W. MENG, Q. YANG, Y. YING, Y. SUN, AND Y. SUN, *Adaptive power acquisition control of variable-speed wind energy conversion systems under inaccurate wind speed measurement*, in 2013 American Control Conference, IEEE, 2013, pp. 4271–4276.

[65] U. D. A. MIRANDA, L. ROLIM, AND M. AREDES, *A dq synchronous reference frame current control for single-phase converters*, in 2005 IEEE 36th power electronics specialists conference, IEEE, 2005, pp. 1377–1381.

[66] O. MOFID AND S. MOBAYEN, *Adaptive sliding mode control for finite-time stability of quad-rotor uavs with parametric uncertainties*, ISA transactions, 72 (2018), pp. 1–14.

[67] O. MOFID, S. MOBAYEN, C. ZHANG, AND B. ESAKKI, *Desired tracking of delayed quadrotor uav under model uncertainty and wind disturbance using adaptive super-twisting terminal sliding mode control*, ISA transactions, 123 (2022), pp. 455–471.

[68] D. MÜLLER, C. VEIL, AND O. SAWODNY, *Disturbance observer based control for quasi continuum manipulators*, IFAC-PapersOnLine, 53 (2020), pp. 9808–9813.

[69] V. NEKOUKAR AND N. M. DEHKORDI, *Robust path tracking of a quadrotor using adaptive fuzzy terminal sliding mode control*, Control Engineering Practice, 110 (2021), p. 104763.

[70] W. L. OBERKAMPF, J. C. HELTON, C. A. JOSLYN, S. F. WOJTKIEWICZ, AND S. FERSON, *Challenge problems: uncertainty in system response given uncertain parameters*, Reliability Engineering & System Safety, 85 (2004), pp. 11–19.

[71] K. OHISHI, M. NAKAO, K. OHNISHI, AND K. MIYACHI, *Microprocessor-controlled dc motor for load-insensitive position servo system*, IEEE transactions on industrial electronics, (1987), pp. 44–49.

[72] P. N. PARASKEVOPOULOS, *Modern control engineering*, CRC Press, 2017.

[73] R.-E. PRECUP, T. KAMAL, AND S. Z. HASSAN, *Advanced control and optimization paradigms for wind energy systems*, Springer, 2019.

[74] Z. QIU, J. SUN, M. JANKOVIC, AND M. SANTILLO, *Nonlinear internal model controller design for wastegate control of a turbocharged gasoline engine*, Control Engineering Practice, 46 (2016), pp. 105–114.

[75] H. RAZAVI, K. MERAT, H. SALARIEH, A. ALASTY, AND A. MEGHDARI, *Observer based minimum variance control of uncertain piecewise affine systems subject to additive noise*, Nonlinear Analysis: Hybrid Systems, 19 (2016), pp. 153–167.

[76] P. S. REDDY, S. C. PATWARDHAN, AND K. Y. RANI, *Robust trajectory tracking in a reactive batch distillation process using multirate nonlinear internal model control*, Industrial & Engineering Chemistry Research, 58 (2019), pp. 11364–11381.

[77] B. REN, Q.-C. ZHONG, AND J. CHEN, *Robust control for a class of nonaffine nonlinear systems based on the uncertainty and disturbance estimator*, IEEE Transactions on Industrial electronics, 62 (2015), pp. 5881–5888.

[78] K. SASAKI AND Z.-J. YANG, *Disturbance observer-based control of uavs with prescribed performance*, International Journal of Systems Science, 51 (2020), pp. 939–957.

[79] S. SAXENA AND Y. V. HOTE, *Advances in internal model control technique: A review and future prospects*, IETE Technical Review, 29 (2012), pp. 461–472.

[80] M. SHAFIQ AND M. HASEEBUDDIN, *U-model-based internal model control for non-linear dynamic plants*, Proceedings of the Institution of Mechanical Engineers, Part I: Journal of Systems and Control Engineering, 219 (2005), pp. 449–458.

[81] H. SHAKHATREH, A. H. SAWALMEH, A. AL-FUQAHA, Z. DOU, E. ALMAITA, I. KHALIL, N. S. OTHMAN, A. KHREISHAH, AND M. GUIZANI, *Unmanned aerial vehicles (uavs): A survey on civil applications and key research challenges*, Ieee Access, 7 (2019), pp. 48572–48634.

[82] Y. SHTESSEL, C. EDWARDS, L. FRIDMAN, A. LEVANT, ET AL., *Sliding mode control and observation*, vol. 10, Springer, 2014.

[83] S. SIEBERLING, Q. CHU, AND J. MULDER, *Robust flight control using incremental nonlinear dynamic inversion and angular acceleration prediction*, Journal of guidance, control, and dynamics, 33 (2010), pp. 1732–1742.

[84] J. SINGH, K. CHATTERJEE, AND C. VISHWAKARMA, *Two degree of freedom internal model control-pid design for lfc of power systems via logarithmic approximations*, ISA transactions, 72 (2018), pp. 185–196.

[85] J.-J. E. SLOTINE, W. LI, ET AL., *Applied nonlinear control*, vol. 199, Prentice hall Englewood Cliffs, NJ, 1991.

[86] E. J. SMEUR, Q. CHU, AND G. C. DE CROON, *Adaptive incremental nonlinear dynamic inversion for attitude control of micro air vehicles*, Journal of Guidance, Control, and Dynamics, 39 (2016), pp. 450–461.

[87] B. SONKER, D. KUMAR, AND P. SAMUEL, *Design of two degree of freedom-internal model control configuration for load frequency control using model approximation*, International Journal of Modelling and Simulation, 39 (2019), pp. 27–37.

[88] J. SU, W.-H. CHEN, AND J. YANG, *On relationship between time-domain and frequency-domain disturbance observers and its applications*, Journal of Dynamic Systems, Measurement, and Control, 138 (2016).

[89] H. SUN, Y.-H. CHEN, AND H. ZHAO, *Adaptive robust control methodology for active roll control system with uncertainty*, Nonlinear Dynamics, 92 (2018), pp. 359–371.

[90] W. SUN, Z. ZHAO, AND H. GAO, *Saturated adaptive robust control for active suspension systems*, IEEE Transactions on industrial electronics, 60 (2012), pp. 3889–3896.

[91] X. SUN, L. CHEN, H. JIANG, Z. YANG, J. CHEN, AND W. ZHANG, *High-performance control for a bearingless permanent-magnet synchronous motor using neural network inverse scheme plus internal model controllers*, IEEE Transactions on Industrial Electronics, 63 (2016), pp. 3479–3488.

[92] X. SUN, Z. SHI, G. LEI, Y. GUO, AND J. ZHU, *Analysis and design optimization of a permanent magnet synchronous motor for a campus patrol electric vehicle*, IEEE Transactions on Vehicular Technology, 68 (2019), pp. 10535–10544.

[93] G. SZAFRANSKI AND R. CZYBA, *Different approaches of pid control uav type quadrotor*, (2011).

[94] E. TAL AND S. KARAMAN, *Accurate tracking of aggressive quadrotor trajectories using incremental nonlinear dynamic inversion and differential flatness*, IEEE Transactions on Control Systems Technology, 29 (2020), pp. 1203–1218.

[95] A. TAYEBI AND S. MCGILVRAY, *Attitude stabilization of a vtol quadrotor aircraft*, IEEE Transactions on control systems technology, 14 (2006), pp. 562–571.

[96] T. UMENO, T. KANEKO, AND Y. HORI, *Robust servosystem design with two degrees of freedom and its application to novel motion control of robot manipulators*, IEEE Transactions on Industrial Electronics, 40 (1993), pp. 473–485.

[97] V. UTKIN, *Variable structure systems with sliding modes*, IEEE Transactions on Automatic control, 22 (1977), pp. 212–222.

[98] S. VAIDYANATHAN AND C.-H. LIEN, *Applications of sliding mode control in science and engineering*, vol. 709, Springer, 2017.

[99] H. WANG, S. LI, J. YANG, AND X. ZHOU, *Continuous sliding mode control for permanent magnet synchronous motor speed regulation systems under time-varying disturbances*, Journal of Power Electronics, 16 (2016), pp. 1324–1335.

[100] S. WANG, J. NA, AND Y. XING, *Adaptive optimal parameter estimation and control of servo mechanisms: theory and experiments*, IEEE Transactions on Industrial Electronics, 68 (2020), pp. 598–608.

[101] S. WANG, L. TAO, Q. CHEN, J. NA, AND X. REN, *Usde-based sliding mode control for servo mechanisms with unknown system dynamics*, IEEE/ASME Transactions on Mechatronics, 25 (2020), pp. 1056–1066.

[102] T. WANG, Z. PING, Y. HUANG, AND J.-G. LU, *Nonlinear internal model based two-step controller design for pmsm position servo system*, in 2019 IEEE 15th International Conference on Control and Automation (ICCA), IEEE, 2019, pp. 1264–1269.

[103] X. WANG, S. SUN, E.-J. VAN KAMPEN, AND Q. CHU, *Quadrotor fault tolerant incremental sliding mode control driven by sliding mode disturbance observers*, Aerospace Science and Technology, 87 (2019), pp. 417–430.

[104] X. WANG, E.-J. VAN KAMPEN, Q. CHU, AND P. LU, *Stability analysis for incremental nonlinear dynamic inversion control*, Journal of Guidance, Control, and Dynamics, 42 (2019), pp. 1116–1129.

[105] Y.-C. WANG, D. SHEU, AND C.-E. LIN, *A unified approach to nonlinear dynamic inversion control with parameter determination by eigenvalue assignment*, Mathematical Problems in Engineering, 2015 (2015).

[106] X. XIANG, C. LIU, H. SU, AND Q. ZHANG, *On decentralized adaptive full-order sliding mode control of multiple uavs*, ISA transactions, 71 (2017), pp. 196–205.

[107] N. XIE, Y. YU, AND C. SUN, *An image-based decoupling controller of quadrotor for moving target tracking*, Journal of Control and Decision, (2022), pp. 1–12.

[108] J.-J. XIONG AND G. ZHANG, *Discrete-time sliding mode control for a quadrotor uav*, Optik, 127 (2016), pp. 3718–3722.

[109] J.-J. XIONG AND E.-H. ZHENG, *Position and attitude tracking control for a quadrotor uav*, ISA transactions, 53 (2014), pp. 725–731.

[110] J. XU, C. CHEN, D. GAO, S. LUO, AND Q. QIAN, *Nonlinear dynamic analysis on maglev train system with flexible guideway and double time-delay feedback control*, Journal of Vibroengineering, 19 (2017), pp. 6346–6362.

[111] X.-G. YAN, S. K. SPURGEON, AND C. EDWARDS, *Variable structure control of complex systems*, Communications and Control Engineering, (2017).

[112] P. C. YOUNG, *Stochastic, dynamic modelling and signal processing: time variable and state dependent parameter estimation*, Nonlinear and nonstationary signal processing, (2000), pp. 74–114.

[113] F. M. ZAIHIDEE, S. MEKHILEF, AND M. MUBIN, *Application of fractional order sliding mode control for speed control of permanent magnet synchronous motor*, Ieee Access, 7 (2019), pp. 101765–101774.

[114] K. ZHANG, Y. SHI, AND H. SHENG, *Robust nonlinear model predictive control based visual servoing of quadrotor uavs*, IEEE/ASME Transactions on Mechatronics, 26 (2021), pp. 700–708.

[115] W. ZHANG, Q. ZHU, S. MOBAYEN, H. YAN, J. QIU, AND P. NARAYAN, *U-model and u-control methodology for nonlinear dynamic systems*, Complexity, 2020 (2020), pp. 1–13.

[116] X. ZHANG, J. HU, AND Z. LIU, *Fuzzy adaptive internal model control for a pneumatic muscle actuator*, in Proceedings of the 2019 11th International Conference on Machine Learning and Computing, 2019, pp. 546–550.

[117] Z. ZHAO, X. HE, AND C. K. AHN, *Boundary disturbance observer-based control of a vibrating single-link flexible manipulator*, IEEE Transactions on Systems, Man, and Cybernetics: Systems, 51 (2019), pp. 2382–2390.

[118] E.-H. ZHENG, J.-J. XIONG, AND J.-L. LUO, *Second order sliding mode control for a quadrotor uav*, ISA transactions, 53 (2014), pp. 1350–1356.

[119] D. ZHOLTAYEV, M. RUBAGOTTI, AND T. D. DO, *Adaptive super-twisting sliding mode control for maximum power point tracking of pmsg-based wind energy conversion systems*, Renewable Energy, 183 (2022), pp. 877–889.

[120] Q. ZHU, S. GHAURI, AND J. NA, *U-model based control system formulisation and design for wind energy conversion systems*, in 2016 UKACC 11th International Conference on Control (CONTROL), IEEE, 2016, pp. 1–6.

[121] Q. ZHU AND L. GUO, *A pole placement controller for non-linear dynamic plants*, Proceedings of the Institution of Mechanical Engineers, Part I: Journal of Systems and Control Engineering, 216 (2002), pp. 467–476.

[122] Q. ZHU, R. LI, AND X. YAN, *U-model-based double sliding mode control (udsm-control) of nonlinear dynamic systems*, International Journal of Systems Science, 53 (2022), pp. 1153–1169.

[123] Q. ZHU, S. LI, AND D. ZHAO, *A universal u-model based control system design*, in Proceedings of the 33rd Chinese Control Conference, IEEE, 2014, pp. 1839–1844.

[124] Q. ZHU, L. LIU, W. ZHANG, AND S. LI, *Control of complex nonlinear dynamic rational systems*, Complexity, 2018 (2018).

[125] Q. ZHU, Y. WANG, D. ZHAO, S. LI, AND S. A. BILLINGS, *Review of rational (total) nonlinear dynamic system modelling, identification, and control*, International Journal of Systems Science, 46 (2015), pp. 2122–2133.

[126] Q. ZHU, K. WARWICK, AND J. DOUCE, *Adaptive general predictive controller for nonlinear systems*, in IEE Proceedings D (Control Theory and Applications), vol. 138, IET, 1991, pp. 33–40.

[127] Q. ZHU, Z. YIN, Y. ZHANG, J. NIU, Y. LI, AND Y. ZHONG, *Research on two-degree-of-freedom internal model control strategy for induction motor based on immune algorithm*, IEEE Transactions on Industrial Electronics, 63 (2015), pp. 1981–1992.

[128] Q. ZHU, W. ZHANG, J. NA, AND B. SUN, *U-model based control design framework for continuous-time systems*, in 2019 Chinese control conference (CCC), IEEE, 2019, pp. 106–111.

[129] Q. ZHU, W. ZHANG, J. ZHANG, AND B. SUN, *U-neural network-enhanced control of nonlinear dynamic systems*, Neurocomputing, 352 (2019), pp. 12–21.

[130] Q. ZHU, D. ZHAO, AND J. ZHANG, *A general u-block model-based design procedure for nonlinear polynomial control systems*, International Journal of Systems Science, 47 (2016), pp. 3465–3475.

[131] Q. M. ZHU, *Identification & control of nonlinear systems*, PhD thesis, University of Warwick, 1989.